



European
Commission

JRC SCIENCE AND POLICY REPORTS

Multi-walled Carbon Nanotubes, NM-400, NM-401, NM-402, NM-403: Characterisation and Physico-Chemical Properties

*JRC Repository: NM-series of
Representative Manufactured
Nanomaterials*

Kirsten Rasmussen, Jan Mast, Pieter-Jan De
Temmerman, Eveline Verleysen, Nadia Waegeneers,
Frederic Van Steen, Jean Christophe Pizzolon, Ludwig
De Temmerman, Elke Van Doren, Keld Alstrup Jensen,
Renie Birkedal, Per Axel Clausen, Yahia Kembouche,
Nathalie Thieriet, Olivier Spalla, Camille Guiot, Davy
Rousset, Olivier Witschger, Sébastien Bau, Bernard
Bianchi, Boris Shivachev, Louiza Dimowa, Rositsa
Nikolova, Diana Nihtianova, Mihail Tarassov, Ognyan
Petrov, Snejana Bakardjieva, Charles Motzkus,
Guillaume Labarraque, Caroline Oster, Giulio Cotogno
and Claire Gailliard

NANOGENOTOX



Co-funded by
the Health Programme
of the European Union
Grant Agreement n°2009 21 01

2014



Report EUR 26796 EN

Joint
Research
Centre

European Commission

Joint Research Centre
Institute for Health and Consumer Protection

Contact information

IHCP Communication Office
Address: Joint Research Centre, via E. Fermi 2749, I-21027 Ispra (VA)
E-mail: jrc-ihcp-communication@ec.europa.eu
Tel.: +39 0332 78 9618
<https://ec.europa.eu/jrc>

Legal Notice

This publication is a Science and Policy Report by the Joint Research Centre, the European Commission's in-house science service. It aims to provide evidence-based scientific support to the European policy-making process. The scientific output expressed does not imply a policy position of the European Commission. Neither the European Commission nor any person acting on behalf of the Commission is responsible for the use which might be made of this publication.

All images © NANOGENOTOX Joint Action 2013

JRC91205
EUR 26796 EN
ISBN 978-92-79-39648-9 (PDF)
ISBN 978-92-79-39649-6 (print)

ISSN 1831-9424 (online)
ISSN 1018-5593 (print)

doi:10.2788/10753

Luxembourg: Publications Office of the European Union, 2014

© European Union, 2014

Reproduction is authorised provided the source is acknowledged

Abstract

In 2011 the JRC launched a Repository for Representative Test Materials that supports both EU and international research projects, and especially the OECD Working Party on Manufactured Nanomaterials' (WPMN) exploratory testing programme "Testing a Representative set of Manufactured Nanomaterials" for the development and collection of data on characterisation, toxicological and ecotoxicological properties, as well as risk assessment and safety evaluation of nanomaterials. The JRC Repository responds to a need for availability of nanomaterial from a single production batch to enhance the comparability of results between different research laboratories and projects.

The present report presents the physico-chemical characterisation of the multi-walled carbon nanotubes (MWCNT) from the JRC Repository: NM-400, NM-401, NM-402 and NM-403. NM-400 was selected as principal material for the OECD WPMN testing programme. MWCNTs are produced by catalytic chemical vapour deposition. Each of these NMs originates from one batch of commercially manufactured MWCNT. They are nanostructured, i.e. they consist of more than one graphene layer stacked on each other and rolled together as concentric tubes. The MWCNT NMs may be used as a representative material in the measurement and testing with regard to hazard identification, risk and exposure assessment studies. The results are based on studies by several European laboratories participating in the NANOGENOTOX Joint Action.

JRC Repository: NM-Series of Representative Manufactured Nanomaterials

Multi-walled Carbon Nanotubes, NM-400, NM-401, NM-402, NM-403: Characterisation and Physico-Chemical Properties

Kirsten Rasmussen, Giulio Cotogno, Claire Gaillard

European Commission, Joint Research Centre, Institute for Health and Consumer Protection, Italy

**Jan Mast, Pieter-Jan De Temmerman, Eveline Verleysen, Nadia Waegeneers,
Frederic Van Steen, Jean Christophe Pizzolon, Ludwig De Temmerman,
Elke Van Doren**

Veterinary and Agrochemical Research Centre (CODA-CERVA), Belgium

Keld Alstrup Jensen, Renie Birkedal, Per Axel Clausen, Yahia Kembouche

National Research Centre for the Working Environment (NRCWE), Denmark

Nathalie Thieriet

L'Agence nationale de sécurité sanitaire de l'alimentation, de l'environnement et du travail (ANSES),
France

Olivier Spalla, Camille Guiot

Commissariat à l'énergie atomique et aux énergies alternatives (CEA), France

Davy Rousset, Olivier Witschger, Sébastien Bau, Bernard Bianchi

Institut National de Recherche et de Sécurité (INRS), France

Charles Motzkus, Guillaume Labarraque, Caroline Oster

Laboratoire National de métrologie et d'essais (LNE), France

Boris Shivachev, Louiza Dimowa, Rositsa Nikolova, Diana Nihtianova,

Mihail Tarassov, Ognyan Petrov, Snejana Bakardjieva

Institute of Mineralogy and Crystallography (IMC-BAS), Bulgaria

Abstract

The European Commission's Joint Research Centre (JRC) provides scientific support to European Union policy including nanotechnology. In 2011 the JRC launched, within this context, a Repository for Representative Test Materials (RTMs), based on preparatory work started in 2008. It supports both EU and international research projects, and especially the OECD Working Party on Manufactured Nanomaterials (WPMN). The WPMN leads an exploratory testing programme "Testing a Representative set of Manufactured Nanomaterials" for the development and collection of data on characterisation, toxicological and ecotoxicological properties, as well as risk assessment and safety evaluation of nanomaterials. The purpose is to understand the applicability of the OECD Test Guidelines for the testing of nanomaterials as well as end-points relevant for such materials.

The JRC Repository responds to a need within nanosafety research: the availability of nanomaterial from a single production batch to enhance the comparability of results between different research laboratories and projects. The availability of representative nanomaterials to the international scientific community furthermore enhances and enables development of safe materials and products.

The present report presents the physico-chemical characterisation of the multi-walled carbon nanotubes (MWCNT) from the JRC Repository: NM-400, NM-401, NM-402 and NM-403. NM-400 was selected as principal material for the OECD test programme "Testing a representative set of manufactured nanomaterials".

NM-400, NM-401, NM-402, NM-403 were produced by catalytic chemical vapour deposition. Each of these NMs originates from one respective batch of commercially manufactured MWCNT. They are nanostructured, i.e. they consist of more than one graphene layer stacked on each other and rolled together as concentric tubes. The MWCNT NMs may be used as a representative material in the measurement and testing with regard to hazard identification, risk and exposure assessment studies.

The results for many endpoints are presented in this report, including size and size distribution, specific surface area and electron microscopy images. The results are based on studies by several European laboratories participating in the NANOGENOTOX Joint Action.

Table of contents

1. Introduction	9
1.1.Production of MWCNT	10
1.2.About this report.....	10
2. Overview of the JRC NM-Series of Representative Test Materials	11
2.1.Representativeness of the materials in the NM-series	12
2.2.The OECD WPMN and Testing the NM-Series	14
2.3.Characterisation of the NM-series.....	16
3. Materials, Methods and End-points.....	18
4. Chemical composition	22
4.1.Elemental Composition by EDS, ICP-OES and ICP-MS	22
4.2.Presence of catalysts by TGA and DTA	27
4.3.Presence of catalysts by XRD	31
4.4.Chemical composition, observations and conclusions	32
5. Raman spectroscopy	34
6. Hydrochemical reactivity, solubility and biodurability	35
6.1.Results, Hydrochemical pH reactivity	36
6.2.Hydrochemical O ₂ Activity	40
6.3. <i>In vitro</i> dissolution and solubility	44
6.4.Estimation of biodurability	47
6.5.Conclusions.....	47
7. SAXS and USAXS measurements and data treatment.....	49
7.1.Size and structure of fractal aggregates by SAXS	51
8. Brunauer, Emmett and Teller (BET) measurements.....	55
8.1.BET results	56
8.2.Comparison of producers' BET data and measured BET	57
8.3.Comparison of SAXS and BET data	57
9. XRD measurements	58
9.1.XRD analysis.....	58
10. Transmission Electron Microscopy (TEM)	60
10.1.TEM. Sample preparation and measurements	60
10.1.1.Sample preparation	60
10.1.2.Recording of the electron micrographs	61
10.2.Results for Transmission Electron Microscopy.....	61
10.3.Interlaboratory comparison.....	63
11. Dustiness	66
11.1.Experimental setup of Vortex Shaker Method and results.....	66
11.2.Results for the Vortex Shaker Method.....	71

12. Conclusions	76
12.1.Characterisation	77
12.2.Summary of the characterisation of each MWCNT NM.....	78
12.2.1.NM-400, summary of physico-chemical characterisation	79
12.2.2.NM-401, summary of physico-chemical characterisation	83
12.2.3.NM-402, summary of physico-chemical characterisation	87
12.2.4.NM-403, summary of physico-chemical characterisation	90
12.2.5.MWCNT NMs, overview of physico-chemical characterisation	93
13. References	98
A. Appendix. The Sensor Dish Reader System	101
B. Appendix. SOP for Small Angle X-ray Scattering.	104

List of abbreviations

2D	Two Dimensional
BET	Brunauer, Emmet and Teller
BF	Bright Field
BSA	Bovine Serum Albumin
CCVD	Catalytic Chemical Vapour Deposition
CEA	Commissariat à l'énergie atomique et aux énergies alternatives, France
CEN	Comité Européen de Normalisation
CLS	Centrifugal Liquid Sedimentation
CODA-CERVA	Veterinary and Agrochemical Research Centre, Belgium
CPC	Condensation Particle Counter
DLS	Dynamic Light Scattering
ELPI	Electrical Low Pressure Impactor
EM	Electron microscopy
EDS / EDX	Energy-Dispersive X-ray spectroscopy
FWHM	Full-Width Half-Maximum
GLP	Good Laboratory Practice
h	hours
ICP	Inductively Coupled Plasma
ICP-MS	Inductively Coupled Plasma – Mass Spectrometry
ICP-OES	Inductively Coupled Plasma – Optical Emission Spectrometry
IHCP	Institute for Health and Consumer Protection (JRC)
IMC-BAS	Institute of Mineralogy and Crystallography, Bulgaria
INRS	Institut National de Recherche et de Sécurité, France
ISO	International Organisation for Standardization
ISO/TC 229	ISO/Technical Committee on Nanotechnologies
JRC	Joint Research Centre, European Commission
L / l	Litre
LNE	Laboratoire national de métrologie et d'essais, France
lpm	Litre per minute
ml / mL	Millilitre
MWCNT	Multi Walled Carbon Nanotubes
MWCNT NMs	NM-400, NM-401, NM-402 and NM-403
NIST	National Institute of Standards and Technology, USA
NM	Nanomaterial
NRCWE	National Research Centre for the Working Environment, Denmark
OECD	Organisation for Economic Co-operation and Development

pH	Acidity value
RH	Relative Humidity
rpm	Rounds Per Minute
RTM	Representative Test Material
s	second
SAED	selected area electron diffraction
SAXS	Small Angle X-ray Scattering
SCENIHR	Scientific Committee for Emerging and Newly Identified Health Risks
SD	Standard Deviation
SDR	Sensor Disk Reader
SEM	Scanning Electron Microscopy
SEM-EDS	Scanning Electron Microscopy-Energy Dispersive Spectroscopy
SOP	Standard Operating Procedure
SSA	Specific surface area
TEM	Transmission Electron Microscopy
TGA	Thermogravimetric Analysis
USA	United States of America
USAXS	Ultra Small Angle X-ray Scattering
VS	Vortex Shaker
WPMN	Working Party on Manufactured Nanomaterials
wt %	weight percent
XRD	X-ray Diffraction

1. Introduction

Over the past decade, nanomaterials have gained an increasing attention and they are subject to numerous international research projects aiming at both evaluating their potential for technological innovation and understanding possible adverse effects (Morris et al., 2011). It is of special interest to identify if the nano form induces adverse effects (e.g. other effects, or different potency) different to non-nano forms of the same chemistry.

For nanosafety research purposes, availability of nanomaterial from a single batch is desirable to enhance the comparability of results between different laboratories and research projects and to overcome questions related to whether a nanomaterial tested in a project is the same or just similar to a nanomaterial tested in other project(s). Addressing this need and supporting the OECD Working Party on Manufactured Nanomaterials (WPMN) programme for "Testing a Representative set of Manufactured Nanomaterials", the European Commission's Joint Research Centre (JRC) established a Repository with Representative Test Materials (RTMs) hosting different types of nanomaterials. The role of Representative Test Materials is described in a recent publication (Roebben et al., 2013).

One of the nanomaterials tested by the OECD WPMN is multi-walled carbon nanotubes (MWCNT), which are widely used as structural composites, and also in energy applications such as the lithium ion battery. MWCNT can be found in final products such as conductive polymers and composites (automobile and electronic), aerospace structural parts, sporting goods and sensors (<http://www.cefic.org/Documents/Other/Benefits%20of%20Carbon%20Nanotubes.pdf>). According to the new market research report "Global CNT Market - SWCNT, MWCNT, Technology, Applications, Trends & Outlook (2011 - 2016)", carbon nanotubes are the fastest growing segment in nanomaterial technology market across the globe (<http://www.prweb.com/releases/carbon-nanotubes/market/prweb11141047.htm>).

A substantial part of the information in this report comes from a Joint Action, NANOGENOTOX, see <http://www.nanogenotox.eu>, which was co-financed by the Executive Agency of the Directorate General for Health and Consumers of the European Commission and 11 EU member states. In NANOGENOTOX, characterisation and testing of MWCNT were important tasks. MARINA (<http://www.marina-fp7.eu/>) is another example of EU projects testing the materials from the JRC Repository. Furthermore, some of the analytical measurements (ICP-MS) were performed by Duke University (UK), and this contribution is gratefully acknowledged.

1.1. Production of MWCNT

The JRC Repository MWCNTs are produced by 4 different producers. The industrial production process is catalytic chemical vapour deposition (CCVD), which currently is one of the principal techniques to synthesise MWCNT. In the CCVD process hydrocarbon vapour passes through a tubular reactor at high temperature (600 -1200 °C) in the presence of metal catalyst material. The hydrocarbon vapour is thus decomposed into carbon and hydrogen species. MWCNTs grow in the reactor and are collected upon cooling the system to room temperature. MWCNTs synthesis is controlled by adjusting the parameters such as hydrocarbon sources, catalyst (type and size), temperature, pressure, gas-flow rate, deposition time and reactor geometry (Kumar and Ando, 2010).

1.2. About this report

This report presents the characterisation data and methods for MWCNT from the JRC Repository: NM-400, NM-401, NM-402 and NM-403; the abbreviation "MWCNT NMs" is used when describing all 4 MWCNT, otherwise a reference is made to the nanomaterial(s) tested.

Chapter 2 introduces the JRC Repository for representative nanomaterials and the link to the OECD Working Party on Manufactured Nanomaterials (WPMN). Chapter 3 describes the materials, methods and end-points and presents an overview of the end-points tested and the methods applied for each end-point.

The following chapters 4 to 9 describe in details the physico-chemical characteristics examined and the applied methodology. The characterisation includes properties such as size distribution measured by Transmission Electron Microscopy (TEM) and Dynamic Light Scattering (DLS) and specific surface area (SSA) was analysed through techniques such as BET¹ and small-angle X-ray scattering (SAXS). Quantitative elemental analysis of MWCNT was performed by EDS-analysis (Energy-dispersive X-ray) and different ICP (Inductively Coupled Plasma) methods. Impurities quantity was also estimated by Thermogravimetric Analysis (TGA). For the dustiness testing, INRS used the vortex shaker method. Table 4 gives an overview of the end-points investigated, methods applied and the institutions involved. The conclusions are presented in chapter 10, and include a summary of results for each of the MWCNT NMs.

A list of abbreviations has been included before the introduction. Furthermore, details on the methods applied are given in appendices A to B as available and relevant.

¹ Brunauer–Emmett–Teller gas adsorption: Stephen Brunauer, Paul Hugh Emmett, and Edward Teller developed a theory that aims to explain the physical adsorption of gas molecules on a solid surface and serves as the basis for an analysis technique, named after them by the initials of their last names, BET, for the measurement of the specific surface area of a material.

2. Overview of the JRC NM-Series of Representative Test Materials

The European Commission's Joint Research Centre (JRC) established the JRC Nanomaterials Repository for the NM-series of Representative Test Materials. The JRC Repository is hosted at the Institute for Health and Consumer Protection in Italy.

Table 1. List of representative Nanomaterials in the JRC Repository (2013).

NM code	Type of material*	Label name	Other information
NM-100	Titanium Dioxide	Titanium Dioxide	
NM-101	Titanium Dioxide	Titanium Dioxide	anatase
NM-102	Titanium Dioxide	Titanium Dioxide, anatase	anatase
NM-103	Titanium Dioxide	Titanium Dioxide thermal, hydrophobic	rutile
NM-104	Titanium Dioxide	Titanium Dioxide thermal, hydrophilic	rutile
NM-105	Titanium Dioxide	Titanium Dioxide rutile-anatase	anatase-rutile
NM-110	Zinc Oxide, uncoated	Zinc Oxide	
NM-111	Zinc Oxide, coated	Zinc Oxidecoatedtriethoxycaprylsilane	
NM-200	Silicon Dioxide	Synthetic Amorphous Silica PR-A-02	precipitated
NM-201	Silicon Dioxide	Synthetic Amorphous Silica PR-B-01	precipitated
NM-202	Silicon Dioxide	Synthetic Amorphous Silica PY-AB-03	thermal
NM-203	Silicon Dioxide	Synthetic Amorphous Silica PY-A-04	thermal
NM-204	Silicon Dioxide	Synthetic Amorphous Silica PR-A-05	precipitated
NM-211	Cerium Dioxide	Cerium (IV) Oxide precipitated, uncoated, cubic	
NM-212	Cerium Dioxide	Cerium (IV) Oxide precipitated, uncoated	
NM-300K	Silver	Silver<20 nm	
NM-300K DIS	Silver - dispersant	Ag - dispersant	
NM-330	Gold		
NM-330 DIS	Gold - dispersant	Gold - dispersant	
NM-400	MWCNT	Multi-walled Carbon Nanotubes	
NM-401	MWCNT	Multi-walled Carbon Nanotubes	
NM-402	MWCNT	Multi-walled Carbon Nanotubes	
NM-403	MWCNT	Multi-walled Carbon Nanotubes	
NM-600	Nanoclay	Bentonite	

* Nanomaterials, even of the same chemical composition, may be available e.g. in various sizes and/or shapes, which may influence their chemical and physical properties

Currently, the JRC Repository contains eight of the nanomaterial chemistries tested in the OECD WPMN Testing Programme and a total of 22 representative nanomaterials, see Table 1. The chemistries are titanium dioxide, zinc oxide, silicon dioxide, cerium dioxide, silver, gold, multi-walled carbon nanotubes and bentonite. Furthermore, the dispersants for silver and gold are also available from the JRC Repository. The sub-sampling was done in collaboration with the Fraunhofer Institute for Molecular Biology and Applied Ecology, and each nanomaterial was homogenised and sub-sampled into vials under reproducible (Good Laboratory Practice [GLP]) conditions). Each nanomaterial in the JRC Repository originates from a random single industrial production batch, produced within industrial specifications.

Thus, to the extent feasible for industrial materials, all sub-samples from one material should be identical and differences in test results between laboratories for the same end-point should not be attributed to differences in the material tested. The nanomaterials were allocated an identifying code with the following format: the letters "NM" followed by a dash and three digits (NM-XXX), the NM-series. In 2014 the code format was changed to JRCNM<5digit number><letter><six digit number>.

The materials are studied in projects investigating properties of nanomaterials at all levels of co-operation: national, European and global. More than 10,000 individual vials have been distributed to research institutions, national authorities, industrial research laboratories and other scientific stakeholders in the EU, Switzerland, USA, Canada, Australia, China, Russia, Japan, and Korea. Several research projects have been undertaken to investigate properties of nanomaterials using the representative nanomaterials from the JRC Repository.

Study results for the WPMN Testing Programme are collated in a JRC database, JRC NANOhub, and are made available to the OECD through access to the database. The combination of availability of representative test nanomaterials and data in the JRC NANOhub builds a foundation for research and product development, thus supporting innovation and competitiveness for nanotechnology industries.

2.1. Representativeness of the materials in the NM-series

To reliably address the scientific questions of nanomaterial-induced effects for toxicity, ecotoxicity and environmental fate and behaviour, representative test nanomaterials are important: they must be relevant for industrial application and commercial use, and be characterised by a critical mass of study results. Representative test materials allow enhanced comparison of test results, robust assessment of data, and pave the way for appropriate test method optimization, harmonisation and validation and may finally serve as performance standards for testing.

In the following, the concept of Representative Test Material (RTM) is briefly outlined clarifying the difference to reference materials. Reference Material (RM) is the generic name for materials which have a proven and sufficient homogeneity and stability in terms of a defined intended use; for certified reference materials, there is a certified value for the property of interest. Reference Materials and Certified Reference Materials need to be produced and used applying the conditions and terms standardised and described in ISO Guides 30 to 35 relating to reference material production. Currently, only a small number of certified reference materials exist in the field of manufactured nanomaterials, for example gold nanoparticles (certified size) and single-wall carbon nanotube soot (certified

composition) from the USA National Institute of Standards and Technology (NIST) and colloid silica (certified size) from the European Commission (JRC-IRMM).

The nanomaterials in the JRC Repository are representative test materials. For RTMs the following definition was proposed by Roebben et al. (2013):

*A **representative test material (RTM)** is a material from a single batch, which is sufficiently homogeneous and stable with respect to one or more specified properties, and which implicitly is assumed to be fit for its intended use in the development of test methods which target properties other than the properties for which homogeneity and stability have been demonstrated.*

An RTM is not a reference material for the tests for which it is intended to be used, because homogeneity and stability are not demonstrated for the corresponding measurand. However, an RTM is more valuable than an ordinary test material, since it has been checked for homogeneity and stability in terms of one or more specified properties. RTMs are extremely useful tools in intra- or interlaboratory development of methods for which reference materials are not (yet) available. Thus, the JRC's NM-series of representative test materials are complementary to (certified) Reference Materials as illustrated in Table 2.

Table 2. Essential characteristics of the concept 'representative test material' compared to the existing concepts of reference material and certified reference material.

	Representative Test Material	Reference Material	
		Not certified	Certified
Parent material	Representative for a class of materials to be investigated with the target method(s)		
Homogeneity / stability	Assumed for the measurands of interest, demonstrated for other measurands	Demonstrated for the measurands of interest	Demonstrated for the measurands of interest
Assigned property value	None	None, or indicative only.	Certified for the measurand of interest

The OECD WPMN uses the term “Representative Manufactured Nanomaterial” for the nanomaterials selected for testing, which are assumed to be representative for a large fraction of nanomaterials on the market. The nanomaterials in the NM-series are a (random) sample from one industrial production batch, produced within industrial specifications. The NM-series ensures that this particular sample has been homogenised, and is sub-sampled into vials under reproducible (GLP) conditions, and the stability of the sub-samples is monitored. Thus, to the extent feasible for industrial materials, all sub-samples from one material should be identical and differences in test results between laboratories for the same end-point should not be attributed to differences in the material tested.

2.2. The OECD WPMN and Testing the NM-Series

In 2006, international recognition of the need of a deeper understanding of nanomaterials, including relevant characterisation information as well as hazard profiles, led to the establishment of the WPMN under the Chemicals Committee of the OECD. The WPMN leads one of the most comprehensive nanomaterial research programmes "Safety Testing of a Set of Representative Manufactured Nanomaterials", established in 2007.

The WPMN agreed on a list of Representative Manufactured Nanomaterials to be tested and relevant end-points to test for exploratory purposes. The nanomaterials listed in the testing programme are (2014): fullerenes, single-wall and multi-wall carbon nanotubes, cerium dioxide, zinc oxide, iron, gold, silver, titanium dioxide, silicon dioxide, nanoclay and dendrimers. Some of these materials are hosted in the JRC Repository.

For MWCNT in the OECD testing programme, NM-400 was selected as the principal material, i.e. a full data set, as listed in Table 3, should be provided for this material; the other multi-walled carbon nanotubes, NM-401, NM-402 and NM-403 are alternate materials (that is sponsored nanomaterials that are tested on some, but not all endpoints) and data available on these materials was submitted to the OECD testing programme as well.

Data in the OECD testing programme regarding characterisation, toxicological and ecotoxicological effects are generated in Phase 1 to understand the hazard profiles of the nanomaterials. A Phase 2 is planned and will start by evaluating the data received in Phase 1, and especially the test guidelines applied to identify their applicability and necessary modifications (if any). Further testing may be considered if needed.

The endpoints addressed within Phase 1 are presented in Table 3. The Guidance Manual for the Testing of Manufactured Nanomaterials (OECD 2010) describes in detail the information expectations for each end-point and all end-points have to be addressed.

In addition to the listed endpoints in the Guidance Manual for Sponsors (GMS), the GMS advises (p. 25): *"To aid in assuring the identical nature of the sponsored MN, the material used in different tests should be obtained preferably in a single lot, and stored and manipulated in comparable, if not identical procedures."* and further *"Sponsors will identify the source of test nanomaterials, including all known aspects of material production, the manufacturer, facility location, lot number, and any other pertinent information as noted in Annex I "Nanomaterial Information/Identification"."* Thus, the GMS recommends ensuring that, as far as possible, the testing of all endpoints is performed with a nanomaterial from one batch, and the JRC Repository assists the WPMN in doing this.

Table 3. Endpoints agreed by the OECD WPMN for the Representative Manufactured Nanomaterials.

Nanomaterial Information / Identification		Environmental fate	
1	Nano material name	27	Dispersion stability in water
2	CAS number	28	Biotic degradability
3	Structural formula / molecular structure	29	Ready biodegradability
4	Composition of NM being tested (incl. degree of purity, known impurities or additives)	30	Simulation testing on ultimate degradation in surface water
5	Basic Morphology	31	Soil simulation testing
6	Description of surface chemistry (e.g. coating or modification)	32	Sediment simulation testing
7	Major commercial uses	33	Sewage treatment simulation testing
8	Known catalytic activity	34	Identification of degradation product(s)
9	Method of production (e.g. precipitation, gas phase)	35	Further testing of degradation product(s) as required
Physical-chemical Properties and Material Characterization		36	Abiotic degradability and fate
10	Agglomeration / aggregation	37	- Hydrolysis, for surface modified nanomaterials
11	Water solubility	38	Adsorption - desorption
12	Crystalline phase	39	Adsorption to soil or sediment
13	Dustiness	40	Bioaccumulation potential
14	Crystallite size	41	Bioaccumulation in sediment
15	Representative TEM picture(s)	Environmental toxicology	
16	Particle size distribution	42	Effects on pelagic species (short/ long term)
17	Specific surface area	43	Effects on sediment species (short/ long term)
18	Zeta potential (surface charge)	44	Effects on soil species (short/ long term)
19	Surface chemistry (where appropriate)	45	Effect on terrestrial species
20	Photo-catalytic activity	46	Effect on micro-organisms
21	Pour density (must be completed)	47	Other relevant information
22	Porosity	Mammalian toxicology	
23	Octanol-water partition coefficient, where relevant	48	Pharmacokinetics (ADME)
24	Redox potential	49	Acute Toxicity
25	Radical formation	50	Repeated dose toxicity
26	Other relevant information (where available)	IF AVAILABLE	
		51	Chronic toxicity
Material safety		52	Reproductive toxicity
57	Flammability	53	Developmental toxicity
58	Explosivity	54	Genetic toxicity
59	Incompatibility	55	Experience with human exposure
		56	Other relevant test data

The provision of the JRC NM-Series to the OECD WPMN test programme enables the development of the comprehensive data set on characterisation nanomaterial properties and toxicological and ecotoxicological behaviour, as described above. In June 2012 the OECD WPMN recommended the development of a risk assessment/safety evaluation methodology for nanomaterials, based on, among others, this data set.

2.3. Characterisation of the NM-series

For nanomaterials it is known that their hazardous properties can be affected by for example shape, size and surface area, because these parameters affect the transport properties of the particles (absorption, distribution, and excretion).

In addition, one of the issues raised consistently in the discussions under the OECD WPMN is the test item preparations and dispersion protocols for the nanomaterials. A “test item” is simply (the actual fraction of) the sample tested. This discussion is linked to the characterisation of the nanomaterials for which a number of relevant scenarios have been identified, and among these are:

Characterisation

- I. as received
- II. as dispersed
- III. during testing

These scenarios reflect that many of the nanomaterials tested are insoluble (in water and other media) or only slightly soluble nanoparticles, and their physico-chemical properties as well as their (eco)toxicological effects are closely linked also to their physical surroundings. Thus, to acquire an in-depth understanding of the nanomaterials, material characterisation should be performed for a number of the different stages of the nanomaterials' use cycle. Table 3, sections "nanomaterial information" and "physico-chemical properties", list the characterisation end-points. Most of these may be measured both for the dry material and in dispersion; however, obviously some belong to a specific preparation form for the measurement: dustiness is a dry measurement whereas the water/octanol partitioning coefficient can be measured only in solution. Additional issues could be relevant, e.g. if the physical state and preparation of the material tested is representative for production and use, taking into account the chain of actors and life cycle.

Below is described a number of issues to consider for the characterisation.

I. “as received” is the characterisation of the properties of a RTM as received, and typical preparations are dry or aqueous.

II and III. “as dispersed” and **"during testing"** are for the nanomaterials undergoing further sample preparation steps, which should be assessed with regard to influence on measurement results, such as particle size determinations for the different scenarios: dry material, in aqueous or physiological media.

In addition to the physico-chemical characterisation, data relating to (eco)toxicological effects are also requested in the OECD Test Programme. For this kind of testing, the test item

preparation needs to be carefully considered. The characterisation of matrix-dependent properties of the prepared test item is an important issue for nanomaterials. Results are dependent on the matrix composition and protocols used.

For the testing, RTMs can be better used and brought into a matrix under defined conditions and applying defined procedures, and availability of protocols also for the matrices should minimise sources of uncertainties and methodological errors. Thus, dispersion protocols have been developed for test item preparation for use in test systems for (eco)toxicological testing or environmental fate analysis, comprising conditioning and choice of matrix components. Hence, the prepared test item should fulfil the requirements of the test method under GLP conditions and be representative for the selected exposure route. Test items are prepared for environmental testing in the compartments soil, water, sediment, sewage treatment plants as well as for oral, dermal, (intravenous) and inhalation toxicity testing, in the form it is assumed to reach the biological entity in the test system.

Depending on the various protocols used, different results may be obtained for the same parameter measured. Also the effect of a particle's 'corona', the molecules surrounding it in a given medium, has been acknowledged (Cedervall et al., 2007), emphasising that the constituents of the corona depend on the medium. Biophysical characterisation, such as corona composition, kinetics/exchange rates, corona structure and depletion effects/changes in matrix kinetics are therefore required in support of understanding of test item properties.

The determination of a property should be addressed by the selection of the appropriate measurand and the corresponding measurement method. For nanomaterials, the "appropriate measurand" is not yet fully understood for all endpoints, and extensive discussion and guidance development take place in several international fora: the Scientific Committee on Emerging and Newly Identified Health Risks (SCENIHR 2010), the OECD WPMN, the Comité Européen de Normalisation Technical Committee 352 Nanotechnologies (CEN/TC 352), and the International Standardisation Organisation (ISO) under Technical Committee 229 Nanotechnologies (ISO/TC 229). In addition, for the measurements, an uncertainty estimate should be described based on the Guide for Uncertainty in Measurements.

3. Materials, Methods and End-points

The multi-walled carbon nanotubes NM-400, NM-401, NM-402 and NM-403 (all four together are the "MWCNT NMs") are available as black powders in amber coloured vials containing 250 mg or less under argon atmosphere. Each individual vial has a unique sample identification number.

This chapter gives an overview of institutions involved in the testing, the end-points tested and associated method(s), as well as the equipment used to characterise the MWCNT NMs.

The testing was performed by several European research institutes (alphabetical order):

CEA	Commissariat à l'énergie atomique et aux énergies alternatives, France
CODA-CERVA	Veterinary and Agrochemical Research Centre, Belgium
IMC-BAS	Institute of Mineralogy and Crystallography, Bulgaria
INRS	Institut National de Recherche et de Sécurité, France
LNE	Laboratoire National de métrologie et d'Essais
NRCWE	National Research Centre for the Working Environment, Denmark

The data was generated in the context of several European projects, for example the Joint Action NANOGENOTOX, which was co-financed by DG SANCO and participating of EU member states. NANOGENOTOX was co-ordinated by L'Agence nationale de sécurité sanitaire de l'alimentation, de l'environnement et du travail (ANSES), France.

Table 4 lists the physico-chemical characterisation end-points agreed by the OECD WPMN and gives an overview for each NM of the characterisation performed, methods used, and institution(s) involved. The test conditions and results are described in chapter 4 and onwards. As shown in Table 4, the following tests and measurements were performed: small-angle X-ray scattering (SAXS) and ultra small-angle X-ray scattering (USAXS). The particle size distribution was analysed from TEM micrographs and the specific surface area was measured by BET, and SAXS and USAXS. The elemental analyses were also performed by ICP-OES (inductive coupled plasma (ICP) with optical emission spectrometry), ICP-MS (inductive coupled plasma (ICP) with mass spectrometry), EDS (energy dispersive X-ray spectroscopy) and TGA (Thermogravimetric Analysis). The solubility was tested simultaneously with analysis of O₂ and pH reactivity in three media (Gambles solution, Caco2 medium and the NANOGENOTOX diluted BSA-water dispersion) using an SDR (Sensor Dish Reader) system for detection. The MWCNT were also analysed by RAMAN and XRD.

Table 4. MWCNT NMs: physico-chemical characterisation performed and institutions involved.

Physico-chemical Properties and Material Characterization (from OECD list)	NM characterised				Method	Institution(s)	Chapter
	400	401	402	403			
Agglomeration/ aggregation	x	x	x	x	TEM	CODA-CERVA, IMC-BAS	10
Water solubility *)	Endpoint not investigated						
Crystalline phase	x	x	x		XRD	IMC-BAS, NRCWE	9
	x	x	x		Raman	NRCWE	5
Dustiness	x	x	x	x	Vortex shaker method	INRS	9
Crystallite size	Endpoint not relevant						
Representative TEM picture(s)	x	x	x	x	TEM	CODA-CERVA	10
	x	x	x			IMC-BAS	
Particle size distribution	x	x	x	x	TEM	CODA-CERVA, IMC-BAS	10
	x	x	x				
Specific surface area (SSA)	x	x	x		BET	IMC-BAS	8
	x	x	x	x	SAXS/USAXS	CEA	7
Zeta potential (surface charge)	Endpoint not investigated						
Surface chemistry (where appropriate).	Endpoint not investigated						
Photo-catalytic activity	Endpoint not relevant						
Porosity	x	x	x		BET	IMC-BAS	8
Octanol-water partition coefficient, where relevant	Endpoint not relevant						
Loss in ignition	Endpoint not investigated						
Redox potential (by O ₂)	x	x	x		SDR	NRCWE	6
OH radical formation, acellular					SDR	NRCWE	6
	x	x	x				
Other relevant information (where available) Elemental analysis/impurities	x	x	x	x	Semi quantitative ICP-OES	CODA-CERVA	4.1
	x		x		Semi quantitative ICP-MS	LNE	4.1
	x	x	x	x	Quantitative ICP-MS	Duke University	4.1
	x	x	x		Semi quantitative EDS	IMC-BAS	4.1
Other relevant information (where available)	x	x	x	x	TGA	NRCWE	4.2
	x	x			DTA	IMC-BAS	4.2
Presence of catalysts	x		x		XRD	NRCWE	4.3
Solubility in Gambles solution Caco2 medium NANOGENOTOX batch dispersion medium	x	x	x	x		NRCWE	6
	x	x	x	x		NRCWE	6
	x	x	x	x		NRCWE	6

The institutes participating to the characterisation of the multi-walled carbon nanotubes used a number of different apparatus and equipment when performing the measurements. Table 5 gives an overview of equipment and conditions.

Table 5. Overview of apparatus used by the institutes for the testing.

Method	Institution	Apparatus and methodology and descriptive text
BET	IMC-BAS	High-speed surface area and pore size analyser NOVA 4200e (Quantachrome)
DTA	IMC-BAS	A STA781 and DTA 675 from Stanton Redcroft was used for the differential thermal analysis (DTA). The heating rate was 10 °C /Min.
EDS	IMC-BAS	Philips TEM420 at 120 kV acceleration voltage
ICP-MS	LNE	Quadripolar PQ Excell VG elemental ICP/MS
	Duke University	Agilent Technologies 7700 Series ICP-MS with an ASX-500 Series ICP-MS Autosampler (Agilent Technologies, Santa Clara, CA, USA)
ICP-OES	CODA-CERVA	Inductively coupled plasma-optical emission spectrometry using a Varian 720-ES, Agilent Technologies
Raman	NRCWE	Horiba Jobin-Yvon Labram HR Raman spectrometer, coupled to a Park Systems XE-100 AFM. Laser wavelength: 632.82 nm (helium-neon)
SAXS and USAXS	CEA/LIONS	<p>The main set up components used for SAXS and USAXS experiments are:</p> <ul style="list-style-type: none"> ▪ X-ray generator : Rigaku generator RUH3000 with copper rotating anode ($\lambda = 1.54 \text{ \AA}$), 3kW ▪ Home- made optic pathways and sample holders (with two channel-cut Ge (111) crystals in Bonse/Hart geometry for USAXS set up, cf Lambard (1992). ▪ Flux measurement for SAXS set up : pico amperemeter Keithley 615 ▪ Flux measurement for USAXS set up : DonPhysik ionization chamber ▪ Detector for SAXS set up : 2D image plate detector MAR300 ▪ Detector for USAXS set up: 1D high count rate CyberStar X200 associated to a scintillator/ photomultiplier detector. <p>All experimental parameters are monitored by computer by a centralized control-command system based on TANGO, and interfaced by Python programming. 2D images are treated using the software <i>ImageJ</i> supplemented with specific plug-ins developed at CEA/LIONS, see O. Taché, 2006.</p>
SDR	NRCWE	24-well Sensor Disc Reader (SDR) system [O ₂ and pH fluorescent sensors] from PreSens Precision Sensing GmbH, Germany
Sonication	CEA	Ultrasonic probe equipped with a standard 13 mm disruptor horn: Sonics & Materials, VCX500-220V, 500 W, 20 kHz
	CODA-CERVA	Vibracell™ 75041 ultrasonifier (750 W, 20 kHz, Fisher Bioblock Scientific, Aalst, Belgium). 13 mm horn (CV33)
	INRS	Ultrasonic probe equipped with a 14 mm Ti disruptor horn: Heilscher UP200H (200W)
	NRCWE	Ultrasonic probe equipped with a standard 13 mm disruptor horn: Branson Bransonic 400W
TEM	CODA-CERVA	Tecnai™ G2 Spirit microscope (FEI, Eindhoven, The Netherlands) with biotwin lens configuration operating at 120 kV
	IMC-BAS	Philips TEM420 at 120 kV acceleration voltage
TGA	NRCWE	A Mettler Toledo TGA/SDTA 851e was used with oxygen atmosphere. The heating rate was 10 K/min and the temperature range was from 25 °C to 1000 °C. The sample holders used for the TGA measurements were made of alumina and had a volume of 70 μL or 150 μL .
Vortex Shaker Method	INRS	Vortex dustiness test system modified and optimized at INRS. CPC: Model 3785 Water-based Condensation Particle Counter (TSI, USA)

Method	Institution	Apparatus and methodology and descriptive text
XRD	IMC-BAS	Bruker D2 Phaser diffractometer in reflection mode with theta-theta geometry. Cu X-rays were generated by a sealed Cu X-ray tube run at 30 kV and 10 mA and focused using a Ni filter and a fixed 0.2° divergence slit. Data generated with a step size of 0.02 degree 2theta and with a step time of 10 s and collected scintillation detector with opening angle 0.2°. Since the instrument does not use a monochromator, the raw data contains reflections from both K α 1 and K α 2 rays. For data comparison, the K α 2 contribution was therefore stripped from the data using the EVA software (Bruker).
	NRCWE	Bruker D8 Advanced diffractometer in reflection mode with Bragg-Brentano geometry. The analysis were made using CuK α 1 X-rays (1.5406 Å) generated using a sealed Cu X-ray tube run at 40 kV and 40 mA. The x-ray beam was filtered for CuK α 2 and focused using a primary beam Ge monochromator and fixed divergence slit 0.2°. The analyses were made in the stepping mode stepping 0.02 degree 2theta per second and data were collected using a linear Particle Size Distribution detector (Lynx-eye) with opening angle 3.3°.

The NANOGENOTOX sample preparation protocol was developed by NRCWE, CEA and INRS and the final dispersion protocol is published on the project's web page at

<http://www.nanogenotox.eu/files/PDF/web%20nanogenotox%20dispersion%20protocol.pdf>

Briefly, the final dispersion following the protocol has a concentration of 2.56 mg/mL and sterile-filtered 0.05 % w/v BSA-ultrapure water. The samples are sonicated (probe sonicator) for 16 minutes, placed in an ice bath, at 400 Watt and 10 % amplitude while controlling that the sonication probe does not touch the walls of the scintillation vial. Use of different sonication conditions (power and amplitude) may require different sonication times. The energy input was calibrated to be in the order of 3,136 MJ/m³.

4. Chemical composition

4.1. Elemental Composition by EDS, ICP-OES and ICP-MS

The elemental composition of any nanomaterial is an essential piece of information for its chemical categorisation; the observed toxicity of a nanomaterial may also be linked to the presence of for example coatings, catalysts and impurities. The elemental composition may be analysed using a range of different techniques. Depending on the technique used, the elemental analysis will range from qualitative to a fully quantitative analysis.

The composition of the MWCNT NMs was analysed using semi-quantitative energy dispersive X-ray spectroscopy (EDS or EDX) on powder tablets by IMC-BAS. Additional semi-quantitative and quantitative analyses were performed using inductive coupled plasma (ICP) with optical emission spectrometry (OES) for detection and determination on extracted elements. Supplementary characterisations were achieved by semi-quantitative and quantitative ICP with mass spectrometry (MS). Where EDS is suitable for major and minor elements, ICP techniques are generally most suitable for detecting and quantification of trace elements in the ppt to ppm levels. The applied techniques are described below.

Energy dispersive X-ray spectroscopy

EDS is short for Energy-dispersive X-ray spectroscopy and is available as an analytical tool in some electron microscopes.

In the present analysis, elements from Na and up were analysed using semi-quantitative analyses, which is an analysis based on factory-defined calibration curves with theoretical corrections for matrix effects, etc. Lighter elements from Be and up may also be quantified depending detectors and instrumental configuration. Oxygen was calculated by difference (assumed to be the residual un-quantified part of the sample). Therefore the sum of all elements adds up to 100 wt %. Due to current quality of detectors and instrument stability, semi-quantitative analyses are relatively reliable for major and minor elements if the samples have a sufficient thickness and as well as a low roughness.

Samples were prepared by pelletizing a known amount of powder, and the results are given in wt % and mass-based parts per million (ppm) depending on the absolute concentrations in the sample.

Table 6 lists the concentration of detected elements in the MWCNT NMs. The major impurities in NM-400 and NM-402 are Al and Fe. NM-401 was found to contain minor impurities dominated by Cu (0.2 wt %) and Zn (0.2 wt %). Similar Cu and Zn content were observed in NM-400, whereas only traces of Cu were found in NM-402.

Table 6. Elemental concentrations by EDS measurements on NM-400, NM-401 and NM-402 performed at IMC-BAS.

Material	C (wt %)	Al* (ppm)	Si* (ppm)	Fe* (ppm)	Co* (ppm)	Cu* (ppm)	Zn* (ppm)	O calculated[#] (wt %)
NM-400	89.81	46100	400	7600	2500	2000	1900	4.15
NM-401	99.19		500			2300	2200	0.6
NM-402	92.97	21100	500	29800		400		1.93

* ppm by weight [#] calculated by difference

Inductively coupled plasma-optical emission spectrometry

All ICP-OES measurements (inductively coupled plasma-optical emission spectrometry) were carried out by CODA-CERVA using a Varian 720-ES (Agilent Technologies). The analyses were performed using the SemiQuant feature, which is designed to provide a fast estimate of the concentration of non-calibrated compounds in samples. The MWCNT NMs were screened for 68 elements: Ag, Al, As, Au, B, Ba, Be, Bi, Ca, Cd, Ce, Co, Cr, Cu, Dy, Er, Eu, Fe, Ga, Gd, Ge, Hf, Hg, Ho, In, Ir, K, La, Li, Lu, Mg, Mn, Mo, Na, Nb, Nd, Ni, P, Pb, Pd, Pr, Pt, Rb, Re, Rh, Ru, S, Sb, Sc, Se, Si, Sm, Sn, Sr, Ta, Tb, Te, Th, Ti, Tl, Tm, U, V, W, Y, Yb, Zn and Zr.

Samples were prepared for analysis by calcinating the MWCNT NMs. For each NM, approximately 10 mg MWCNT was weighed into a platinum crucible. The crucibles were placed in a muffle furnace after which the temperature was progressively increased up to 650°C in 12 hours. This temperature was maintained for 6 hours. The mixture was heated overnight at 80°C in a DigiPREP MS (SCP SCIENCE). After cooling, the ashes were dissolved in 1 ml HNO₃. Next, a few ml double distilled water were added and heated until the boiling point was reached. Double distilled water was then added until 10 ml volume was reached. This solution was screened in semi-quantitative analysis.

Table 7 presents the major impurities found in the MWCNT NMs. The major impurities observed were Al and Fe. Ca was found in one vial of NM-403 but not in all the NM-403 vials analysed.

Table 7. Overview of impurities detected in the MWCNT NMs by semi-quantitative ICP-OES.

Material	Impurities > 0.01%	Impurities 0.005 – 0.01%	Impurities 0.001 – 0.005%
NM-400	Al, Fe, Na, S*	Co	Ca, K
NM-401	S*		Ag
NM-402	Al, Fe, S*	-	-
NM-403	Al, Co, Mg, Mn, Ca		

*Impurity content might be higher for sulphur

Then NM-400, NM-402 and NM-403 were analysed by quantitative ICP-OES for Al, Co and Fe, see Table 8.

Table 8. Overview of the aluminium (Al), iron (Fe) and cobalt (Co) concentrations in NM-400, NM-402 and NM-403 after calcination and analysis by ICP-OES.

Material	Al (mg/kg)	Fe (mg/kg)	Co (mg/kg)
NM-400	2540 ± 14	387 ± 25	161 ± 4
NM-402	2025 ± 35	1255 ± 78	n.d.
NM-403	431 ± 63	n.d.	40 ± 1

n.d.: not detected

Inductively coupled plasma-mass spectrometry

All ICP-MS measurements (inductively coupled plasma-mass spectrometry) were carried out by LNE and Duke University. LNE worked on identifying a suitable extraction procedure and an elemental screening. Duke University achieved a full multi elemental analysis.

LNE prepared the extraction on the basis of the work of Ge et al. (2008). The closed system for mineralization in microwave was achieved by varying sample mass and the mixture of acid for each material. The specific extraction conditions for the three MWCNT NMs are listed in Table 9 to Table 11 and the program of mineralisation used is given in table 12. Then LNE performed semiquantitative analysis on a quadripolar PQ Excell VG elemental ICP/MS in the standard condition.

Table 9. Extraction procedure for NM-400.

NM-400		
10 mg	10 mg	20 mg
9 mL HCl suprapur + 3 mL HNO ₃ suprapur	7 mL HNO ₃ suprapur + 3 mL H ₂ O ₂ suprapur	12 mL HNO ₃ suprapur + 1 mL H ₂ O ₂ suprapur
Intact particles	Mineralization Dissolution completed OK	Mineralization Dissolution completed OK

Table 10. Extraction procedure for NM-401.

NM-401			
5 mg	10 mg	5 mg	7 mg
9 mL HCl suprapur + 3 mL HNO ₃ suprapur	7 mL HNO ₃ suprapur + 1 mL H ₂ O ₂ suprapur	12 mL HNO ₃ suprapur + 1 mL H ₂ O ₂ suprapur	3 mL HNO ₃ suprapur + 3 mL H ₂ O ₂ suprapur
Intact particles	Intact particles	Intact particles	Mineralization Dissolution completed OK

Table 11. Extraction procedure for NM-402.

NM-402		
10 mg	10 mg	20 mg
9 mL HCl suprapur + 10 mL HNO ₃ suprapur	7 mL HNO ₃ suprapur + 1 mL H ₂ O ₂ suprapur	12 mL HNO ₃ suprapur + 1 mL H ₂ O ₂ suprapur
Intact particles	Mineralization Dissolution completed OK	Mineralization Dissolution completed OK

Table 12. Mineralization program used in the sample preparation procedure.

Duration	Energy input
10 min	250 W
5 min	0 W
10 min	500 W
5 min	0 W
10 min	650 W
5 min	0 W
10 min	850 W
5 min	0 W
Wait 5 min	

At Duke University, multi-element metal analysis of MWCNT NMs was performed on an Agilent Technologies 7700 Series ICP-MS with an ASX-500 Series ICP-MS Autosampler (Agilent Technologies, Santa Clara, CA, USA).

To overcome the challenges in chemical digestion of the carbon “skeleton”, MWCNT NMs were weighed into ceramic crucibles (approximately 20-30 mg) and calcinated (or combusted) for 12 hours at 750 °C. Once cooled, 375 µL concentrated HNO₃ and 75 µL concentrated HCl were added to the combusted MWCNT NMs (the ashes). Samples were transferred to 40 mL metal-free glass vials and heated for 1 hour at 100 °C on a heating block. Once ready for analysis, samples were transferred to 15 mL sterile, acid-washed polypropylene centrifuge tubes (VWR, Radnor, PA, USA) and diluted to 15 mL with deionized water for a final concentration of 2% HNO₃ and 0.5% HCl.

Table 13 lists the analytical results from the ICP-MS analysis of MWCNT from Duke University (D.U.) and LNE. NM-400, NM-402 and NM-403 were found to be the most impure MWCNTs (1 and 3 wt %). As observed by EDS, Al and Fe are the most important impurities. However, Mg, Mn and Co are also important elements in NM-403.

The ICP-MS results indicate that when performing toxicity testing, Mn and Ni should also be considered as important elements for (geno)toxicity testing.

Comparing the absolute results obtained by the two ICP-MS and the ICP-OES procedures, we find some inconsistencies. Higher concentrations of Al, Fe, and Co are generally found by the two ICP-MS analyses as compared to the quantitative ICP-OES analyses.

Table 13. Results from the ICP-MS analysis at Duke University (D.U.) and Laboratoire National de métrologie et d'essais (LNE) for specified elements.

Element identified (organisation)	NM-400 ppm	NM-401 ppm	NM-402 ppm	NM-403 ppm
Na (D. U.)	1345 ± 151	581 ± 32	727 ± 120	893 ± 443
Na (LNE)	600	-	-	NA
Mg (D. U.)	-	0 ± 3	-	2231 ± 144
Al (D. U.)	9951 ± 31	59 ± 4	12955 ± 1530	2024 ± 168
K (D. U.)	97 ± 3	57 ± 9	85 ± 7	88 ± 40
Ca (D. U.)	3 ± 2	2 ± 1	2 ± 1	2 ± 1
V (D. U.)	0	1 ± 0	1 ± 0	0
Cr (D. U.)	9 ± 1	3 ± 1	13 ± 1	3 ± 1
Cr (LNE)	14	-	10	NA
Mn (D. U.)	-	-	9 ± 1	2706 ± 182
Mn (LNE)	2	-	17	NA
Fe (D. U.)	1988 ± 26	379 ± 71	16321 ± 664	7 ± 4
Fe (LNE)	4300	NA	16000	NA
Co (D. U.)	693 ± 26	-	2 ± 0	2881 ± 190
Co (LNE)	3700	-	5	NA
Ni (D. U.)	4 ± 0	2 ± 0	9 ± 1	58 ± 4
Ni (LNE)	17	-	11	NA
Cu (D. U.)	3 ± 0	3 ± 3	4 ± 1	1 ± 0
Cu (LNE)	1	-	4	NA
Zn (D. U.)	2 ± 0	2 ± 1	2 ± 0	5 ± 1
Zn (LNE)	-	-	1	NA
As (D. U.)	-	-	-	-
As (LNE)	5	-	-	NA
Mo (D. U.)	-	-	-	-
Mo (LNE)	1	-	1	NA
Ag (D. U.)	-	-	-	-
Ag (LNE)	0.3	-	0.3	-
Sn (D. U.)	NA	NA	NA	NA
Sn (LNE)	0.5	-	0.5	NA
Ba (D. U.)	1 ± 0	1 ± 0	1 ± 0	1 ± 1
Ba (LNE)	0.3	-	0.3	NA
Pb (D. U.)	1 ± 0	-	-	-
Pb (LNE)	1.5	-	1.2	NA
La (LNE)	-	-	0.1	NA
Ce (LNE)	-	-	0.3	NA
wt % of all impurities, (D.U.)	1.41	0.11	3.01	1.09
(LNE)	0.87	-	1.6	NA

- : Not detected. NA: Not analysed or Not reported.

4.2. Presence of catalysts by TGA and DTA

Identification of the potential presence of organic coating was assessed by sample mass-loss during heating using thermogravimetric analysis (TGA) at NRCWE and differential thermal analysis (DTA) at IMC-BAS. In general, thermogravimetric analysis on carbon nanotubes is not straightforward due to non-homogenous material. However, the MWCNTs appear to produce reliable representative results with a test sample size between a few mg and up to more than 10 mg depending on the material.

In TGA measurements, a sample is heated in a gas (usually air, O₂ or N₂) and the weight of the sample is measured as a function of the temperature. The combustion pattern and temperature could indicate the MWCNT quality and presence of other combustible matter. The important three parameters in the weight loss curve are (i) the temperature at which decomposition starts, (ii) the oxidation temperature (point of maximum weight loss which is identified by the peak in the derivative of the weight loss as a function of temperature) and (iii) the residual mass. Decomposition in several steps shows a non-homogenous material containing various types of combustible compounds, which could be also due to different structural carbon nanotubes.

In DTA measurements, the reference and the sample undergo identical thermal cycles; they are either heated or cooled at the same rate. The temperature is measured for both sample and reference, and the difference is calculated. Most transformations such as melting, decomposition etc. are either endothermic or exothermic; that is they either require or release energy. Thus, when such a transformation takes place the temperature of the material will deviate from a reference, which is what is seen by DTA.

Figure 1 and Figure 2 display the results from thermogravimetric analyses of NM-400. The first derivative show more than one decomposition temperature for the two large samples tested, indicating more than one type of carbon material, i.e. NM-400 is not homogeneous. The results for the small sample indicate that it appears to contain only one type of carbon nanotube. Comparing the data, a sample size of at least 8 mg is required for the test sample to be representative.

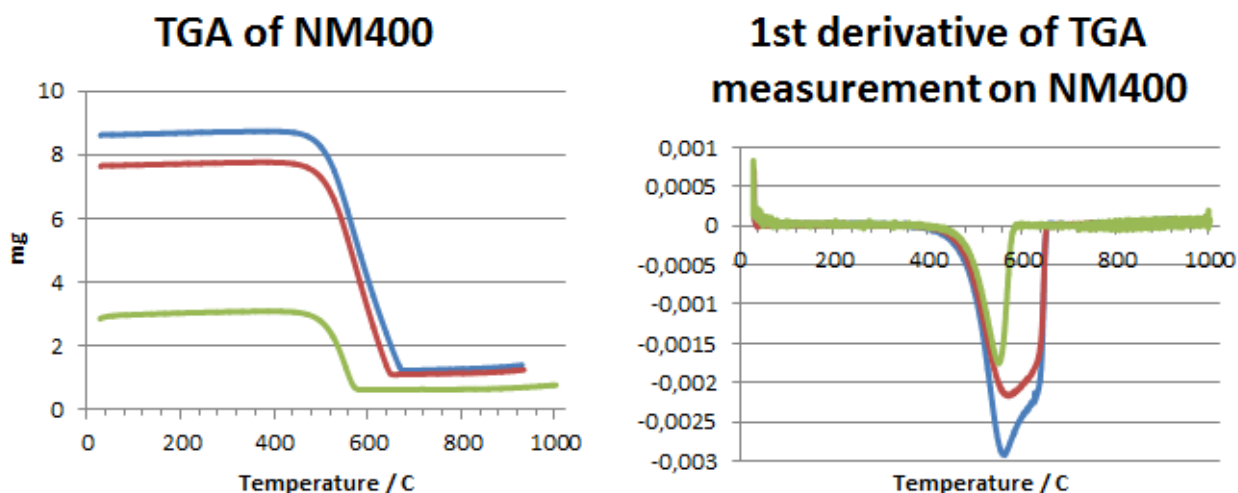


Figure 1. Results from TGA measurement on NM-400.

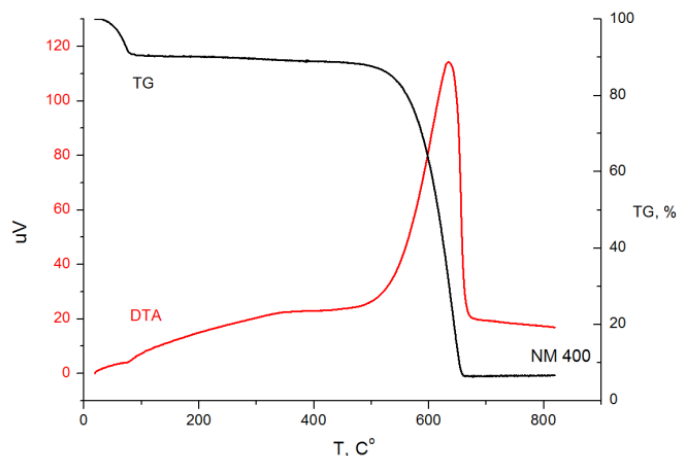


Figure 2. DTA results for NM-400 (red curve, unit (left) is μV [Thermocouple electromotive force]) and TG [thermogravimetric analysis] (black curve, remaining mass in percent (right)).

Figure 3 and Figure 4 show the results from thermogravimetric analyses of NM-401. The curves for the decomposition of different NM-401 masses appear highly repeatable, and the decomposition temperature is approximately the same for all runs. This would indicate a homogenous NM, however, after considering the large amount of residual (catalyst) in the material the material appears to be non-homogenous and at least 4 mg of NM-401 is needed to get a representative sample for the testing. Figure 4 shows the DTA results related to NM-401, indicating a strong exothermic reaction peaking at ca. 750 °C corresponding well to the TGA results.

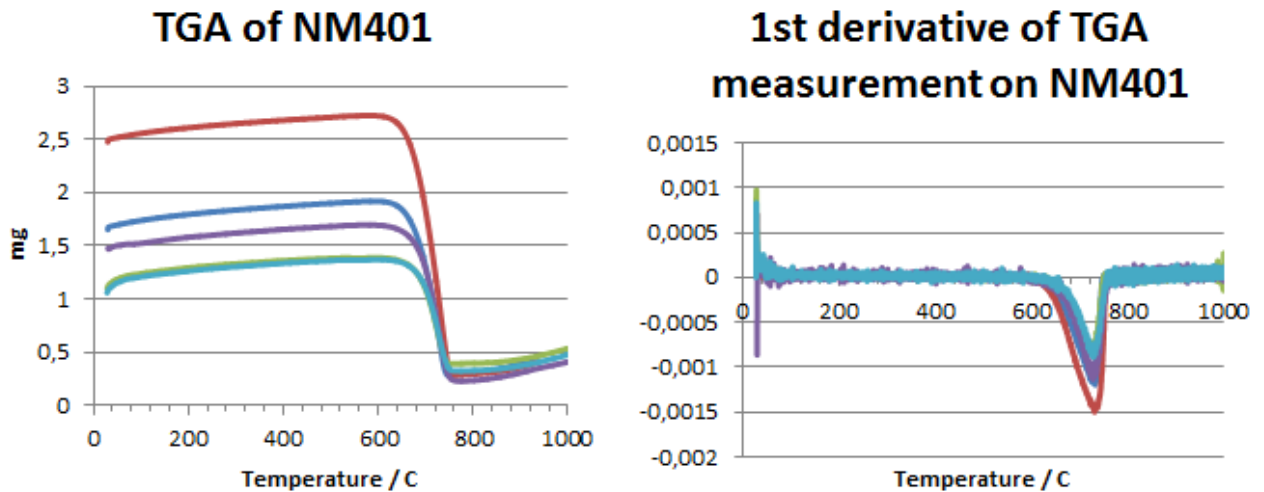


Figure 3. Results from TGA measurement on NM-401.

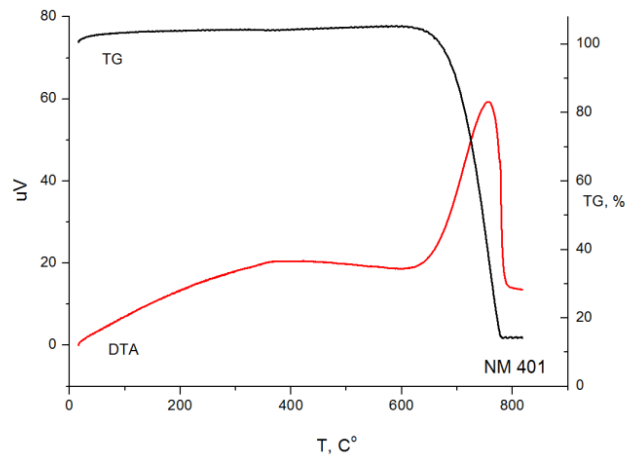


Figure 4. DTA results for NM-401 (red curve, unit (left) is μV [Thermocouple electromotive force]) and TG (black curve, remaining mass in percent (right)).

Figure 5 shows the results from thermogravimetric analyses of NM-402. These analyses indicate a non-homogenous material. The three curves are all different (the green one has one decomposition temperature, the red one has two and the blue one has several peaks). From these data, more than 13 mg is necessary to obtain a representative sample for the testing.

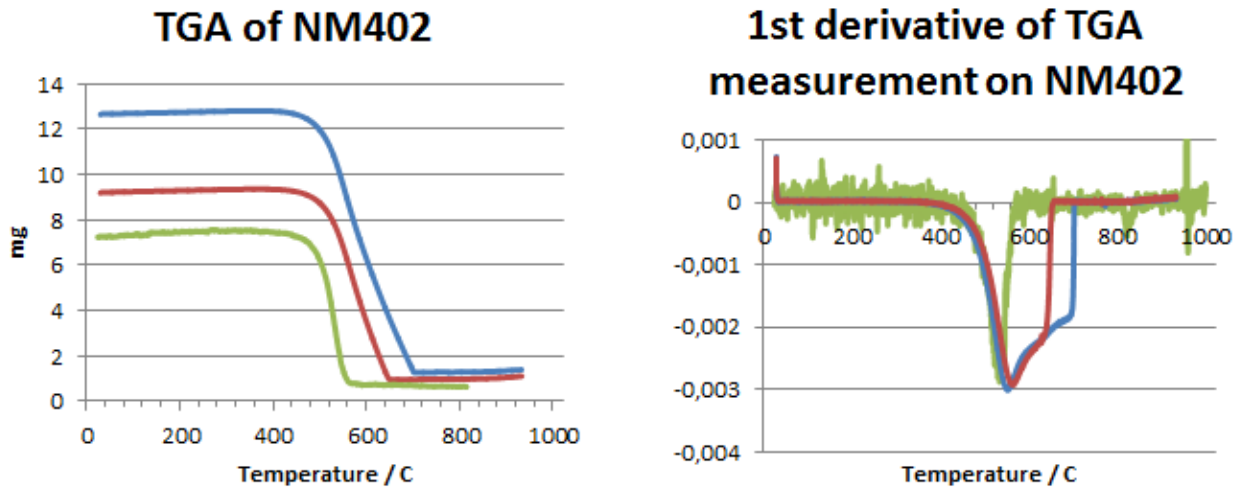


Figure 5. Results from TGA measurement on NM-402.

Figure 6 shows the results from thermogravimetric analyses of NM-403. These analyses indicate that NM-403 is a very uniform material, with a sharp peak for the first derivative of the weight loss as a function of temperature, i.e. the maximum weight loss appears almost instantaneously. The shape of the curves at approximately 400°C marked by an arrow shows a spontaneous combustion.

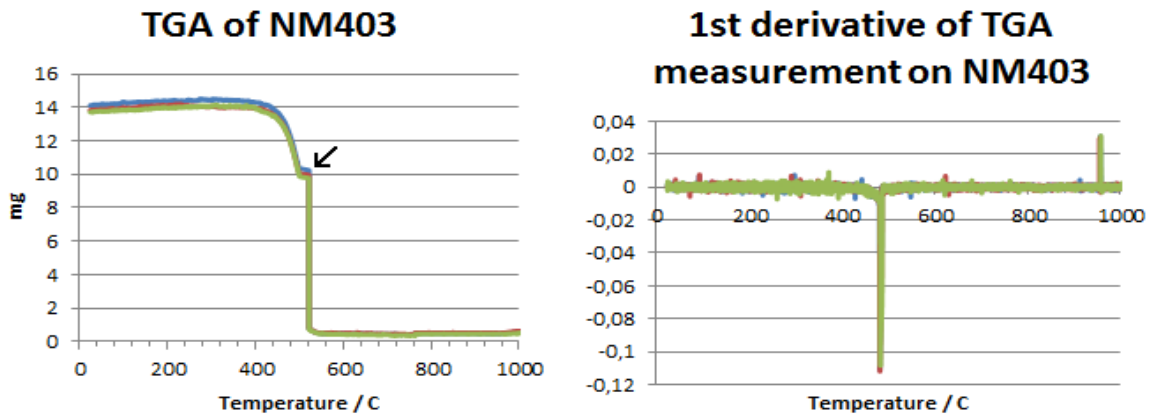


Figure 6. Results from TGA measurement on NM-403.

TGA measurements were completed several times for each MWCNT, and the results can thus be used for several purposes: The MWCNT NMs are not necessarily homogeneous, neither in carbon concentration and catalyst impurities, nor in the dimensions and qualities of the individual tubes. Inhomogeneity in carbon allotropes and tube characteristics will result in different combustion profiles. By several measurements, the amount of catalyst can be determined from a larger volume. By comparing the measurements, one can evaluate the homogeneity of the material and give an estimate of amount of material required to have a

“representative sample”. It must be noted that the catalyst present in the samples may have been oxidised during the material combustion: if this is the case, the weight of the oxygen should be subtracted from the sample weight measured.

The key results on purity of the MWCNT NMs are summarized in Table 14.

Table 14. TGA results on amount of impurities in the MWCNT NMs.

Material	Appear homogeneous	Weight catalyst (%)	Main decomposition temperature (°C)
NM-400	N	16.2 ± 2.9	563 ± 8
NM-401	N	18.1 ± 6.7	729 ± 2
NM-402	N	10.6 ± 0.4	555 ± 9
NM-403	Y	3.2 ± 0.3	482 ± 1

4.3. Presence of catalysts by XRD

Analysis of residuals after TGA measurements

XRD analyses were performed on NM-400 and NM-402 after thermogravimetric analysis. For NM-400, impurities were identified as $\gamma\text{-Al}_2\text{O}_3$, or a closely related structure (or phase). For NM-402, the crystalline material was hematite ($\alpha\text{Fe}_2\text{O}_3$). Figure 7 and Figure 8 show the XRD scans (for the residual after TGA analysis for NM-400 and NM-402, respectively).

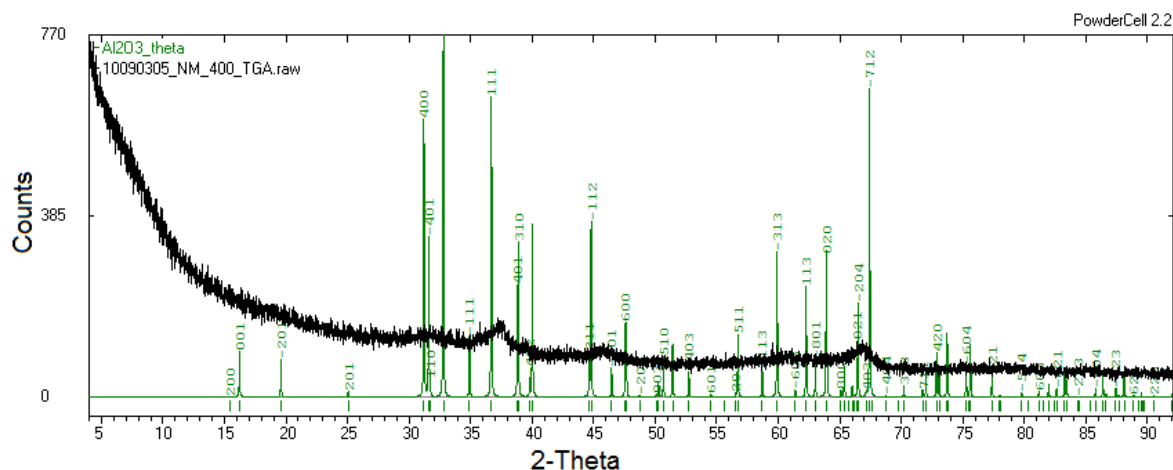


Figure 7. NRCWE diffraction data on the residual of NM-400 after heating to 1000 °C.

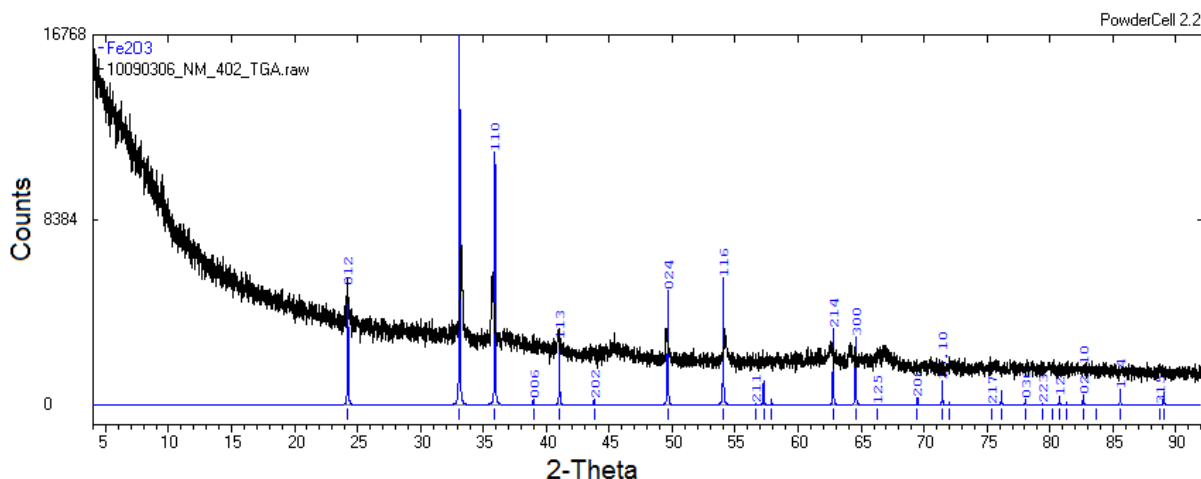


Figure 8. NRCWE diffraction data on the residual of NM-402 after heating to 1000 °C.

4.4. Chemical composition, observations and conclusions

As expected, all the analytical methods applied indicate that the main elemental component of the MWCNT NMs is carbon, and impurities are only a minor part. Depending on analytical technique, several additional elements and compounds were attributed to the different MWCNT NMs, see Table 15 that lists the impurities identified. The ICP-OES analysis, see also Table 7, identified a number of impurities above 0.01% for NM-400, NM-401, NM-402 and NM-403. Also the results from the ICP-MS, listed in Table 13, showed that Fe and Na were detected in all the MWCNT NMs. As EDS is the only analytical method that detected Cu and Zn, the signal from the EM grid/stub should be checked to understand if this contributed to the result, as Zn and Cu are typically found in such carriers.

Table 15. Elements (impurities) detected in the MWCNT NMs according to analytical method.

Material	EDS	ICP-OES	XRD	ICP-MS
NM-400	Al, Si, Fe, Co, Cu, Zn	Al, Fe, Na, S (above 0.01%)	Al	Al, Fe, Na, Co
NM-401	Si, Cu, Zn	S	N.A.	Fe, Na, Co
NM-402	Al, Si, Fe, Cu	Al, Co, Mg, Mn, Ca	Fe	Al, Fe, Na
NM-403	N.A.	-	N.A.	Al, Mg, Na, Mn, Co

N.A. not applied

The analyses of the MWCNT NMs showed clearly different elemental profiles of the different MWCNTs suggesting that they were produced using different catalysts. However, the results were relatively inconsistent both regarding which elements that were detected and their concentrations. The differences in elemental profiles is naturally partly caused by the different detection limits of the methods, where SEM EDS becomes questionable around 0.01 wt%, and ICP-MS and ICP-OES have detection limits in the ppm and ppt range,

respectively. However, presence of undetected elements and the very different concentration levels obtained for same elements are of concern.

First, large differences were observed between the EDS and ICP-OES data obtained in the screening analysis. By ICP-OES, relatively high impurity concentrations were only found in NM-400 and NM-402 and dominated by Al (>1 wt %). The relatively high Al concentrations in these two NMs are in agreement with the results from the EDS analyses. All other elements determined by ICP-OES were in concentrations lower than 0.01 wt %. This is in contrast to the EDS analyses of NM-400, NM-401 and NM-402, which indicated that Fe, Co, Cu, and Zn may also be present in concentrations higher than 0.01 wt %; it should be checked for Cu and Zn if the measurement refers to the grid/stub of the EM. Specifically, the Fe concentration was found to be 7600 and 29800 ppm in NM-400 and NM-402, respectively.

Table 16 lists the total elemental concentrations reported for each of the analyses and the total incombustible residual from the TGA analyses.

Table 16. Overview of the summed aluminium, iron and cobalt concentrations (wt %) in the MWCNT after total impurity and catalyst amount was quantified by the different listed analytical methods.

Method (laboratory)	NM-400 (wt %)	NM-401 (wt %)	NM-402 (wt %)	NM-403 (wt %)
EDS metals	6.05	0.5	5.18	
ICP MS metals (D.U.)	1.47	0.11	3.01	1.09
ICP MS metals (LNE)	0.87	-	1.6	
ICP OES metals (CODA- CERVA)	0.31	-	0.33	0.10
EDS metals incl. Oxygen	10.2	1.1	7.11	
TGA metals incl. Oxygen (NRCWE)	16.2	18.1	10.6	3.2

Comparing the results for some of the key catalyst impurities, it is evident that the ratios between the analyses vary depending on the procedures used. Lowest concentrations were obtained by the procedure used by CODA-CERVA followed by the procedures used by Duke University (D.U.) (ICP-MS), LNE (ICP-MS), and IMC-BAS (EDS). It is anticipated that the explanation for these more or less systematic differences is caused by the different digestion procedures used rather than instrumental settings and qualities. This is further supported by the fact that the highest concentrations were generally obtained by EDS, which is a non-destructive method. However, semi-quantitative EDS is still the methods associated with the largest analytical uncertainty and more precise measurements are required for final conclusions. Relating the elemental analyses of the MWCNT NMs with the results of the TGA-analysis further supports this hypothesis.

5. Raman spectroscopy

Raman spectroscopy yield information about the purity, defects and tube alignment, and assists in the distinction the presence of MWCNTs relative to other carbon allotropes. Hence Raman spectroscopy can be used to evaluate the quality of MWCNT and was completed on NM-400, NM-401 and NM-402. RAMAN is considered very useful for analysis of carbon materials as this is one of the few techniques that can give a qualitative measurement of a “large” sample. Each band in the Raman spectrum corresponds to a specific vibrational frequency of a chemical bond.

The Raman spectrum of sp³-hybridized carbon-carbon bond, the so-called D-band (for Defect or Diamond), shows a single sharp peak between ca. 1290 cm⁻¹ and 1360 cm⁻¹ depending on the tube and the frequency of the laser. Carbon atoms in hexagonal arrangement such as graphite, graphene, and MWCNT etc. with sp² hybridized bonds shifts the Raman peak to a higher frequency at 1582 cm⁻¹, the so-called G-band (for Graphite), which may consist of several modes and have two branches. The G' band, which is an overtone of the D band, is at about 2700 cm⁻¹. For MWCNT the intensity of the D-band increases compared to the G-band with increasing number walls in the MWCNT.

The results from the current analysis show that NM-401 had a spectroscopic profile with a high G-band intensity and low D-band (Figure 9). This suggests that the MWCNT in NM-401 has a more graphitic structure than NM-400 and NM-402 (Figure 9). Interestingly NM-401 was found to have the largest tube diameters and NM-400 and NM-402 the smallest tube diameters among the similar MWCNT characterized by TEM (Table 28). The influence of graphite particle impurities must also be considered in further analysis.

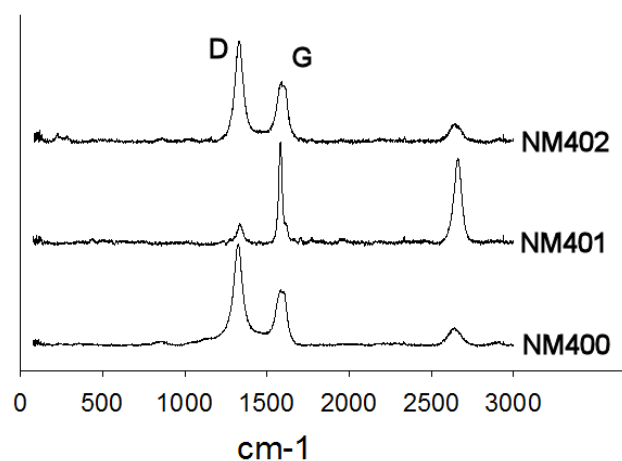


Figure 9. Results from Raman spectroscopy analysis of the MWCNTs. NM-401 with low D/G band ratios. NM-400 and NM-402 with high D/G band ratios.

6. Hydrochemical reactivity, solubility and biodurability

The 24-hour hydrochemical reactivity, solubility and inferred biodurability of the MWCNT NMs were investigated by NRCWE. The tests were completed in the NANOGENOTOX batch dispersion medium (sterile filtered 0.05 % w/v BSA water with 0.5% v/v ethanol pre-wetting) and two synthetic biological media relevant for assessing the NM behaviour in the lung-lining fluid (low-Ca Gambles solution) and intestinal system (Caco2 cell medium).

Data on the hydrochemical reactivity of NMs and their biodurability may be important to better understand the biochemical reactivity of nanoparticles and dissolution in contact with specific biofluids. When particles come in contact with biofluids, reactions may take place causing e.g. changes in pH, adsorption of ions or biomolecules, dissolution, and electron loss or gain, which can result in formation of reactive oxygen species (ROS), often considered as being one of the most important parameters of hydrochemical reactivity (e.g. Dick et al., 2003; Xia et al., 2006).

Biodurability is another classical test, originally established to analyse the degradation (dissolution) rate of asbestos, minerals and man-made fibres in synthetic lung-fluids (e.g. Forster and Tiesler, 1993; Christensen et al., 1994; Sebastian et al., 2002). Recently, the development of biodurability testing has gained new interest (Wiecinski et al., 2009; Xinyuan et al., 2010; Osmond-McCloud et al., 2011; Cho et al., 2011). Quantification of biodurability is usually done by weighing residual particles on a filter sample and/or measurement of specific constituent elements. However, representative retrieval of NMs from small volume dispersions may be associated with some difficulty.

In this analysis, we performed a batch dissolution test of the hydrochemical reactivity and solubility under external environmental control mimicking *in vitro* toxicological test conditions. For the experiments, we used a commercial 24-well pH and O₂ Sensor Dish Reader (SDR) system (PreSens GmbH; Germany). Dispersions were prepared as described in the generic NANOGENOTOX dispersion protocol to mimic the treatment used for toxicological studies presented here.

The SDR system enables simultaneous measurement in 24 wells down to one second resolution, and thus a variety of data can be established as function of dose and time. The test conditions using the SDR system are maintained by a cell-incubator and consequently directly corresponds to the conditions of a given *in vitro* exposure event (here 37°C and 5% CO₂ for lung conditions). One drawback is that the measurable pH-range is limited to pH 5 to 9. The range in O₂ concentrations is wide and varies from 0 to 250% O₂ saturation (0 to 707.6 µmol/l). Due to the principle link between electron activity and oxygen fugacity (e.g.

Nordstöm and Munoz, 1994), the variation in O₂ may correspond to values obtained by direct redox potential measurement.

As a final output from the SDR studies, the measured amount of soluble NM (concentrations of dissolved elements) after the 24-hour incubation in each of the three incubation media is reported. For this, liquid samples were carefully extracted, filtered and centrifuged to remove dispersed NM in the liquid sample. Quantification was done as a commercial service by ICP-OES (Si) and ICP-MS (Al) without further acid treatment other than stabilization. The concentrations of dissolved elements give indication on the durable fraction (total – the dissolved amount) in the three media. However, the values are still indicative as high-precision analysis was not performed on the starting materials.

6.1. Results, Hydrochemical pH reactivity

As explained in Appendix A, four concentrations and six dose response measurements are made in one test round. Figure 10 to Figure 12 show the temporal pH evolution in each of the tested NM incubations considering the highest dose experiments compared to the reference (zero-dose). The results show that most of the NMs have negligible to minor influence on the pH-evolution in the three test media. If there is a pH reaction, it normally occurs within the first few hours. It is particularly noteworthy that pH-evolution paths are mostly controlled by the different test media.

The pH in the 0.05% BSA water batch dispersion medium typically increases from near or below the pH 5 lower detection limit to between pH 5 and 6 within the first hour. Addition of nanomaterial to the BSA water appears generally to cause a small elevation in the pH as compared to the reference medium. The Gambles solution medium has slightly basic pH values, typically starting between pH 7 and 9. The protocol should ensure that pH adjustment in this type of static experiment without online pH control at least makes proper pH adjustment in the initial step of the test. By deviation from protocol, this was not done in these tests. The Caco2 cell medium normally has an initial pH around 7 to 8.

MWCNT should be inactive towards pH as such, but the presence of several catalyst and processing impurities such as chlorides and sulphates could affect pH as well as reaction with catalyst particles. However, only non-systematic potential effects were observed as pH increases over a certain time-interval in e.g. NM-400 and NM-401 in BSA water and Caco2 medium, NM-402 in BSA-water and Gambles solution.

As a general conclusion, it is found that the selected incubation medium and the incubator atmosphere are the primary controllers of the temporal pH evolution for the nanomaterials. Noting that the MWCNT NMs had a not unimportant content of catalysts, interpretation of the

results should be done cautiously, as the catalysts, not the carbon, could be the component causing observed changes.

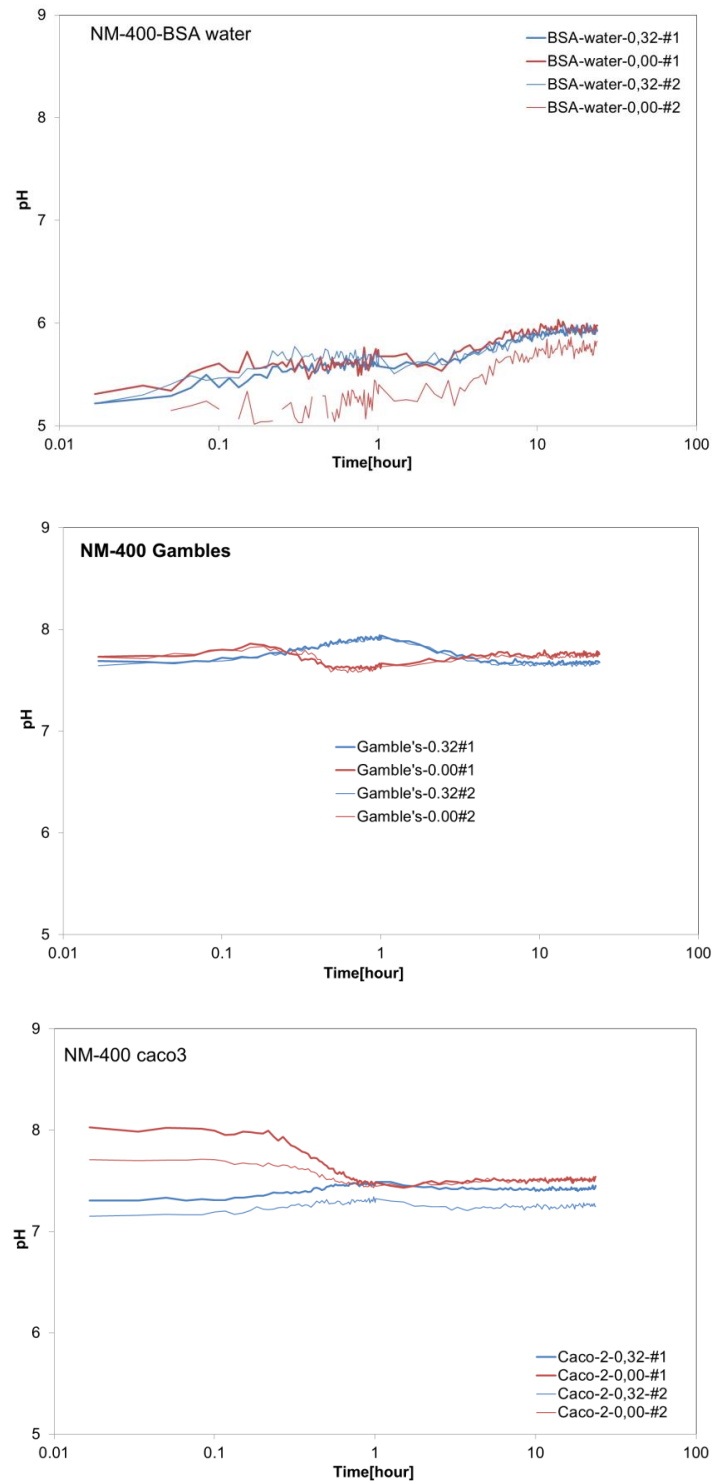


Figure 10. pH-evolution during 24-hour incubation of NM-400 in 0.05% BSA water NANOGENOTOX batch dispersion (top); Gambles solution (centre); and Caco2 cell medium (bottom). The particle concentrations in the Gambles solution and Caco2 cell medium were dosed from the batch dispersion tested in (top).

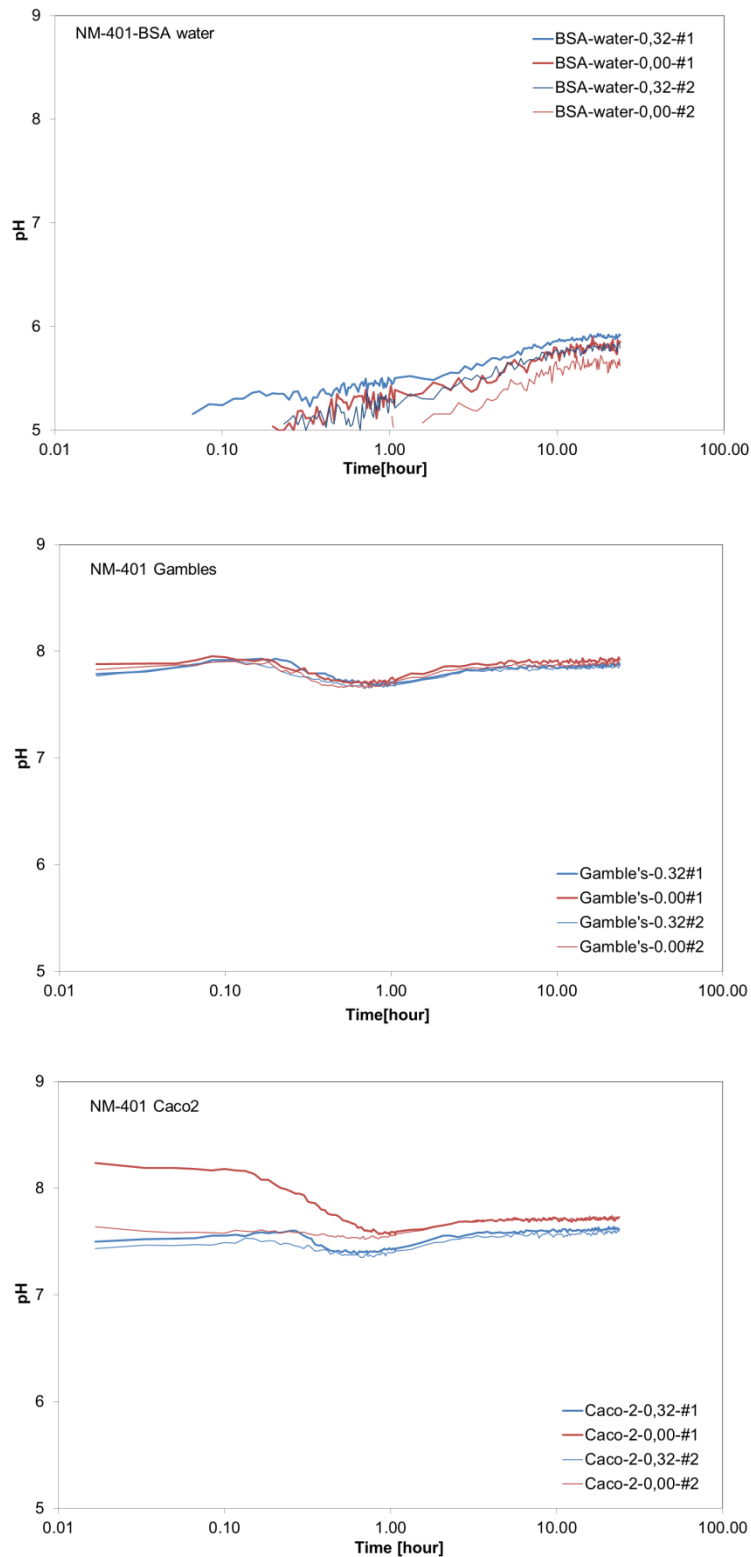


Figure 11. pH-evolution during 24-hour incubation of NM-401 in 0.05% BSA water NANOGENOTOX batch dispersion (top); Gambles solution (centre); and Caco2 cell medium (bottom). The particle concentrations in the Gambles solution and Caco2 cell medium were dosed from the batch dispersion tested in (top).

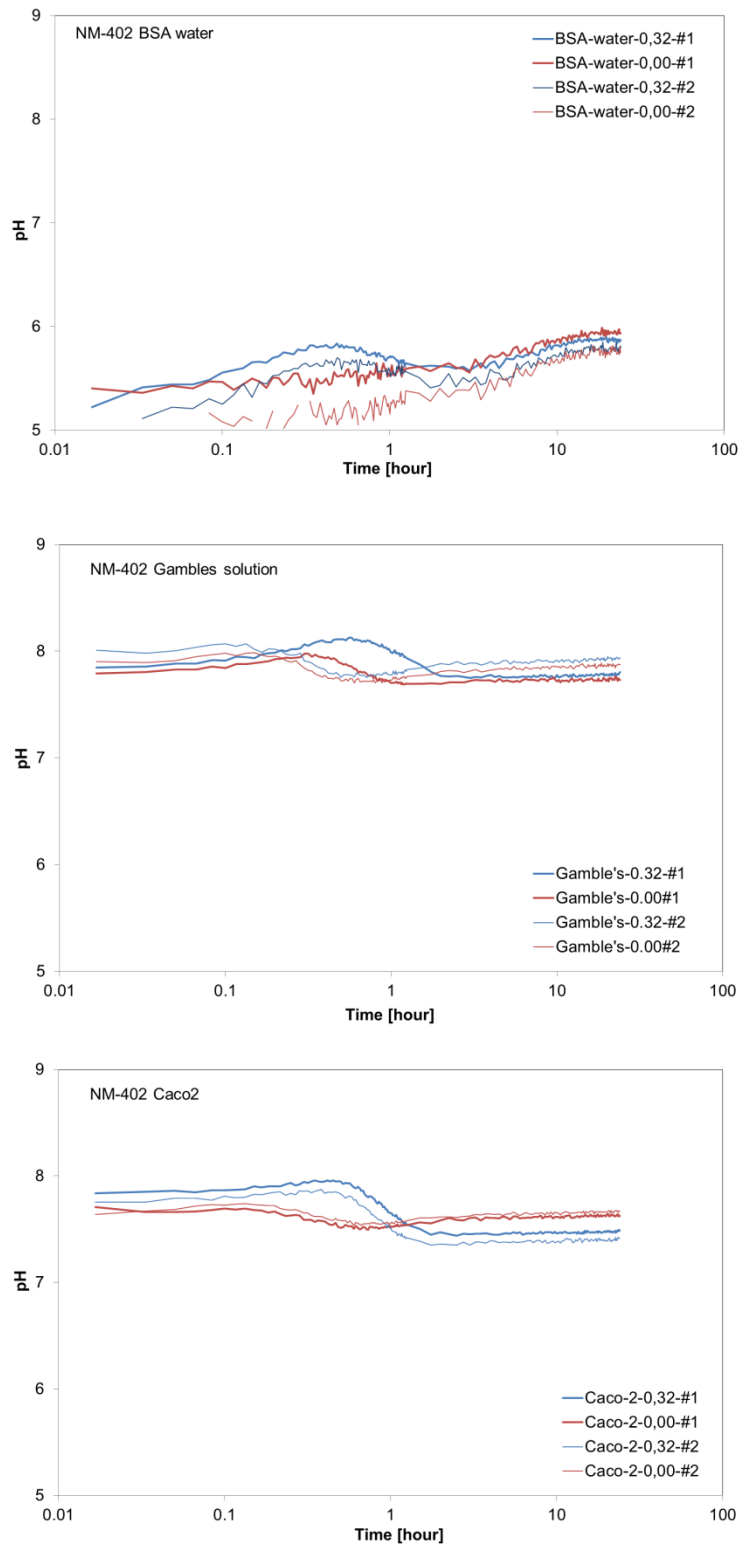


Figure 12. pH-evolution during 24-hour incubation of NM-402 in 0.05% BSA water NANOGENOTOX batch dispersion (top); Gambles solution (centre); and Caco2 cell medium (bottom). The particle concentrations in the Gambles solution and Caco2 cell medium were dosed from the batch dispersion tested in (top).

6.2. Hydrochemical O₂ Activity

The hydrochemical O₂ activity is also measured using the SDR system, see Appendix A, for information on these analyses. The temporal evolution of O₂ was expressed as $dO_2 = O_{2, \text{dose}} - O_{2, \text{medium control}}$, where $O_{2, \text{medium control}}$ is the O₂ from the control, which is medium without any NM added, and $O_{2, \text{dose}}$ is the O₂ from the dispersed sample at a given dose. Figures 13 to 15 show the temporal variation in dO_2 (average of two experiments) and show that the MWCNT NMs have a wide range of reactivity. Interestingly, the reactivity may not be exerted to similar degrees in the different media.

In BSA water batch dispersions, only NM-402 was able to induce significant increase of the oxygen level. NM-400 and NM-401 had minor to negligible effects on O₂.

NM-400 and NM-402 caused increased dO_2 in Gambles solution and Caco2 medium, whereas NM-401 only caused dO_2 increase in Gambles solution.

For all MWCNT NMs, the maximum dO_2 change is in the order of 40 μmol/ml. Considering the applied doses, this suggests that the particle reactivity easily can exceed 1 μmol O₂/mg.

This type of analysis is still in development and a clear data interpretation is not possible at this point in time. It is, however, evident that the MWCNT NMs (including impurities) do react and have influence on the O₂ concentrations in Gambles solution and currently, the interpretation of the dO_2 variations is that all these MWCNT NMs are redox-active in Gambles solution and two of them are reactive in Caco2 medium. This activity may be due to direct electron transfer processes or caused by changes in the O₂ concentration due to dissolution-related reactions of the impurities.

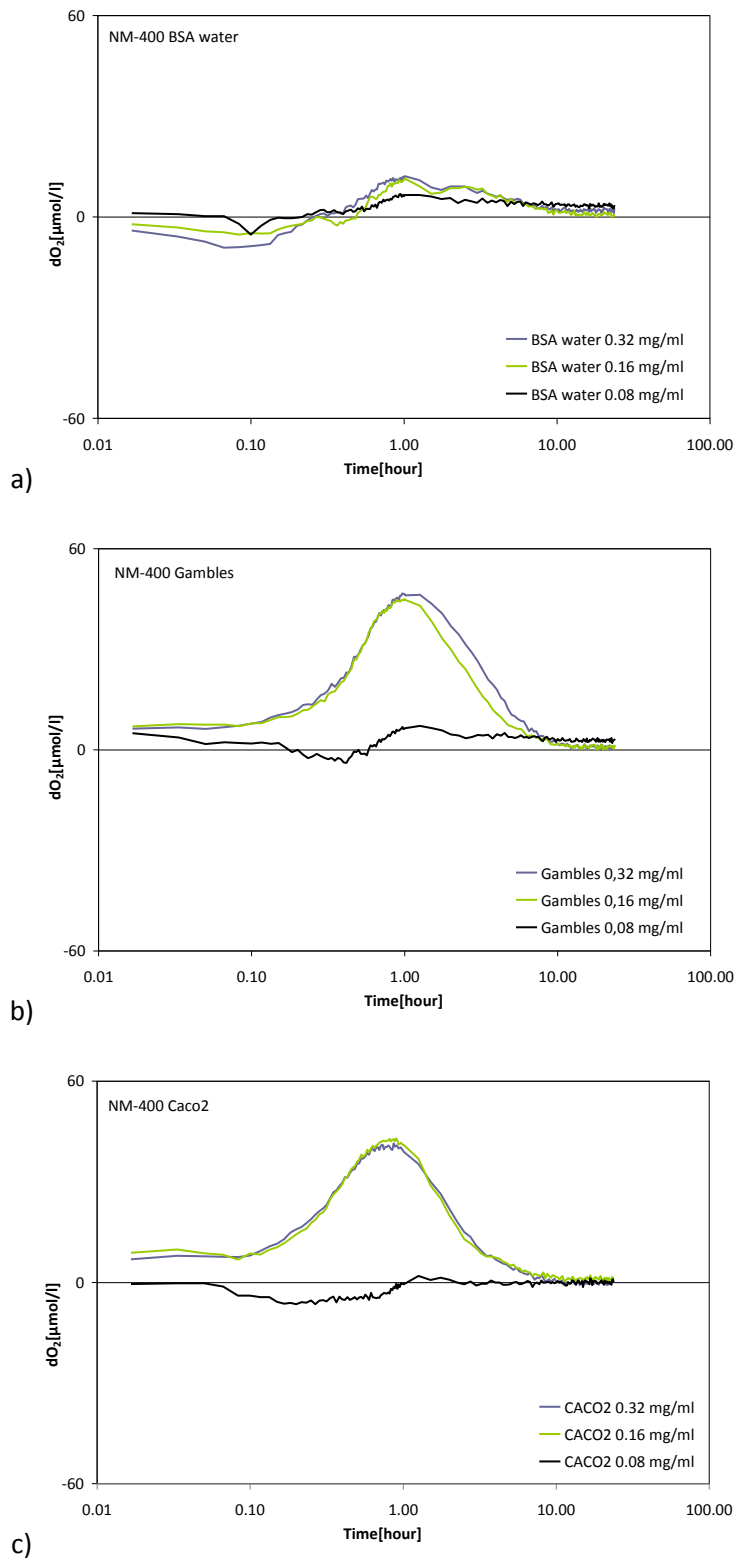


Figure 13. O_2 -evolution during 24-hour incubation of NM-400 in a) 0.05% BSA water NANOGENOTOX batch dispersion; b) Gambles solution; and c) Caco2 cell medium. The particle concentrations in the Gambles solution and Caco2 cell medium were dosed from the batch dispersion tested in a).

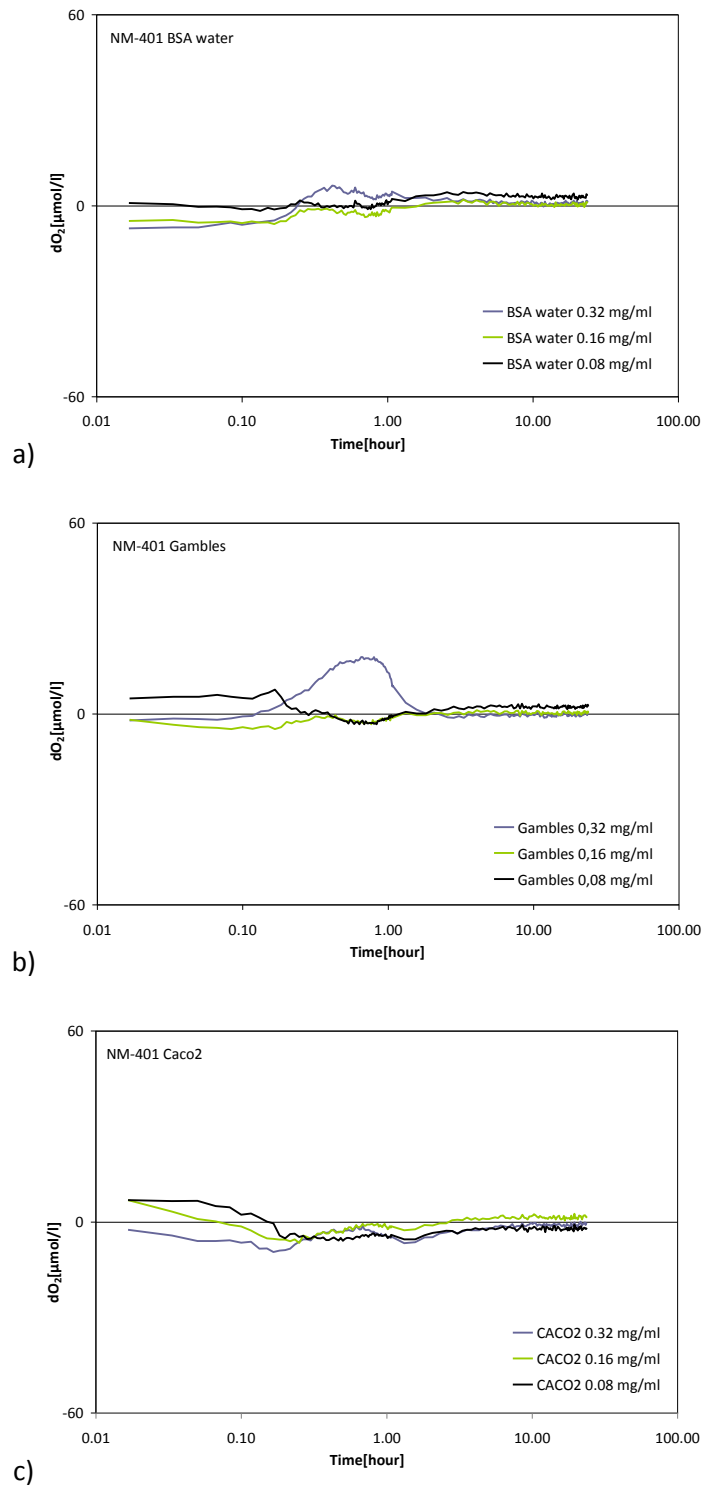


Figure 14. O_2 -evolution during 24-hour incubation of NM-401 in a) 0.05% BSA water NANOGENOTOX batch dispersion; b) Gambles solution; and c) Caco2 cell medium. The particle concentrations in the Gambles solution and Caco2 cell medium were dosed from the batch dispersion tested in a).

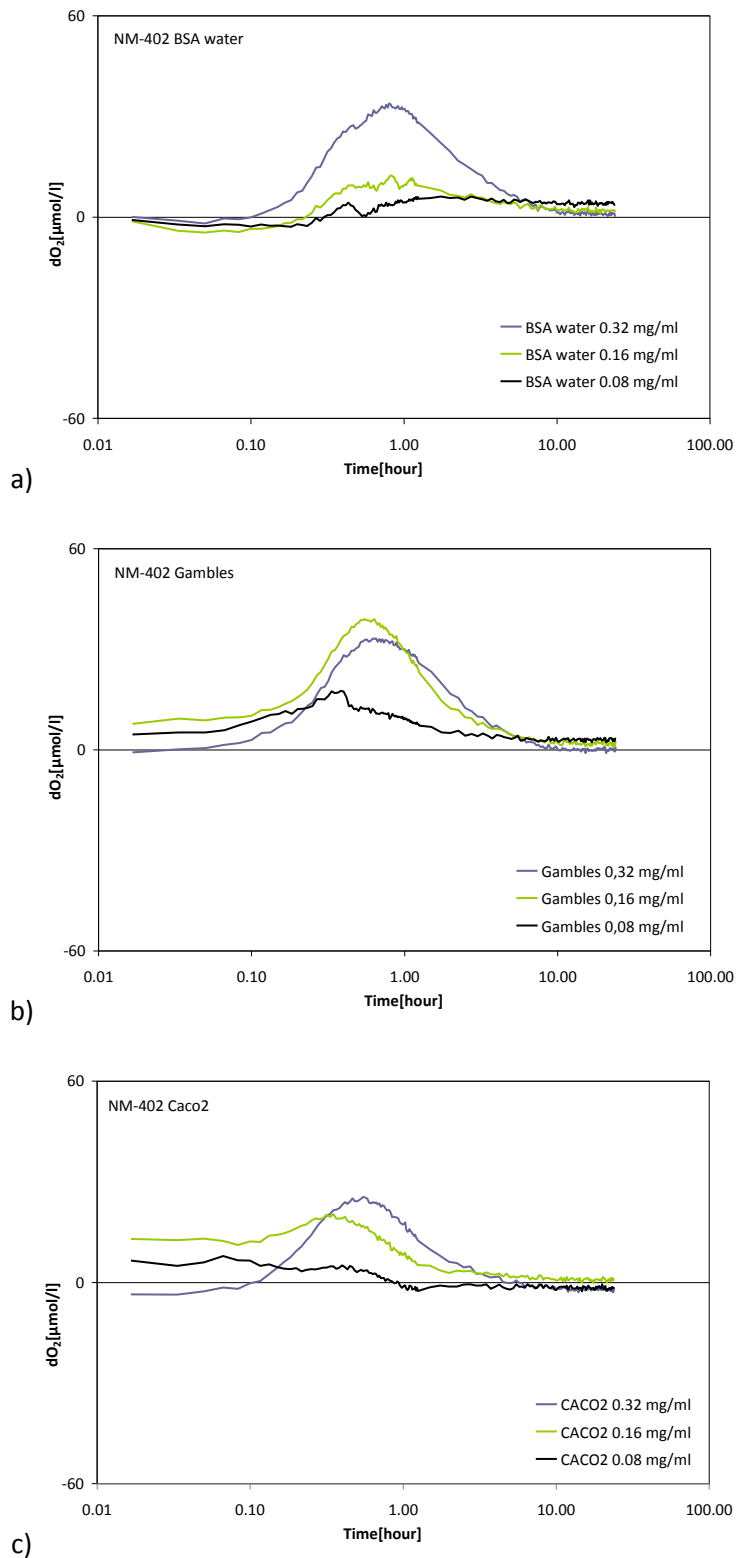


Figure 15. O_2 -evolution during 24-hour incubation of NM-402 in a) 0.05% BSA water NANOGENOTOX batch dispersion; b) Gambles solution; and c) Caco2 cell medium. The particle concentrations in the Gambles solution and Caco2 cell medium were dosed from the batch dispersion tested in a).

6.3. *In vitro* dissolution and solubility

The *in vitro* dissolution and solubility were investigated by analysing the three media without any MWCNT, giving the media background. Then known amounts of the MWCNTs were added for 24 hours to the three media, the background subtracted and the resulting concentrations are the 24 h solubility of the impurities (Table 19).

Table 17 presents the elemental analyses of the carefully centrifuged and filtered particle-free three media, the BSA batch solution, Gambles solution and the Caco2 medium, which show that the three media give only minor background concentrations of Ti, Si, Al, Fe, Co, and Ni, which were the key target elements for assessing the 24-hour NM dissolution ratios.

Table 17. Elemental concentrations in the investigated incubation media (n=2).

MDL [€]	Element	unit	BSA	σ	Gambles	σ	Caco2	σ
1	K	mg/l	<	<	<	<	160	<
1	Si		<	<	<	<	<	
0.05	Fe		<	<	<	<	0.31	0.36
30	Al	$\mu\text{g/l}$	<	<	<	<	<	<
5	Ti		7.6	1.0	10.2	1.4	11.5	1.3
1	Cr		0.9	0.7	1.3	0.4	1.8	0.6
5	Co		<	<	<	<	<	<
1	Ni		1.8	0.8	1.97	0.33	2.4	1.5
5	Zn		22.3	11.5	11.0	3.8	88	7

[€] MDL = Minimum detection limit; < = not detected or below MDL. Measurements were performed twice, i.e. n=2

Table 18 lists the elemental concentrations used for the assessment of the MWCNT NMs' solubility and biodurability. As mentioned in Chapter 4, the quantitative ICP data made on the MWCNT MN are uncertain due to apparent incomplete extraction efficiencies. Therefore, the assessment of 24-hour solubility limits and biodurable fraction must be considered approximate.

Table 18. Elemental concentrations ($\mu\text{g/g}$) in the MWCNT NMs used for assessment of dissolved fraction and particle biodurability, as measured by ICP-MS, Duke University (Table 13), which provided a complete dataset for the impurities and the NMs.

Material	Al	Fe	Co	Ni
NM-400	9 951 \pm 31	1 988 \pm 26	693 \pm 26	4
NM-401	59 \pm 4	379 \pm 71		2
NM-402	12 955 \pm 1530	16 321 \pm 664	2	9 \pm 1
NM-403	2 024 \pm 168	7 \pm 4	2 881 \pm 190	58 \pm 4

Table 19 lists the elemental compositions in the three incubation media corrected for the background concentrations in the incubation media. It is clear that most elements are present in relatively low concentrations. However, for proper assessment of the amount of dissolved matter, the calculation must be made using the applied elemental dose in the experiments. For this analysis, 0.32 mg/ml NMs powder was dosed into each incubation medium.

Table 19. Background-corrected elemental concentration in the test mediums after 24-hour dissolution tests with MWCNT NM (n=2).

MDL	Unit		NM-400	σ	NM-401	σ	NM-402	σ	NM-403	σ
0.05% BSA										
0.05	mg/l	Fe	0.23	0.05	-	-	-	-	7.4	0.2
30	$\mu\text{g/l}$	Al	50	11	-	-	-	-	22	31
5	$\mu\text{g/l}$	Co	32	4	-	-	-	-	448	40
1	$\mu\text{g/l}$	Ni	3.8	2.1	<	1.1	<	1.1	8.4	1.4
Gambles solution										
1	mg/l	Fe	0.09	0.03	-	-	0.08	-	-	-
30	$\mu\text{g/l}$	Al	322	20	-	-	196	-	322	-
5	$\mu\text{g/l}$	Co	36	1	-	-	553	10	-	-
1	$\mu\text{g/l}$	Ni	6.3	7.0	0.3	0.6	<	0.5	10.6	0.5
Caco2										
1	mg/l	Fe	<	0.51	-	-	<	0.5	<	0.5
30	$\mu\text{g/l}$	Al	-	-	-	-	-	-	22	31
5	$\mu\text{g/l}$	Co	30.1	1.0	-	-	-	-	455	10
1	$\mu\text{g/l}$	Ni	2.7	4.3	<	2.2	<	2.2	8	2.3

MDL: Minimum detection limit in the raw analysis; - denotes not detected; < denotes background corrected concentration lower than 0.1 x MDL. Measurements were performed twice, i.e. n=2

The elemental dose concentration was determined by simple multiplication of element concentration (Table 17) in $\mu\text{g/mg}$ with the applied dose 0.32 mg sample/ml medium. These concentration data were used to calculate the weight percent of dissolved element using the background-corrected elemental concentrations in the three incubation media after 24-hour incubation (Table 19). The results from these calculations are shown in Figure 16.

In the dissolution experiments with MWCNT, the actual degradation of MWCNT cannot be assessed from pure elemental analyses. It is assumed that the tubular and graphite carbon material in the MWCNT NMs are non-degradable at the applied test conditions. However, the catalyst and impurity materials identified by elemental analysis and electron microscopy (see chapters 4 and 10) may behave differently. In this study, Al, Co, Fe and Ni were used as indicators for the catalyst dissolution. Following similar calculations as above, Figure 16 shows the dose concentrations and the percent dissolved element in the three incubation media. It is evident that Al and/or Fe are the major impurities in the MWCNT NMs. The

measured concentrations of Al and Fe do reach percent levels in NM-400 (1.0 wt % Al; 0.2 wt % Fe) and NM-402 (1.3 wt % Al; 1.6 wt % Fe).

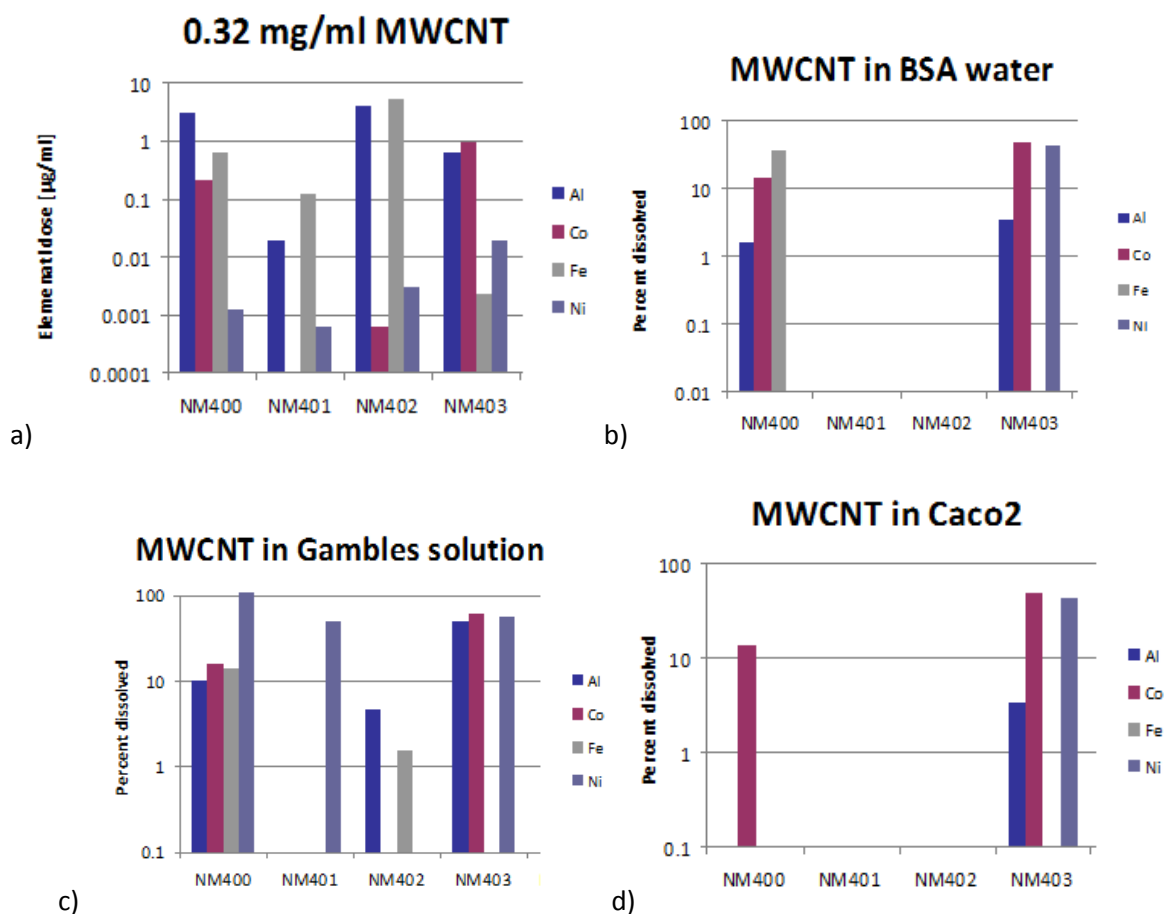


Figure 16. a) Elemental dose for most abundant elements in the MWCNT NMs. Weight percent dissolved element in b) BSA water; c) Gambles solution; and d) Caco2 cell medium.

Due to the relatively low measured elemental concentrations in the MWCNT NMs, the most reliable data are to be expected for Al and Fe in NM-400 and NM-402, Al and Co in NM-403. The concentrations of the four selected elements may be too low in NM-401 (≤ 0.06 wt %) for reliable assessment even by ICP-OES (Table 18, Figure 16). However, the data are still included as an indication, because some of the elements were sometimes detected in the test medium after the 24-hour dissolution test.

As seen from Figure 16, the results from the analyses suggest slightly different behaviour of the catalyst materials in the three different incubation media. For NM-401 and NM-402, no dissolution was detected in BSA water and Caco2 cell medium (Figure 16b and d). Some degree of dissolution was observed for all other material and medium combinations

For very low concentration elements in the MWCNT, higher percentages of dissolution were often found. For example, about half of the was found to be dissolved in the test of NM-401 (Figure 16c). Sometimes, the calculated dissolved Ni fraction even exceeded 100% (NM-

400) which may be due to sensitivity of very low concentration levels, inhomogeneity and potentially insufficient extraction of the metals in the analysis of the powder materials. The fraction of dissolved Co was also relatively high in all test media (14 to 60 wt %). For these two elements, the observed high dissolved fractions may be due to MWCNT elemental concentrations too low for quantification, material inhomogeneity, or too low yield in the elemental analyses on the powders. The materials are indeed known to be inhomogeneous and low elemental quantification yield of the MWCNT has also been indicated (as indicated in Chapter 12). Therefore, the dissolution data on especially the low concentration impurities in the MWCNT should only be considered indicative.

6.4. Estimation of biodurability

The results from the 24-hour reactivity and dissolution tests can give some indication on the biodurability of the nanomaterials. MWCNT contained several different impurity elements due to Al and different transition metal catalyst particles.

It is assumed that the carbon structure is not degradable in the three incubation media and the given test conditions. However, the associated catalyst impurities appear to dissolve, at least partially, during the 24-hour reactivity and dissolution test. For the elements with relatively high abundance, the dissolved fraction did not exceed 50 wt %. For Al (good tracer for NM-400; NM-402; and NM-403), up to ca. 3 wt % was observed to dissolve in BSA water, 5 to 50 wt % were dissolved in Gambles solution and up to ca. 3 wt % were dissolved in Caco2 medium. For Fe (good tracer for NM-400 and NM-402), 0 to 36 wt % was dissolved in BSA-water and ca. 2 to 14 wt % was dissolved in Gambles solution, whereas in Caco2 cell medium no dissolved fraction was measurable. For Co (good tracer for NM-403) 49 wt % was dissolved in BSA-water, 60 wt % was dissolved in Gambles solution, and 50 wt % was dissolved in Caco2 cell medium. Consequently, the biodurability of the catalysts appears to be high to moderate and, remembering that these analyses are made on minor and trace elements, appear to vary considerably between materials and media. This suggests that the speciation of the individual impurity elements may not be the same across all materials.

6.5. Conclusions

Under *in vitro* test conditions, pH reactivity tests revealed negligible to moderate effects on pH of the tested NMs in 0.05 % w/v BSA-water, Gambles solution, and Caco2 cell medium. However, relatively large variations could occur during the course of the experiment, which are tentatively assumed to be due to small fluctuations in CO₂ concentrations delivered from external pressure tanks.

O₂ reactivity tests showed some material and medium-dependent effects on dO₂ (difference between O₂ concentration in dosed and reference vials). NMs generally caused increased dO₂ values. Yet, NM-402 was the only material to notably increase dO₂ values in BSA-water.

The NMs dissolution and biodurability revealed material-dependent behaviour, partially linked to presence of associated impurity phases in MWCNT. The carbon materials in MWCNT are assumed to be highly durable in the selected incubation media and test conditions. However, the associated metal impurities and catalysts have moderate to high levels of dissolution, which is important to include in the evaluation of any toxicity studies as the impurities may influence the outcome of such studies. For NM-401 and NM-402 (relative high concentrations of Fe and Al + Fe, respectively), no dissolution was observed in BSA-water and Caco2 cell medium. In MWCNT NMs containing Co, 13-16 wt % (NM-401) to 43-60 wt % (NM-403) was dissolved in all three media. The calculated dissolved fraction sometimes exceeded 100% which may be due to sensitivity of very low concentration levels, inhomogeneity and potentially insufficient extraction of the metals in the analysis of the powder materials.

7. SAXS and USAXS measurements and data treatment

Small-angle X-ray scattering (SAXS) is a technique based on the interaction between X-rays and matter to probe the structure of materials. The processed data are the intensity, I , of X-ray scattered by a sample as a function of angular position of a detector, see Figure 17.

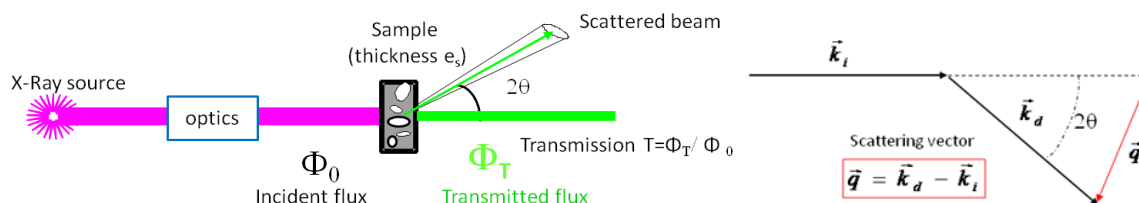


Figure 17. Schematic set up for SAXS and physical quantities.

The intensity is expressed in absolute scale, cm^{-1} , independent from test parameters such as X-ray wavelength, experimental background, time of acquisition and sample thickness. 2D raw data images are converted into diffractograms displaying the scattered intensity I as a function of scattering vector q defined by:

$$q = \frac{4\pi \sin \theta}{\lambda}$$

λ : X-ray wavelength

Ultra small angle X-ray scattering (USAXS) measurements give access to X-ray scattering data for a smaller range of q and then complement the SAXS diffractograms. It requires a specific and very precise set-up, usually different from the one used for SAXS. General theorems of experimental physics have been developed for the interpretation of the diffractograms to extract different properties of nanostructured materials, such as shape of nanoparticles, surface area, interactions occurring, etc.

In the high q range, diffractograms display an intensity decrease in a q^{-4} trend, called the “Porod region”, corresponding to the “real space” to the scale of the interfaces (for smooth interfaces). Therefore, for a sample with two phases, the asymptotic limit of the “Porod’s plateau”, when data are represented as $Iq^4 = f(q)$, is related to the total quantity of interface Σ (in m^2/m^3) between the two phases, as follows (Porod’s law):

$$\Sigma [m^{-1}] = \frac{\lim_{plateau} (I \cdot q^4)}{2\pi(\Delta\rho)^2}$$

$\Delta\rho$ is the difference in scattering length density between the two phases.

To treat raw SAXS data and obtain absolute intensities, the intensity by the thickness of the scattering material need to be normalised. For powder samples where sample thickness has no real meaning, a model system is used, in which the effective thickness of material crossed by X-rays, e_B , is considered and it corresponds to a thickness equivalent to the material arranged in a fully dense (no inner or outer porosity) and uniform layer. The sample transmission is related to this equivalent thickness by the following equation:

$$e_B = -\frac{1}{\mu} \ln(T_{exp})$$

where μ : material absorption coefficient for X-rays ($\mu_{MWCNT} = 6 \text{ cm}^{-1}$) and T_{exp} is the experimental transmission (transmitted flux Φ_T /incident flux Φ_0), i.e. transmission of the sample plus cell with regard to the transmission of the empty cell (kapton alone, empty capillary, etc.).

The intensity scaled by this thickness e_B is called I_1 . Porod's law can then be applied for I_1 to calculate the specific surface area of the powder. The optimum parameters for measurements are given in Table 20.

Table 20. Material properties considered and corresponding calculated optimum thickness of dense material for a sample transmission of 0.3.

Material	Density	Scattering length density	Absorption coefficient (μ)	Optimum thickness (e_B)
MWCNT	1.4 g/cm ³	$1.877 \cdot 10^{11} \text{ cm}^{-2}$	6 cm^{-1}	2 mm

SAXS measurements were performed by CEA using kapton capillaries of internal thickness 1.425 mm and run for 3600s. A measurement is considered optimal for a transmission around 0.3 and the optimum thicknesses e_B for the MWCNT NMs are gathered in Table 21.

Table 21. Experimental parameters for the MWCNT NMs.

Material	Cell	e_B (μm)	T_{exp}
NM-400	two sticky kapton films (5 mm cell)	745	0.64
NM-401	two sticky kapton films (15 mm cell)	1124	0.52
NM-402	two sticky kapton films (5 mm cell)	1190	0.5
NM-403	two sticky kapton films (5 mm cell)	1320	0.46

For each MWCNT NM, two SAXS measurements were performed, one with a short acquisition time to prevent saturation of the detector, typically 60 s, and one with a long-time acquisition of 1800 s to lower the signal/noise ratio at high q .

Image treatment and calculations on radial averaged data are described in Appendix B for SAXS and USAXS data. It includes normalization of the intensity by the parameters of the

experiments, e.g. acquisition time, sample thickness, calibration constants determined using reference samples and background subtraction. SAXS data obtained for short time and long-time and USAXS data are merged to get continuous diffractograms for the whole q range.

All specific surface area results together with their uncertainty calculations are presented below. Errors on the Porod's plateaus have been determined manually for each diffractogram, and the uncertainty on the material density is considered to be about 5%.

The specific surface areas of powders are determined on the Porod plateau, see Appendix B. More details on the general principles of measurement and the measurement technique as well as the data treatment are described in Appendix B.

7.1. Size and structure of fractal aggregates by SAXS

All SAXS diffractograms and the corresponding representations in $I(q)q^4$ for MWCNT powders are displayed in Figure 18, Figure 19 and Figure 20. Among the carbon nanotube powders, NM-401 stands out from the others and does not display any real plateau. Therefore, its specific surface area is difficult to assess, but remains very low compared to other NMs, indicating the presence of true aggregates and/or large nanotubes.

The length of nanotubes is not accessible in the q range of the instruments used.

The calculation results for specific surface area of MWCNT powders, expressed in m^{-1} and in m^2/g , together with uncertainty estimations, are reported in Table 22. The diameter calculated in the last column corresponds to the size of dense, perfectly monodisperse carbon nanotubes that would exhibit the same mean surface area.

Table 22. Specific surface area measured by SAXS for the MWCNT NMs.

NM	$\text{Lim } Iq^4$ ($10^{-3} \text{ cm}^{-1} \text{ A}^{-4}$)	Σ (m^{-1})	Specific surface area (m^2/g)	Error on plateau (m^2/g)	+ 5% error on density (m^2/g)	Equivalent diameter for cylinders (nm)
NM-400	5.9	2.65E+08	189.3	± 8.1	± 27.1	15
NM-401	0.9	4.27E+08	>30.5	± 1.5	± 4.6	< 94
NM-402	4.0	1.82E+08	130.3	± 4.2	± 17.2	22
NM-403	5.9	2.65E+08	189.0	± 10.8	± 29.7	15

* *For NM-401 no real plateau is observed so the surface area calculation is only a minimum estimation.

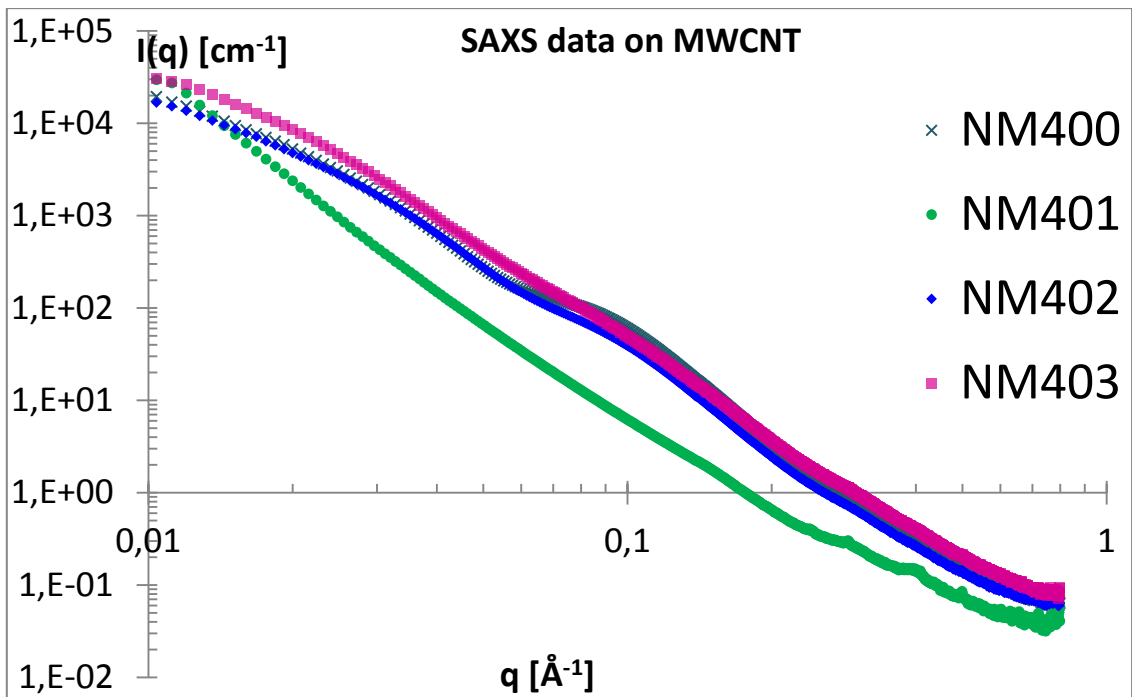


Figure 18. SAXS and USAXS results for MWCNT raw powders NM-400 (blue), NM-401 (green), NM-202 (dark blue), NM-203 (pink).

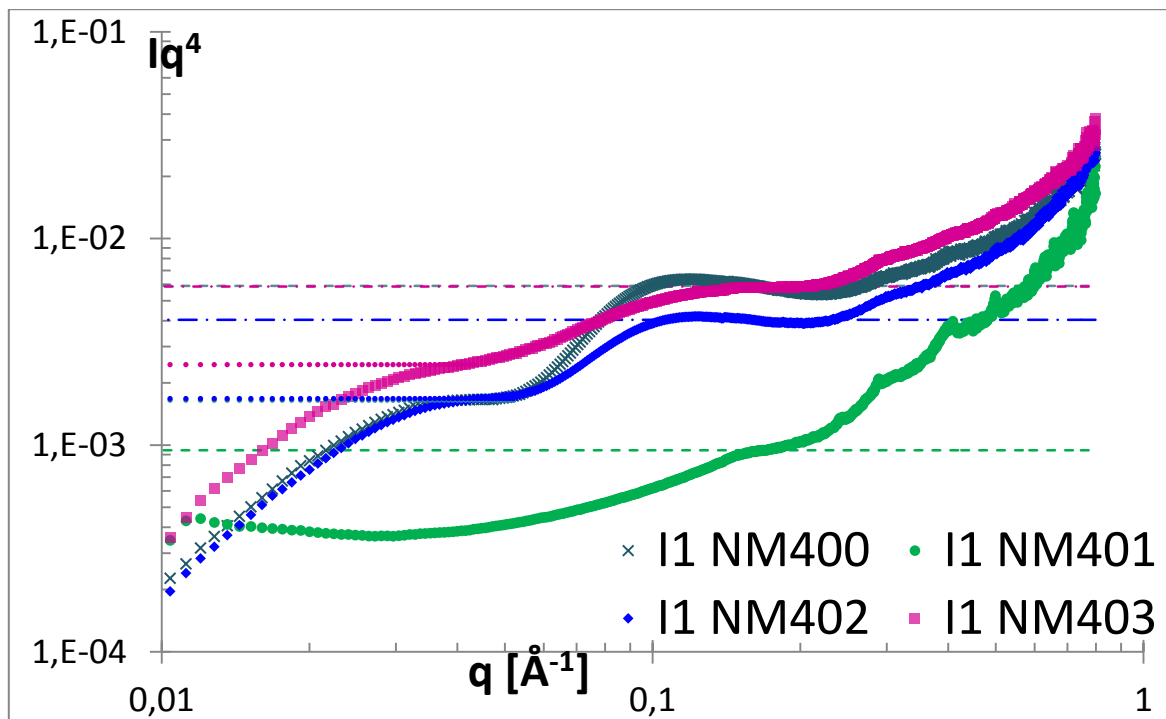


Figure 19. Representation in Iq^4 of SAXS and USAXS results of NM-400 (blue), NM-401 (green), NM-402 (dark blue), NM-403 (pink). The dotted lines are the corresponding Porod's plateaus.

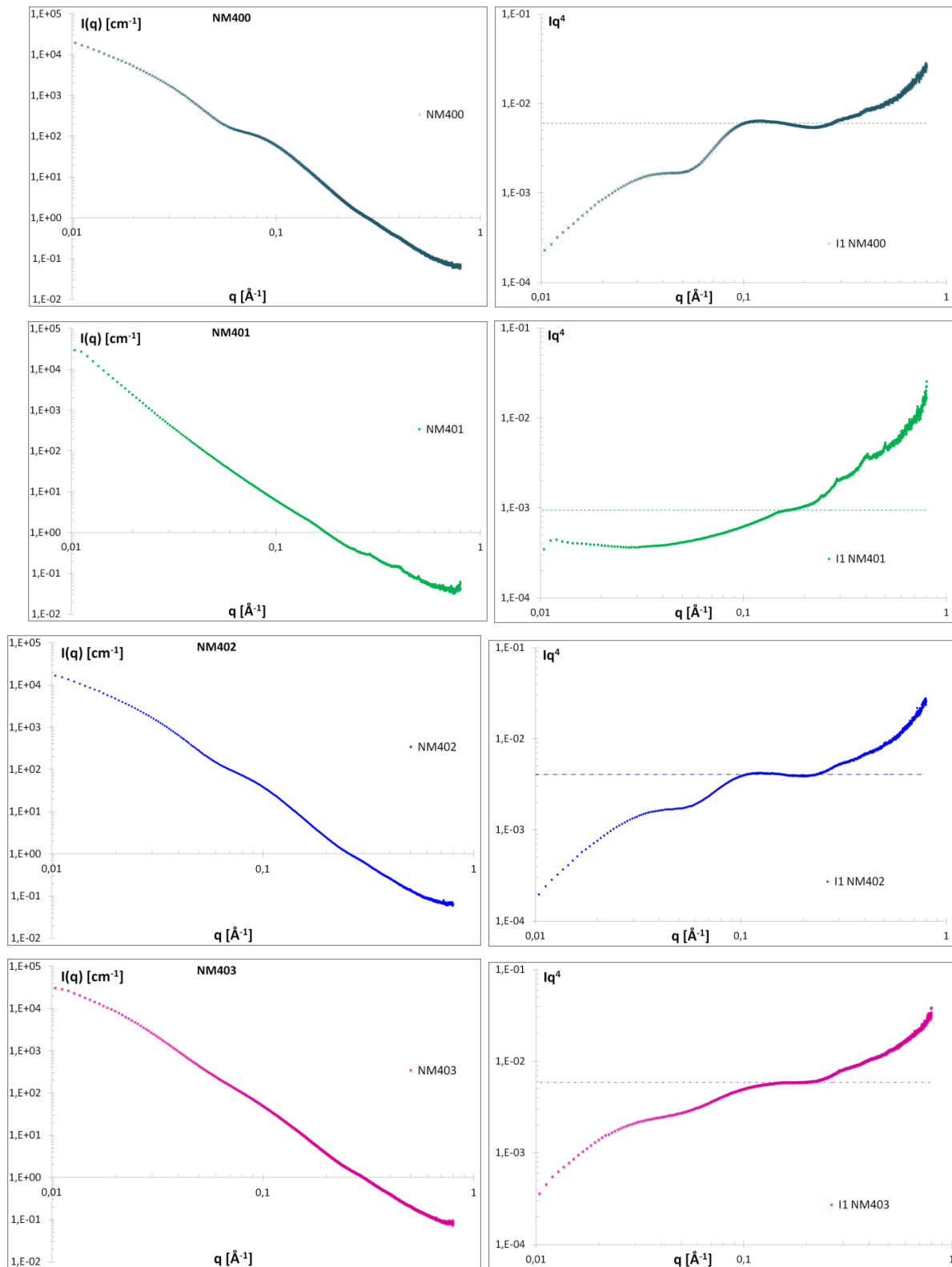


Figure 20. SAXS and USAXS results for raw powders of a) NM-400; b) NM-401; c) NM-402, d) NM-403; $I(q)$ representations on the left; $I(q)^4$ representations q^4 representation revealing Porod's plateaus on the right.

Two plateaus are clearly visible for NM-400, NM-402 and NM-403. The highest plateau reflects the presence of very small carbon nanotubes displaying high specific surface areas. The presence of another plateau for lower q indicates that carbon is arranged in secondary structures of finite size, under the assumption that no major contamination of a scattering impurity is present. NM-400 and NM-402 seem to have a similar secondary structure, but different nanotube units (in terms of size and/or multiwall properties). For NM-403, the two plateaus are less pronounced and the size difference between the primary and secondary structure is smaller. It is not possible to estimate the lengths of the carbon nanotubes in the q range of the instruments used.

The measured concentrations of nanoparticles obtained through the invariant theorem and the specific surface areas corresponding to Porod's plateau were consistent with theoretical concentrations and specific surface areas of dry materials determined by SAXS, see also the measurement of specific surface area by BET.

The order of magnitude of the secondary structures present in NM-400, NM-402 and NM-403, can be estimated from the height of the lower plateaus, assuming a spherical shape. Values are reported in Table 23.

Table 23. Values obtained from the lower plateaus observed for NM-400, NM-402 and NM-403, and derived typical size of secondary structures.

	Low plateau ($10^{-3} \text{ cm}^{-1} \text{ \AA}^{-4}$)	Σ (m^{-1})	Specific surface area (m^2/g)	Estimation of secondary structure size (spherical assumption) (nm)
NM-400	1.65	7.45E+07	53.2	54
NM-402	1.68	7.59E+07	54.2	53
NM-403	2.45	1.11E+08	79	36

Table 25 and Section 8.3 compare the SAXS and BET data, and data from the MWCNT producers. The values measured by SAXS for the surface areas of NM-400 and NM-401 where also BET data from the producers are available (see Table 25), are both below the lowest value in the range given, so it appears that using SAXS for estimating the surface area is not optimal.

8. Brunauer, Emmett and Teller (BET) measurements

The most widely used technique for estimating surface area and porosity is the BET method (Brunauer, Emmett and Teller, 1938). The concept of the theory is an extension of the Langmuir theory for monolayer molecular adsorption to multilayer adsorption with the following hypotheses: (a) gas molecules physically adsorb on a solid in layers infinitely; (b) there is no interaction between each adsorption layer; and (c) the Langmuir theory can be applied to each layer. The BET equation is

$$\frac{1}{v[(p_0/p) - 1]} = \frac{c - 1}{v_m c} \left(\frac{p}{p_0}\right) + \frac{1}{v_m c}$$

where p and p_0 are the equilibrium and the saturation pressure of adsorbates at the temperature of adsorption, v is the adsorbed gas quantity (for example, in volume units), and v_m is the monolayer adsorbed gas quantity. c is the BET constant.

$$c = \exp\left(\left(\frac{E_1 - E_{L1}}{RT}\right) \frac{E_1 - E_{L1}}{RT}\right)$$

where E_1 is the heat of adsorption for the first layer, and E_L is that for the second and higher layers and is equal to the heat of liquefaction.

The equation is an adsorption isotherm and can be plotted as a straight line with the y-axis showing $1/v[(P_0/P)-1]$ and $\phi = P/P_0$ on the x-axis according to experimental results (BET plot). P is the equilibrium pressure and P_0 is the saturation pressure. The value of the slope, A , and the y-intercept, I , of the line are used to calculate the monolayer adsorbed gas quantity V_m and the BET constant c . The following equations are used:

$$v_m = \frac{1}{A + I} \quad \text{and} \quad c = 1 + \frac{A}{I}$$

A total surface area $S_{BET, total}$ and a specific surface area S_{BET} are estimated by the following equations:

$$S_{BET, Total} = \frac{v_m N S}{V} \quad \text{and} \quad S_{BET} = \frac{S_{Total}}{a}$$

where V_m is in units of volume which are also the units of the molar volume of the adsorbate gas, N is Avogadro's number, S is the adsorption cross section of the adsorbing species, V is the molar volume of adsorbate gas, a is the mass of adsorbent (in g).

8.1. BET results

The results for the specific surface area, pore volume and micro-porosity of the MWCNT NMs obtained by IMC-BAS are summarised in Table 24.

The nitrogen adsorption isotherms for the MWCNT NMs are shown on Figure 21 and the curves are very similar in shape suggesting that the MWCNT NMs have the same behaviour.

Table 24. Results of the IMC-BAS BET measurements on the MWCNT NMs.

	BET surface m ² /g	Total pore volume mL/g	Micro surface area m ² /g	Micropore volume mL/g
NM-400	254.00	0.9613	0.0	0.0
NM-401	17.850	0.0776	0.0	0.0
NM-402	226.39	0.8892	15.747	0.0814

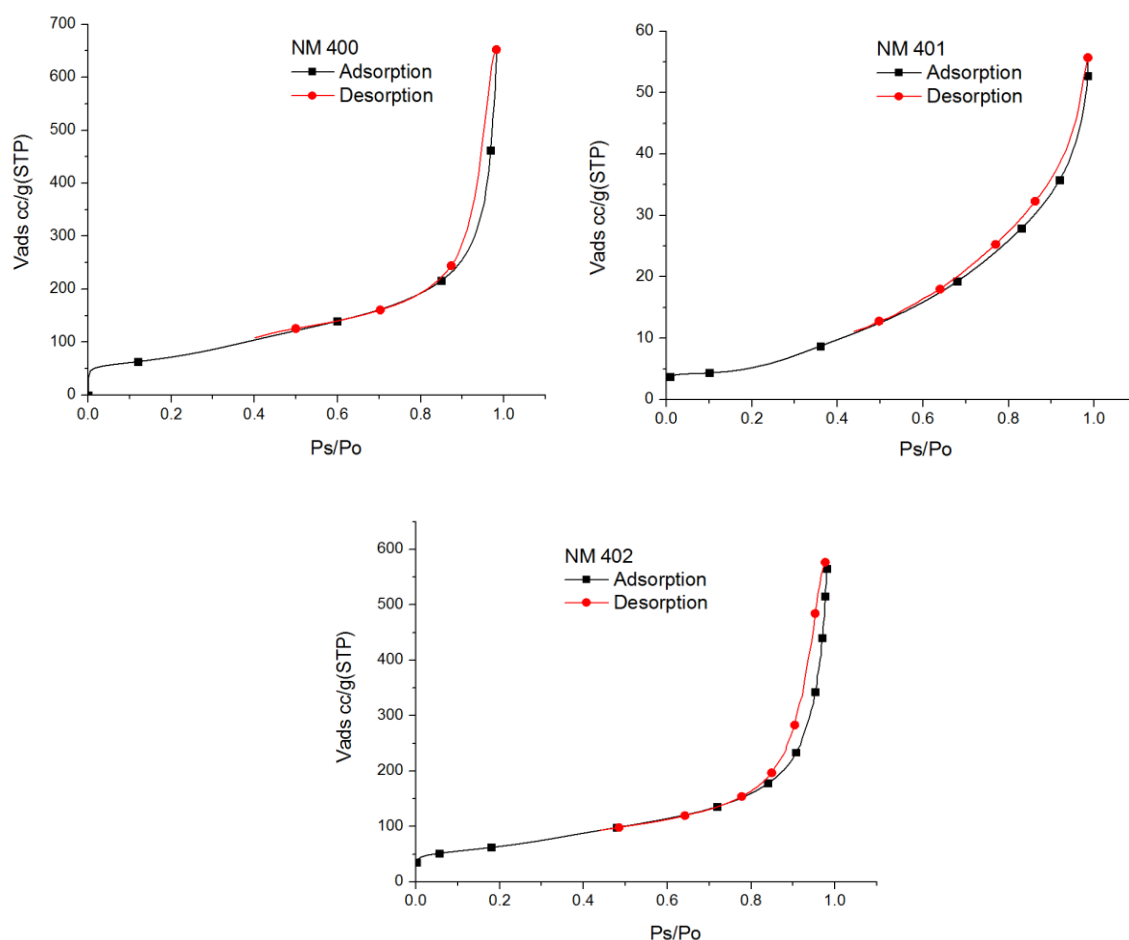


Figure 21. Isotherms of nitrogen sorption experiments by IMC-BAS at 77K for MWCNT NMs giving the adsorbed volume (V_{ads}) in cm³ per gram (cc/g) [y-axis] and P/P_0 on the x-axis. The NM-numbers are mentioned in the title of each plot.

8.2. Comparison of producers' BET data and measured BET

In Table 25 the results from the BET analyses are compared with data provided by manufacturers of the industrial materials. Despite clear differences in absolute numbers, it is evident that there is an overall, and possibly as good as possible, comparability between the three data sets. The results suggest reasonable material homogeneity and/or that both the NANOGENOTOX project and producer instrumental capacity and the SOPs for making BET analysis are of similar quality. However, a final conclusion cannot be made on comparability as the results were not produced using traceable standards for calibration or benchmarking.

Table 25. Comparison of BET data by the manufacturers and measured in the NANOGENOTOX project, and SAXS data.

Material	Tube length Producer (μm)	BET surface Producer m^2/g	BET surface, IMC-BAS m^2/g	SAXS surface, CEA m^2/g
NM-400	~ 1.5	250-300	254	189.3 (± 8.1)
NM-401	5 – 15	40-300	140.46	> 30.5 (± 1.5)
NM-402	0.1 - 10	-	226.4	130.3 (± 4.2)
NM-403	1 -10	-	-	189.0 (± 10.8)

*Data obtained in the EU FP7 NANODEVICE project as a commercial service from QUANTACHROME GmbH & Co. KG ([6] Birkedal et al., 2012).

8.3. Comparison of SAXS and BET data

The MWCNT NMs were analysed for their specific surface area using BET and SAXS, which are two different analytical methods relying on nitrogen gas adsorption and X-ray scattering, respectively. The results show a wide range in the specific surface areas of the NMs analysed with BET. For the SAXS analysis it has been shown in the NANOGENOTOX project that the method can, in principle, be applied as a technique to determine surface area for SiO_2 and TiO_2 . However, the data set for MWCNTs is small and the specific surface area estimated by SAXS for NM-401 is outside (below) the broad range given by the producer, and also the SAXS estimate for NM-400 is below the range given by the producer. The BET measurements fall with the values given by the producer.

In the Specific Surface Area assessment, differences and limitations of the methods also need to be considered. Assessed from the methodology, most of the differences in the obtained results may be explained by the combined errors in density and placement of plateau. Other explanations may come from the difference in thermal treatment and outgassing of the powders before BET analysis. Furthermore, the SAXS analysis indicates two scales of values depending on the range of plateau considered. This is particularly intriguing and should be the matter of further studies to allow a proper comparison with the BET results obtained.

9. XRD measurements

9.1. XRD analysis

X-Ray Diffraction (XRD) analysis is based on the principle that crystalline materials diffract X-rays in a characteristic pattern unique for each material. In this technique, a beam of X-rays is diffracted into many specific directions on regular atomic lattice, which allows determining the atomic and molecular structure of a crystal. XRD can therefore be used to identify different polymorphs, such as typical TiO_2 polymorphs rutile, brookite and anatase. The width of the reflections can also give information about the size of the diffracting domains (crystallites), which for nanoparticles may often (but not always) correspond to particle size.

An important factor in the determination of the particle size by means of XRD is the instrument contribution to the width of the XRD profile. Each instrument has a unique contribution to the X-ray diffraction profile, which should be documented for detailed data comparisons using e.g. a large crystallite standard. For the analysis, IMC-BAS used quartz (SiO_2) (NIST SRM1878, median particle size of 1.4 μm after grinding). To assess the contribution from the instrument, the full width at half maximum, FWHM, was measured on the standards and plotted as a radian angle.

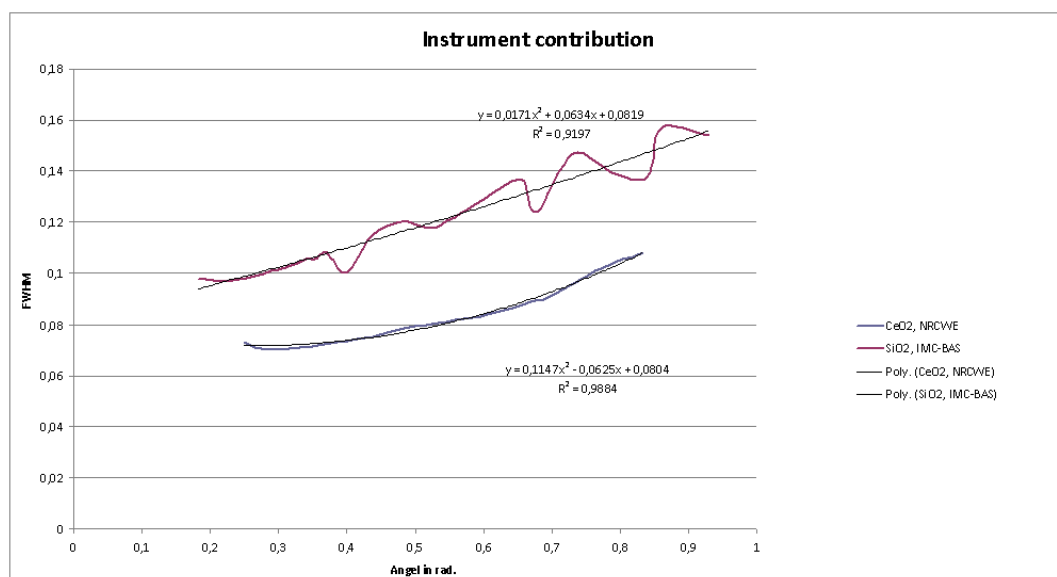


Figure 22. Graph of instrument contribution to the width of the reflections for data collected by IMC-BAS and NRCWE. The x-axis is the angle in radians and the y-axis is FWHM.

Figure 22 shows the theoretical contribution from the instruments at IMC-BAS and at NRCWE. The instrument contribution is found as the FWHM of the reflections in the dataset of standards. 2θ is expressed in radians. For each instrument the best fit for FWHM

(standard) as a function of 2Θ (radians) is found. The difference between the two instruments is calculated for four specific points.

Analyses of raw powder MWCNT

IMC-BAS investigated the possibility to detect catalyst, carbon allotropes and the MWCNT structure by XRD on powders from NM-400, NM-401, and NM-402. The X-ray diffractograms show one significant broad reflection and some smaller ones. All peaks were ascribed to reflections from the carbon nanotubes. Besides carbon nanotubes, graphite may be present in NM-401. The carbon nanotube reflections were used to estimate the wall thickness based on the widths of the reflections. However, it should be strongly emphasized that there is no consensus on whether wall thickness can be properly calculated from powder X-ray diffraction data. The results are summarized in Table 26.

Table 26. Results from the XRD size calculations on NM-400, NM-401 and NM-402 by IMC-BAS.

Material	Size [nm] method		
	XRD / peaks ¹	Rietveld ²	Standard +Rietveld ³
NM-400	2	2.832 (0.641)	3.2(0.6)
NM-401 (+Graphite?)	9	8.58 and 12.22	8.6 (for graphite 2H hkl 002 and 006)
NM-402	2	2.939 (2.061)	

¹ Ognyan Petrov, peak fit, FWHM vs. standard peak;

² Louiza Dimova, Bruker Topas 4.2, standard less;

³ Rosica Nikolova, Fullproof + quartz standard.

The technique and the interpretation of results need further refinement before it can be routinely applied to MWCNT.

10. Transmission Electron Microscopy (TEM)

The TEM experiments were performed by CODA-CERVA and IMC-BAS. Given that the aim for NM characterisation is a sub-1-nm-resolution, TEM is one of the few techniques available that allows this resolution. TEM yields number-based results, allows size measurements as well as also specific shape measurements and characterization of surface topologies on a number basis (per particle). It allows distinguishing between characterization of primary particles and aggregates/agglomerates and was successfully applied to the MWCNT NMs.

The TEM results give both a qualitative and quantitative description. A qualitative description of the NM is provided based on conventional Bright Field (BF) electron microscopy. This description includes (i) representative and calibrated micrographs, (ii) the agglomeration and aggregation status, (iii) the general morphology, (iv) the surface topology, (v) the structure (e.g. crystalline, amorphous) and (vi) the presence of contaminants and aberrant particles. To measure the characteristics of primary particles of the MWCNT NMs, the Feret Min and Feret Max were measured in CODA-CERVA following systematic selection procedure for unbiased random image collection as described by De Temmerman et al., 2012.

10.1. TEM. Sample preparation and measurements

10.1.1. Sample preparation

At CODA-CERVA, the NMs were brought in dispersion (NANOGENOTOX medium and protocol) at a suitable concentration: 0.512 mg/ml of MWCNT and sonication for 16 minutes using a Vibracell™ 75041 ultrasonifier (750 W, 20 kHz, Fisher Bioblock Scientific, Aalst, Belgium) equipped with a 13 mm horn (CV33) at 40% amplitude. This setup resulted in an average horn power of about 26 W and a sample specific energy in the order of 2530 ± 20 MJ/m³. During sonication the samples were cooled in ice water to prevent excessive heating. The suspended NM were brought on pioloform- and carbon coated, 400 mesh copper grids (Agar Scientific, Essex, England) that were pre-treated with 1% Alcian blue (Fluka, Buchs, Switzerland) to increase hydrophilicity.

At IMC-BAS, the NMs were transferred onto carbon-coated copper grids without Alcian blue pre-treatment using a special tool, a platinum (Pt) wire loop (0.2 mm Pt wire, one end of which is bent as loop with external diameter of 2.5-3.0 mm). The following operations were carried out during the transfer of suspension onto EM grids: (i) catching a grid by tweezers with reverse action; (ii) disposing the tweezers on a table surface in a way ensuring direct contact of the grid and the filter paper; (iii) careful sinking and extracting the Pt loop in/from the vessel with suspension of nanoparticles (here, a thin film of nanoparticles suspension is formed in the loop space due to the surface tension); (iv) careful touching the Cu grid placed

on the filter paper by the Pt loop (in this operation, the whole surface of Cu grid in contact with the Pt loop is covered by nanoparticles while liquid medium is absorbed by the filter paper); (iii-iv) operation can be performed 1 or 2 times (the Cu grid covered by nanoparticles is ready for observation immediately or after drying a few seconds at ambient temperature).

10.1.2. Recording of the electron micrographs

At IMC-BAS, well-contrasted BF images of NM were obtained using: (i) a Philips TEM420 at 120 kV acceleration voltage; (ii) EM grids with holey carbon support film; (iii) well calibrated regimes in EM for recording images on photo plates (Kodak electron image film SO-163); (iv) appropriate developing of EM films; (v) high-resolution scanner technique for transferring the image from EM film into digital file, (vi) image processing.

At CODA-CERVA, the samples were also imaged in BF mode using a Tecnai™ G2 Spirit microscope (FEI, Eindhoven, The Netherlands) with Biotwin lens configuration operating at 120 kV at spot size 3. The condenser lens current was chosen so that the beam was parallel and images were taken approximately 500 nm below minimal contrast conditions, where Fresnel fringes were minimal and contrast was judged to be optimal. Micrographs were recorded using a 4*4 K CCD camera (Eagle, FEI). To achieve maximal traceability of information, each micrograph was stored together with its administrative and sample preparation information and the information related to its imaging conditions in a dedicated database integrated in the iTEM software (Olympus, Münster, Germany). Modifications of the TIA image acquisition software (FEI) and of the iTEM software were made to transfer the micrographs and their associated information efficiently in the iTEM database. (i) The TIA protocol for batch conversion of the software-specific SER- and EMI-formats was adjusted to avoid too long file names. (ii) An imaging C- and libtiff library-based module, referred to as the TIA-TAG module, was developed in iTEM. This module reads the information relevant for image analysis and quality control in the private tags of the TIF image files and renders it accessible in a new information tab of the iTEM software. In addition, the TIA-TAG module facilitates calibration of images by automatically converting the pixel size from mm scale to nm scale. (iii) New fields were defined in the iTEM database specifying the sample and its preparation characteristics. Where applicable, drop lists were foreseen to avoid typing errors.

10.2. Results for Transmission Electron Microscopy

Representative images of the MWCNT nanomaterials are shown in Figure 23, Figure 24, Figure 25 and Figure 26 for NM-400, NM-401, NM-402 and NM-403, respectively. It should be noted that the MWCNT nanomaterials show great variation in the types and content of impurities. All MWCNT NMs appear to contain a fraction of μm size particles, which

sometimes was identified as fully euhedral graphite crystals and in NM-400 was corundum crystals (catalyst support material). Inorganic catalyst particles are abundant in the sidewalls of NM-401 and appear to occur mainly at the tube ends in NM-402. It is important to extend the in situ characterization of all MWCNT materials beyond size analysis to fully understand these materials and their potential hazard.

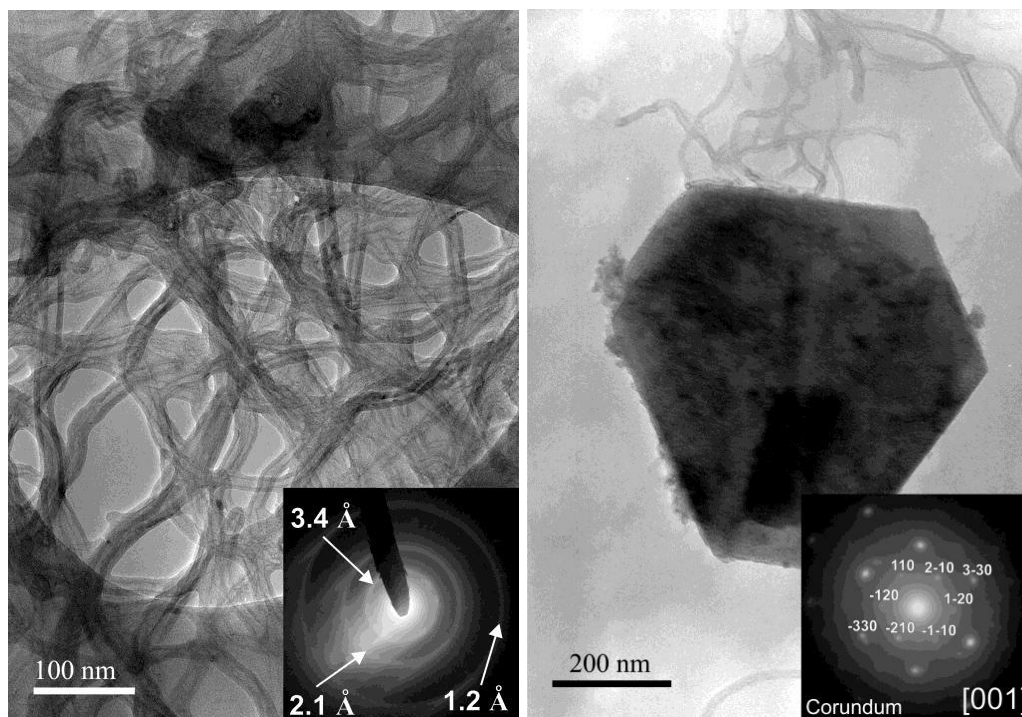


Figure 23. NM-400: A) Representative TEM micrograph of NM-400 (Scale bar 100 nm). Typical selected area electron diffraction (SAED) pattern is shown in insert. B) Example of euhedral foreign particles - catalyst support corundum viewed down [001]. SAED pattern is shown in insert (Scale bar 200 nm).

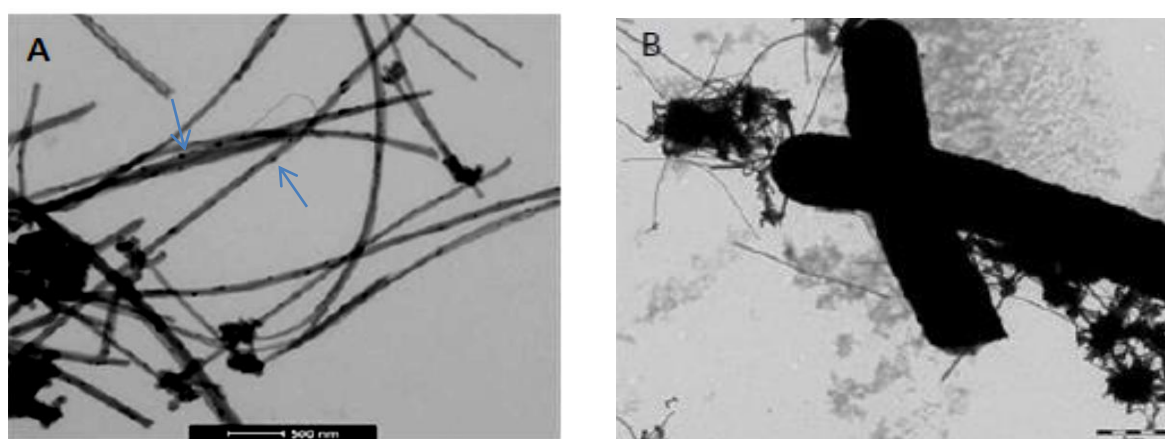


Figure 24. NM-401 A) Representative TEM micrograph of NM-401. Dark spots, of which two are indicated with blue arrows) in the MWCNT sidewall are catalyst impurities (scale bar 500 nm). B) Example of “megatubes” and μm-size dense aggregates and agglomerates in the NM (Scale bar 2 μm).

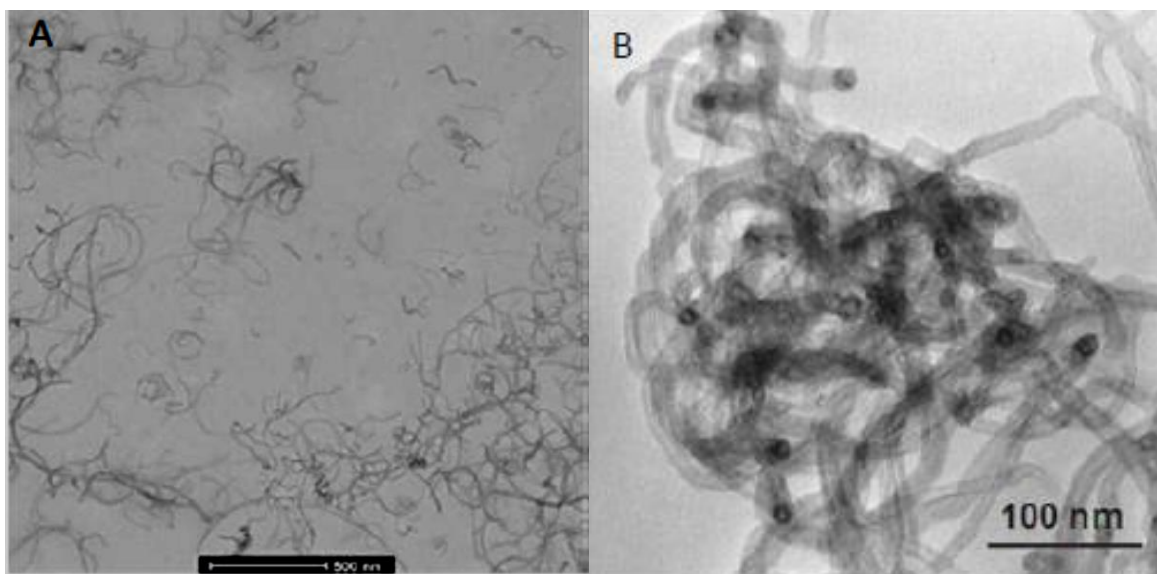


Figure 25. NM-402: A) Representative TEM micrograph of highly dispersed MWCNT in NM-402. B) Image showing the structure of dense “particle” areas, which consist of highly entangled MWCNT.

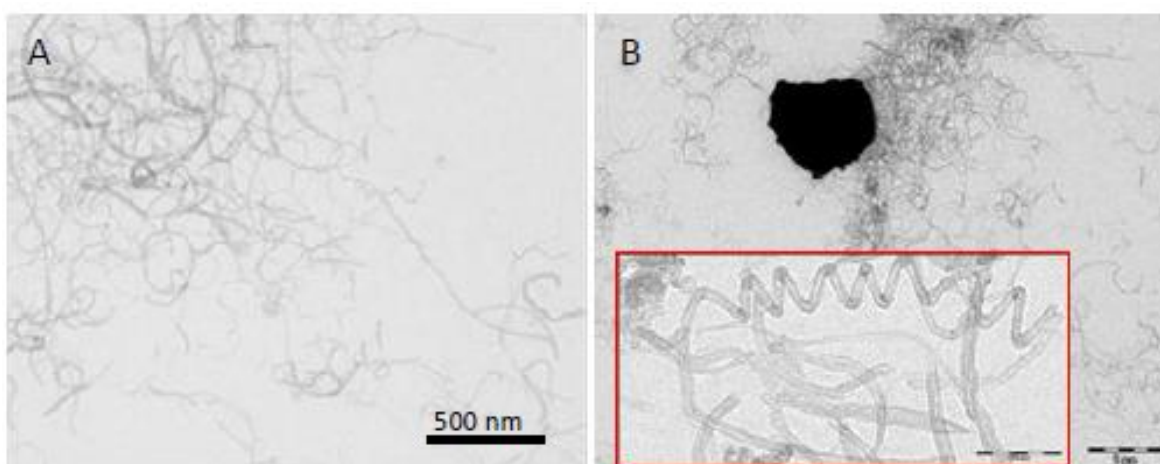


Figure 26. NM-403: A) Representative TEM micrograph of NM-403. B) Example of μm -size dense unidentified impurity particles (Scale bar $1\ \mu\text{m}$) and insert showing different morphologies with bent and spiral shaped MWCNT (Scale Bar $100\ \text{nm}$).

10.3. Interlaboratory comparison

Analysis of the micrographs from TEM shows that the different MWCNT materials may be grouped into two principally different types according to the morphology of the tubes. The general morphology of the MWCNTs within the first group was quite comparable. In section 10.1 the sample preparation and measurement are described.

- Group 1: Highly bent MWCNT (NM-400, NM-402, NM-403)
- Group 2: Straight-wall MWCNT (NM-401)

Quantitative size analysis of the MWCNT based on the TEM micrographs is shown in Table 27. NM-401 is classified as large-diameter MWCNT (ca. 70 to 80 nm average diameter), whereas NM-400, NM-402, and NM-403 are low-diameter MWCNT (ca. 10 to 17 nm average diameter). The number based thickness distribution is given in Figure 27. The large-diameter MWCNTs have a wide size distribution while the low-diameter MWCNT have a narrow size distribution (Figure 27 and Figure 28). The large majority (87-90%) of the large-diameter MWCNTs had a thickness of less than 100 nm. For the low diameter MWCNT all analysed tubes had a thickness of less than 100 nm. Due to the generally high degree of entanglement, it was only possible to complete manual analysis of tube lengths. The average lengths vary from 443 nm (NM-403) to 4.05 μ m (NM-401): ordered by length, NM-403 < NM-400 < NM-402 < NM-401. The length of NM-401 is the one that has the greatest similarity with the MWCNT lengths given by vendors. However, the measured length is influenced by the dispersion protocol used, and the vendors' protocols are unknown so comparison of the measured values is not meaningful; as NM-401 is the thickest MWCNT, a possible conclusion might be that thick MWCNT do not break so easy in pieces (by sonication) as thin MWCNT.

Table 27. Thickness, geodesic length, percentage of particles with a thickness lower than 100 nm and aspect ratio of NM-400, NM-401, NM-402, NM-403 (CODA-CERVA), and manually measured dimensions of the MWCNT nanomaterials (IMC-BAS).

Material	Thickness, CODA-CERVA \pm SD (nm)*	Thickness of nanotube, IMC-BAS \pm SD (nm)*	Thickness of tubewall, IMC-BAS \pm SD (nm)*	Geodesic length, CODA-CERVA \pm SD (nm)*	< 100 nm CODA-CERVA	Aspect ratio* CODA-CERVA	n ^{&} CC	n ^{&} IB
NM-400	11 \pm 3	16.2 \pm 3.5	5.1 \pm 1.0	846 \pm 446	100 %	79 \pm 50	20	36
NM-401	67 \pm 24	61.4 \pm 24.4	-	4048 \pm 2371	90 %	66 \pm 46	43	358
NM-402	11 \pm 3	14.3 \pm 2.7	5.4 \pm 1.2	1372 \pm 836	100 %	125 \pm 66	20	135
NM-403	12 \pm 7	-	-	443 \pm 222	100 %	42 \pm 29	50	-

* Mean \pm standard deviation (SD), n[&]: number of observations, CC: CODA-CERVA, IB: IMC-BAS

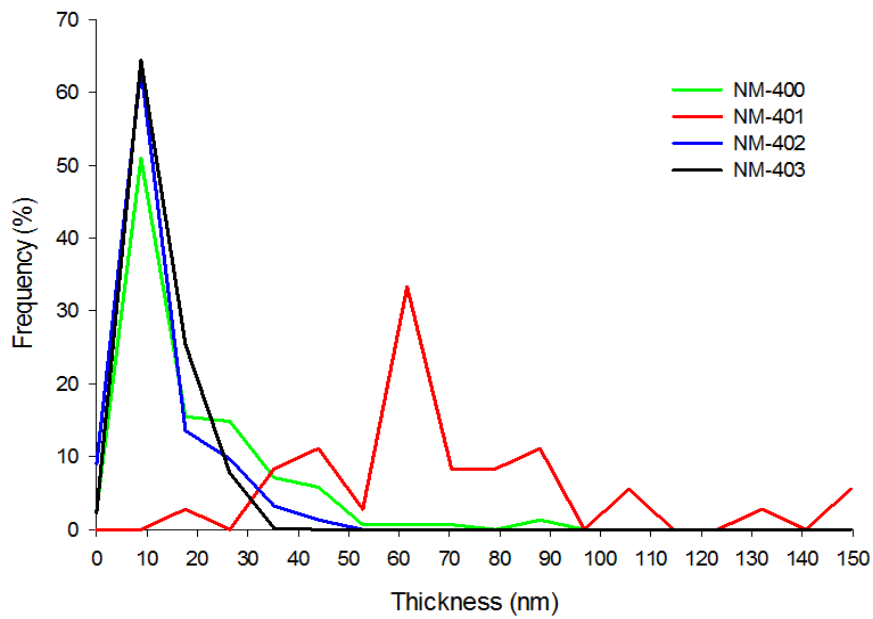


Figure 27. Qualitative TEM image analysis of MWCNT. Graph illustrates the primary thickness as a function of the frequency. Highly bent MWCNT: NM-400, NM-402 and NM-403; Straight-wall MWCNT: NM-401.

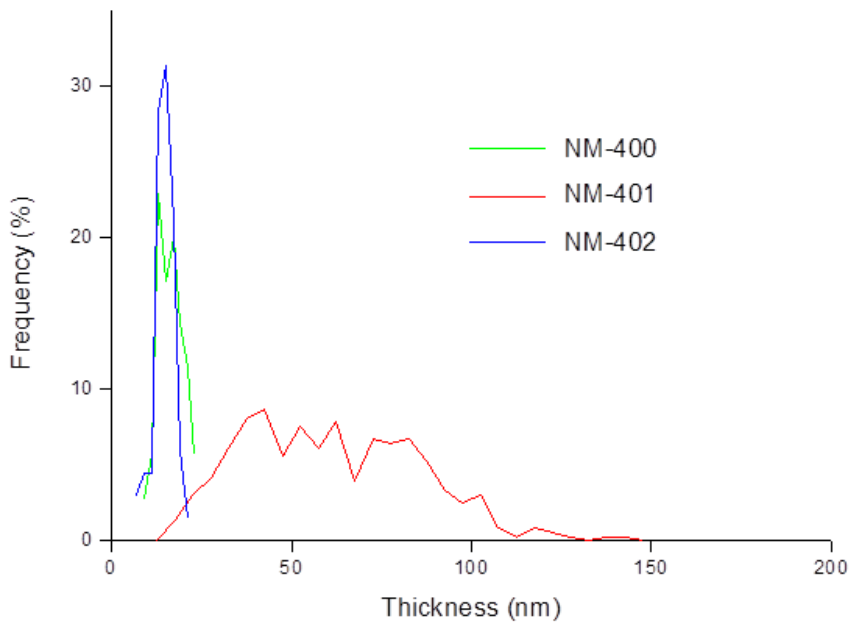


Figure 28. Qualitative TEM image analysis of MWCNT (IMC-BAS). Graph illustrates the primary thickness in function of the frequency. Both Highly bent MWCNT (NM-400 and NM-402) and Straight-wall MWCNT (NM-401) are illustrated on the graph.

11. Dustiness

Dustiness is defined as the propensity of a material to emit dust during agitation. A European standard (EN15051) has been established containing two methods (the rotating drum and continuous drop methods). However, EN15051 is not fully suitable for nanomaterials, as also stated in EN 15051 and was not applied to the MWCNT NMs. Other procedures are therefore currently under investigation, and in this study dustiness was tested using Vortex shaker (VS) method.

It is important to note that dustiness is not an intrinsic physical or chemical defined property of a powder. Its level depends on e.g. characteristic properties of the powders and the activation energy in the simulated handling, and thus different values may be obtained by different test methods.

The Vortex shaker method, or VS method, consists of a centrifuge tube continuously agitated by vibration in which the test material is placed. Originally proposed by Baron et al. (2002), this method was also used later by Isamu et al. (2009). More recently, INRS has developed this approach, particularly in the context of a collaborative project within the network PEROSH (Witschger et al., 2011).

Among the useful features of the VS methods, one is that only little material (less than 6 grams) is needed for a test compared to the traditional methods described in the EN15051 standard (several hundred grams). In addition, the smaller size equipment is easier to place in an approved fume cupboard or safety cabinet, greatly improving the safety of the experimenters.

For the VS method the determination of dustiness in respirable size-fractions was combined with number concentration and size-distribution analysis of the dust particles. For a few of the tests conducted with the VS method, electron microscopy observations were performed. Finally, particle-size distributions data are reported from measurements using Electrical Low-Pressure Impactor (ELPI™ Classic) for the VS method.

The objective of this study is to analyse the propensity of the MWCNT NMs to generate fine dust during simulated agitation of raw powder. The nanomaterial powders were compared with each other according to their index of dustiness. Two indexes have been defined, one based on the number of particles emitted, and the other on the mass of particles emitted.

11.1. Experimental setup of Vortex Shaker Method and results

The vortex shaker method consists of a centrifuge stainless tube agitated by a vortex in which the test powdered material is placed together with 100 µm diameter bronze beads. These are used to help the de-agglomeration of powders. High-efficiency particulate air

(HEPA) filtered air, controlled at 50% relative humidity (RH), pass through the tube in order to transfer the released aerosol to the sampling and measurement section. The protocol developed for the experiments performed at INRS used two different versions of the sampling and measurement section.

All tests conducted with VS method used approximately 0.5 ml powder, which was placed in the sample vial together with 5 g bronze beads (100 μm), used to agitate and de-agglomerate the powder. The sample is allowed conditioning in the 50% RH before the shaker for a powder agitation period of 3600 s (60 min).

The first version of the sampling and measurement was devoted for real-time measurement using ELPI™ Classic (Electrical Low Pressure Impactor) (10 lpm, Dekati) for size distributions according to the equivalent aerodynamic diameter and Condensation Particle Counter (CPC. Model 3786 UWCPC, TSI) for number concentrations. This version was also devoted for collecting airborne particles for subsequent electron microscopy observations. Tests were completed in triplicates for each NM.

The CPC used was the Model 3785 Water-based CPC (TSI, USA). This CPC detects particles from 5 to >3000 nm. It provides a wide, dynamic, particle-concentration range, an essential characteristic for the tests considered. Featuring a single-particle-counting mode with continuous, live-time coincidence correction and a photometric mode, the CPC measures particle number concentrations at $<10^7$ particles/cm³.

ELPI™ is an instrument to measure airborne particle size distribution and concentration in real-time. It operates in the size range of 7 nm – 10 μm in its standard configuration. Because of its wide particle size range and rapid response (< 5 s), the ELPI™ has been considered an ideal measurement instrument for the analysis of the unstable concentrations and size distributions, or the evolution of size distributions that could be observed in these tests. To prevent particle bouncing and charge transfer during the tests, all collection substrates (PVC GELMAN GLA-5000 5 μm / 25 mm) were greased.

The results of the tests performed with this first version of the VS method leads to the determination of:

- Dustiness indices expressed as the total number of particles emitted (based on data from CPC).
- Particle size-distribution of the aerosol (based on data from ELPI™ Classic in its standard configuration).

In the ELPI the measured current signals are converted to (aerodynamic) size distribution using particle size dependent relations describing the properties of the charger, the impactor

stages, and the effective density of the particles. The particle effective density provides a relationship between mobility and aerodynamics sizes. Effective density is a parameter which is complex to measure (Olferta et al., 2007), and values for the MWCNT NMs are not available in the literature.

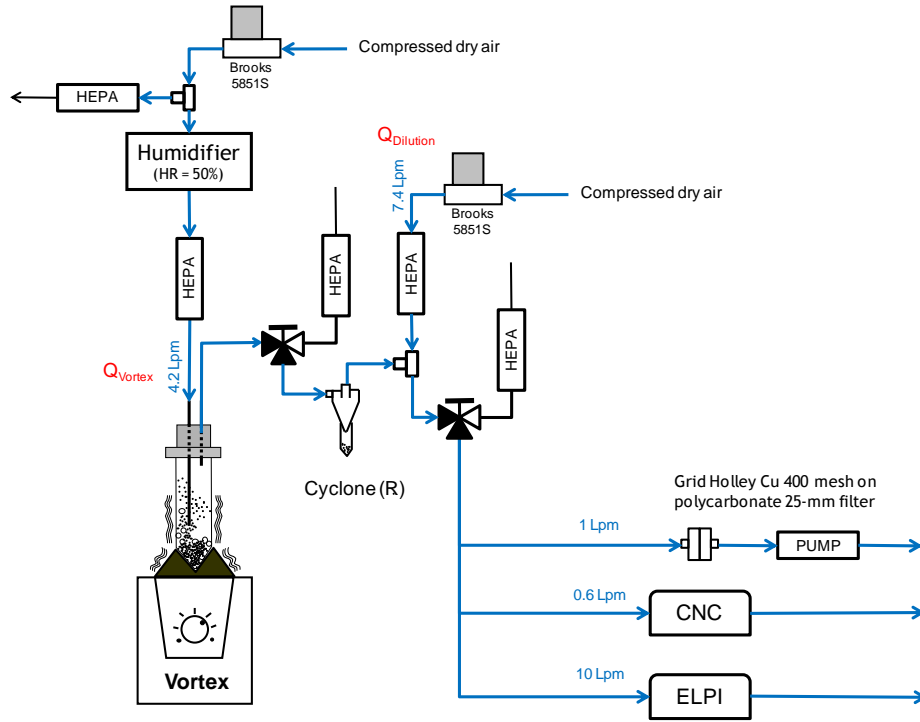


Figure 29. Experimental set-up of the vortex shaker method for measuring number concentrations and particle-size distributions, and for collecting airborne particles for subsequent EM observations.

The following assumption has been made for the data from the ELPI: spherical particle with a density equal to the density of the condensed phase of the material constituting the NM. The density used was 1.75 g/cm^3 for all MWCNT NMs based on Kim et al. (2009). If this assumption is questionable, there is no robust method that can be applied to polydispersed aerosols over a wide size range, such as those used here. However, to assess the effect of this parameter on the results, the number size distributions were also calculated for a density of 1 g/cm^3 .

$S_{Vortex}^{Number(CNC)}$ is the total number of generated particles from the Vortex tube and it was calculated as:

$$S_{Vortex}^{Number(CNC)} = [Q_{Vortex} + Q_{Dilution}] \cdot \Delta t \cdot \sum_{i=0}^T C_{CNC}(t_0 + i \cdot \Delta t)$$

Where:

- T is the time over which the total number of particles is calculated. This time is between 5 and 3600s, the latter is the test duration in the original protocol of the VS method.
- Δt is the step time of the CNC (for all tests it was set as 5 s)
- $C_{CNC}(t_0+i\cdot\Delta t)$ is the number concentration measured during the time interval
- Q_{Vortex} is the total air flow rate passing through the vortex tube (4.2 lpm)
- $Q_{Dilution}$ is the flow rate of dilution air (7.4 lpm).

$DI_{Number(CNC)}$ is the dustiness index in number of particles per gram, and it was calculated as the total number of generated particles divided by the total mass of the test NM in milligrams (unit 1/mg):

$$DI_{Number(CNC)} = \frac{S_{Vortex}^{Number(CNC)}}{m_{NM}}$$

To get information on particle morphology of the emitted aerosol, a simple but specific sampling set-up has been designed (not shown here). TEM copper grids were taped onto 25 mm diameter polycarbonate membrane filters (0.4 or 0.8 μ m). Fibre backing filters were used to support the polycarbonate filters. Air flow was driven by a personal sampling pump at a flow rate of 1 L/min. The duration of the sampling was set to 1 hour. The sampling period was set equal to the duration of a test (1 hour). For some tests, the sample was accumulated over two trials in order to have enough particles to observe. Different TEM copper grids having different carbon films have been used (Carbon film, Quantifoil Holey Carbon Films or Holey Carbon Support Film).

It is important to note that the duration of the test is a relevant test parameter as the process is dynamic. In the original INRS protocol developed, the duration of a test was set equal to 3600 s. But in the first version of the set-up (Figure 29), as the instruments measure in real time, it is possible to perform the calculation for different durations between 0 and 3600 s. In this report, the calculations based on the condensation nuclei counter CNC data were performed for two durations: 180 s and 3600 s. The first duration (180 s) was chosen to be consistent with the NRCWE Small Rotating Drum method based on EN15051 (Schneider and Jensen, 2008). For the second version of the setup, the duration of the test was set to 3600 s, which corresponds to the original protocol of the VS method.

The second version of the setup (Figure 30) is used for collecting respirable mass fraction of the emitted aerosol. The respirable mass fraction is obtained by sampling with a GK2.69 cyclone (BGI, UK). The filters have been pre-weighed and post-weighed following the recommendations of the ISO 15767:2009 on the same analytical balance. Only one test was performed with this setup due to time constraints. Therefore the results are not presented

with a confidence interval based on reproducibility. However, measurement uncertainty has been calculated for each measurement performed.

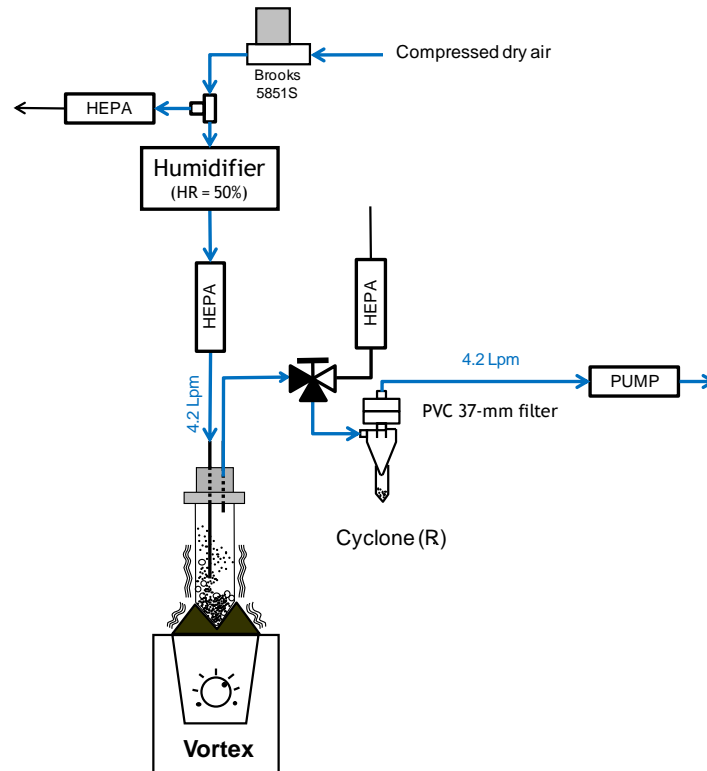


Figure 30. Experimental set-up of the vortex shaker method for collecting respirable mass fraction of the emitted aerosol.

$DI_{Mass(GK2.69)}$ is the dustiness index in respirable mass (mg) of particles per kilogram and it was calculated as the respirable mass of generated particles in milligrams divided by the total mass of the NM tested in kilograms:

$$DI_{Mass(GK2.69)} = \frac{S_{Vortex}^{NumMass(GK2.69)ber(CNC)}}{m_{NM}}$$

The recommendations of the standard ISO 15767:2009 were followed to determine the Limit of Detection (LOD) of the weighing procedure for the filters used for sampling respirable mass of particles during this project. The LOD for the PVC GELMAN GLA-5000 (5 μ m/37 mm) filters was equal to 20 ng. This value is used to determine the LOD expressed in dustiness index.

The preparation of MWCNT NMs for VS testing included: 1) to take a series of 7 samples of 0.5 cm³ from the vial containing the nanomaterial, 2) to accurately weigh the samples. Three samples are devoted for testing with the first version of the set-up, one for the second version (respirable mass fraction measurement) and three for the gravimetric water content

measurement. The gravimetric water content was performed using a HR83 Halogen Moisture Analyzer (Mettler Toledo) and following a drying program defined specifically for small quantities of used NM (Temperature = 160°C; duration = 170 s).

The weighing of the NMs was performed with a XP205 analytical balance (10 µg accuracy, Mettler Toledo) while the weighing of the 37-mm filters from the respirable sampler was performed with a MX5 microbalance (1 µg accuracy, Mettler Toledo).

Particular attention was given to cleaning the experimental device between successive tests. All pipes and other connections were systematically cleaned with water and/or ethanol and dried in an oven, or eventually changed. The checking of the airflows was performed using a primary flow bubble calibrator (Gillian® Gillibrator 2). Prior to each test, the cleanliness of the air was assessed on the basis of measurements made using the condensation nuclei counter. In the case of a non-compliant result, the cleaning was performed again or pipes and other connections changed. The validation of a test depends on several factors such as: 1) the stability of the parameters during the test, 2) a good reproducibility of measured number concentrations, 3) the sequence of steps for the respirable aerosol sampling etc.

The entire set-up was located inside a variable volume fume hood to prevent exposure of the operator. Similarly, all operations like weighing, water content measurement and sample preparation were carried out in a specific containment system that has a unique turbulent-free, low flow design which allows our sensitive balance to operate without fluctuation and protects the operator from exposure to airborne particles that could be released when handling and weighing the MWCNT NMs.

11.2. Results for the Vortex Shaker Method

Table 28 lists the bulk density of the nanomaterials in powders. The results were obtained in tests conducted by INRS.

Table 28. Bulk density of the MWCNT NMs.

Material	Bulk density (g/cm³)
NM-400	0.08
NM-401	0.02
NM-402	0.11
NM-403	0.17

Experimental data obtained with the VS method are summarized in Table 29. Number-based data with the VS method are calculated from the time profiles with 2 test durations 180 s and 3600 s. The mass-based data, obtained with a test duration of 3600 s, correspond to the respirable fraction only as the inhalable fraction was not part of the VS original protocol.

Table 29. Number-based and mass-based dustiness indexes MWCNT NMs.

Material	Test mass (mg)	Dustiness Index			
		Number (number/mg)			Mass (mg/kg)
		T = 180 s		T = 3600 s	
		CPC (SD) ^b	ELPI ^a (SD) ^b	CPC (SD) ^b	Respirable (SD) ^c
NM-400	36.6	1.5E+05 (5.7E+04)	1.9E+05 (1.8E+05)	5.3E+05 (2.0E+05)	<4.2E+02 ^d
NM-401	8.8	4.0E+06 (2.2E+06)	5.2E+06 (3.2E+06)	6.8E+06 (4.7E+06)	<1.7E+03 ^d
NM-402	59.6	1.0E+05 (8.9E+03)	1.0E+05 (6.1E+04)	6.6E+05 (2.1E+04)	4.2E+03 (3.75E-03)
NM-403	86.1	3.9E+04 (1.2E+04)	< LOD	3.5E+05 (3.4E+04)	4.9E+03 (4.39E-03)

a The assumption for calculating the number of particles emitted from the data from the ELPI is: spherical particle with a density equal to the density of the condensed phase of the material constituting the NM. Densities used were 1.75 g/cm³ for all NM-40x; based on Kim et al. (2009).

b standard deviation calculated over 3 repeats

c measurement uncertainty as there was no repeat for this tests

d correspond to the LOD in mass dustiness index

Figure 31 below shows the respirable mass-based indices with the VS method. It is difficult to say something about the MWCNT NMs because for two of them (NM-400 and NM-401) the indexes were below the limit of detection (LODs). However, both NM-402 and NM-403 shows indices quasi-equivalent, well above the LODs.

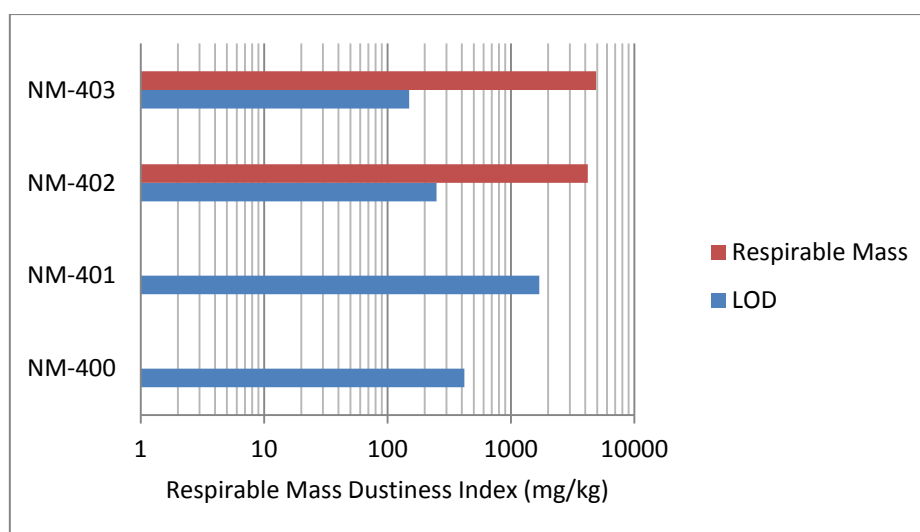


Figure 31. Respirable mass dustiness indices of NMs tested with the VS method. The grey bars correspond to the LOD expressed in mass-based indices. Respirable mass dustiness indices are presented with their measurement uncertainty (which is not visible on the graph as it is below 1%).

Figure 32 shows the number (1/mg) and respirable mass (mg/kg) dustiness indices of NMs tested with the VS method. The MWCNT NMs were classified according to their highest respirable mass index to the lowest. There is no correlation between the two indices presented, respirable mass and number. The ratio between the max and min values is similar for both number and respirable mass indices, around 100. For both NM-400 and NM-

401, the respirable mass collected on the cyclone filter was below the LOD of the weighing procedure. For both NM-400 and NM-401 the values obtained for number of particles emitted are significant while the results expressed as respirable mass are below the detection limit.

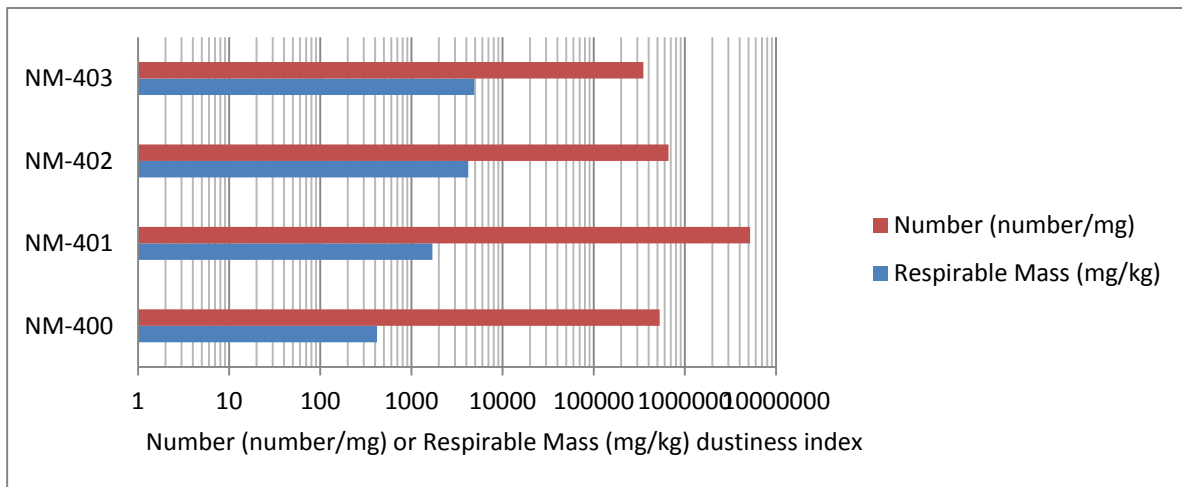


Figure 32. Number (number/mg) and respirable mass (mg/kg) dustiness indices of NMs tested with the VS method.

In Figure 33, the influence of test duration on the calculation of the number dustiness index (number/mg) can be observed.

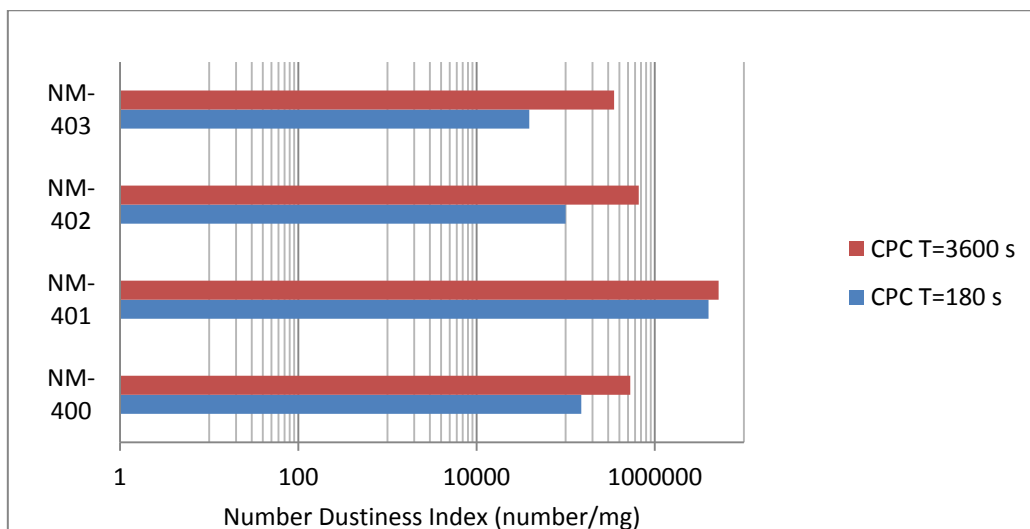


Figure 33. Number (number/mg) dustiness indices for all NMs tested with the VS method as measured by CPC. Comparison of two test times T for calculation: 180 and 3600 s.

Figure 34 shows the particle number size distributions for all MWCNT NMs obtained with the VS method and measured by the ELPI Classic (standard configuration). All distributions are presented as given by the ELPI (aerodynamic equivalent diameter). For each MWCNT, the

particle number size distribution is shown for two values of the particle density. It should be noted that the representation chosen here is for the Y axis is the relative number ($\Delta N/N_{total}$), so that size distributions can directly compared between plots. From the plots for each MWCNT (Figure 34) it is seen that the particle number size distribution of NM-401 is different from the particle number size distribution of NM-400, NM-402 and NM-403, which are rather similar. NM-401 is clearly distinguishable from the others with an aerosol that is characterized by a mode around 300 nm. For the measurements performed using the ELPI it should be noted that the size-distributions obtained are qualitative determinations due to the low number of particles emitted (near the background noise of the instrument).

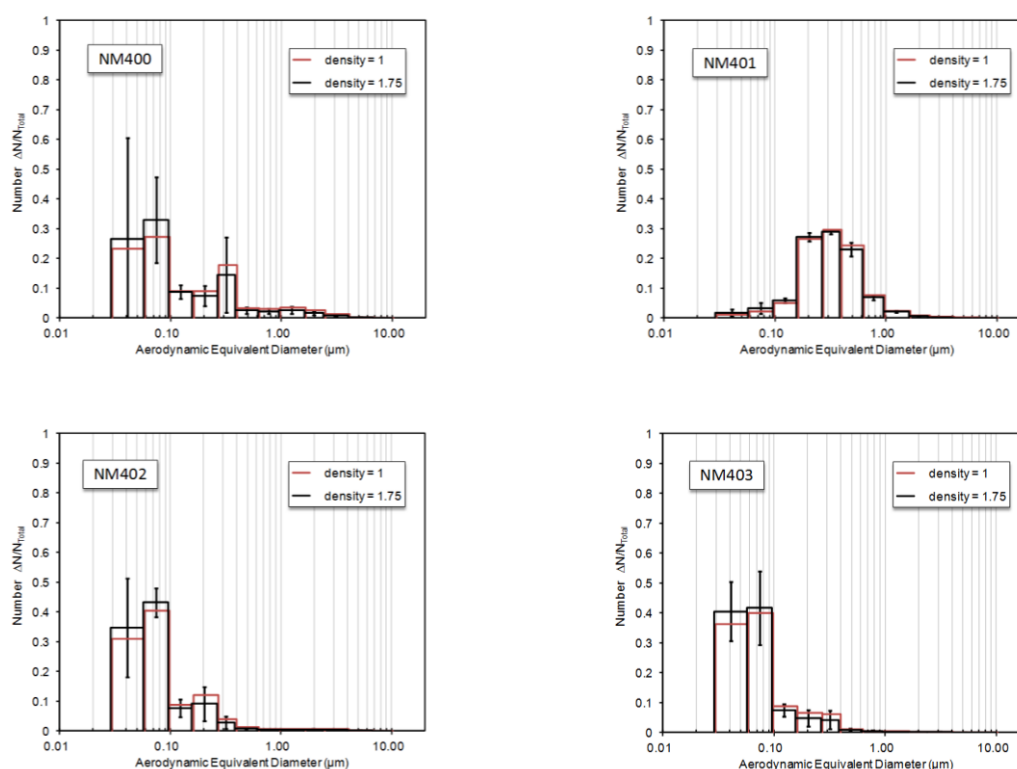


Figure 34. Particle number size distributions for carbon nanotube NMs obtained with the VS method and measured by the ELPI Classic (standard configuration). All distributions are presented as given by the ELPI (aerodynamic equivalent diameter). Densities used were 1.75 g/cm^3 for all MWCNT NMs based on Kim et al. (2009).

Figure 35 shows TEM pictures of NM-401. The photographs qualitatively show the diversity of the particles observed on each grid. For NM-401, the pictures show bundles of carbon nanotubes as well as single fibres of micrometre-sized length. The observation of free tubes generated by dustiness testing is an important information for the assessment of potential exposure associated with handling of MWCNT NMs.

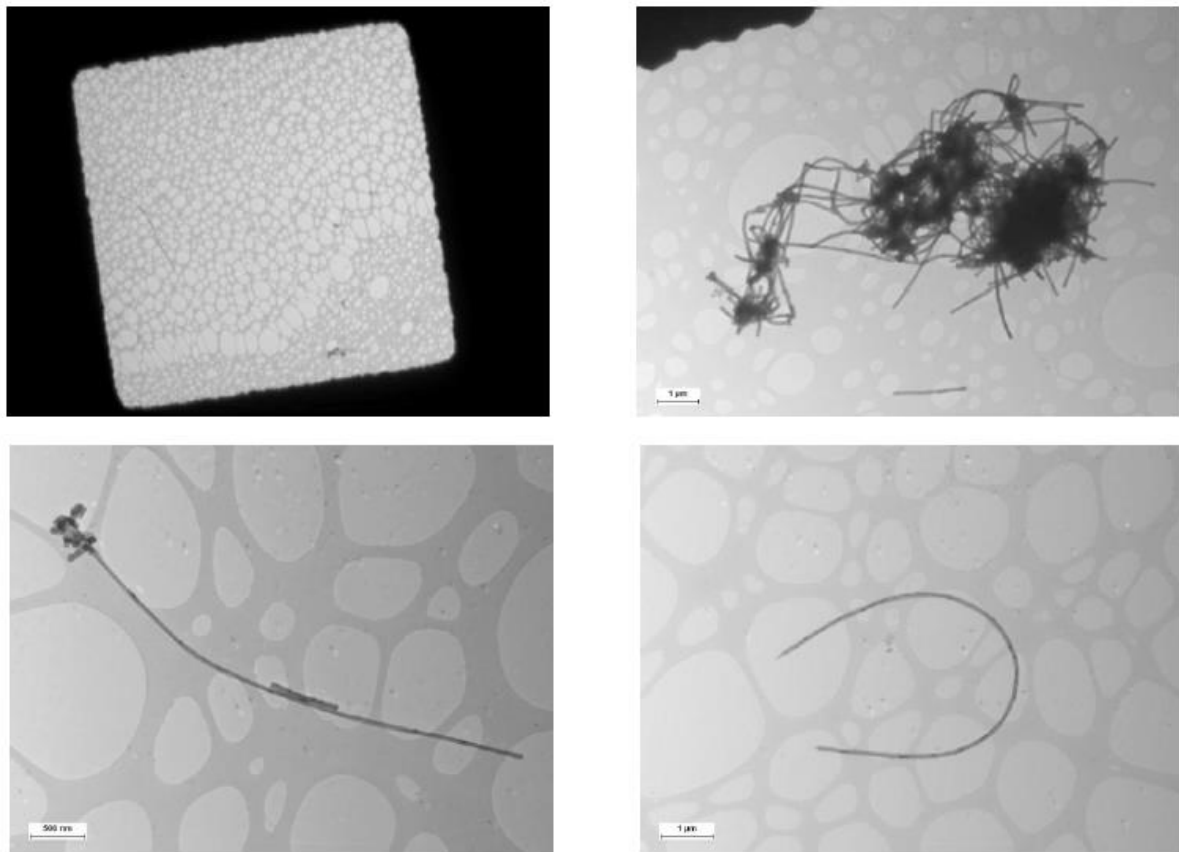


Figure 35. TEM pictures of NM-401. The top row, left, shows the grid from which three parts were enlarged. The top row, right, shows an enlarged area with an example of bundled carbon nanotubes and the bottom row shows two examples of single fibres. The right column has an insert showing a one micron measurement bar, whereas measurement bar for the bottom row, left, is 500 nm.

Dustiness as quantified by particle number or by mass-based dustiness index had a large range, suggesting a corresponding large difference in exposure potential. It is however difficult to say more to the extent the relationship between Dustiness index and actual exposure is not known.

As stated earlier, dustiness is not an intrinsic physical or chemical defined property of a powder, but depends on characteristic properties of the powders and the activation energy in the simulated handling. Therefore different values may be obtained by different test methods (test apparatus, operation procedure, sampling and measurement strategy, *etc.*). It seems obvious that the absence of a harmonized approach concerning the measurement strategies and techniques, metrics and size ranges and the procedures of data analysis and reporting severely limits the comparison of these dustiness methods and results obtained. Number size distributions measured on the aerosols produced during the dustiness testing together with the few TEM pictures observed suggest that it is likely that occupational exposures are characterized by the presence of bundles of MWCNT as well as single tubes.

12. Conclusions

The JRC launched its Repository for representative nanomaterials in 2011 with preparatory work starting in 2008. It hosts more than 20 different types of nanomaterials at the JRC Ispra (Italy) site. The NM-series of representative test nanomaterials was introduced by the JRC to support the OECD Working Party on Manufactured Nanomaterials' programme "Safety Testing of a Set of Representative Manufactured Nanomaterials", established in November 2007, as well as national and international research projects within and outside the EU. The OECD WPMN recommended testing selected nanomaterials for a series of end-points in the OECD nanomaterials testing programme. The multi walled carbon nanotubes, NM-400, NM-401, NM-402 and NM-403 are some of the key materials of the OECD WPMN programme.

Also outside the OECD WPMN, characterisation of nanomaterials and applicable methods are intensively studied to understand nanomaterials both in a regulatory and a scientific context. For example, the JRC published recently a report regarding "Requirements on measurements for the implementation of the European Commission definition of the term "nanomaterial" (see Linsinger et al. 2012) that also evaluates the limits and advantages of the existing methods for characterisation of nanomaterials, and the reader is referred to it for additional information on the applicability areas of the methods.

The physico-chemical characterisation of MWCNT NMs was performed within the NANOGENOTOX project, and by the JRC. Chapter 12.2 gives an overview of the outcome of the physico-chemical characterisation of each of the 4 MWCNT NMs and the measurement methods applied.

A dispersion protocol was first developed which was used for the *in vitro* and *in vivo* experiments with the MWCNT as well as TiO₂ and SiO₂ see <http://www.nanogenotox.eu>; such a protocol is obviously not optimised for the single material type, let alone the individual experiments. Our results show that the sonicator seems to have an important influence on the degree of dispersion and final particle size distribution in the medium. A part of the physico-chemical characterisation was done using the NANOGENOTOX protocol, but for investigating the inherent properties also other dispersion protocols were relevant.

After preparation of the dispersion of the test item, analysis should always be performed to ensure dispersion stability, as successful (liquid) sample splitting can only be conducted if a homogeneous dispersion has been achieved, otherwise a much higher sampling error will be introduced. In addition to errors incurred from sub-sampling steps, stability of the dispersion

is important for nanoparticle characterisation, since only stable dispersions give reliable characterisation data.

12.1. Characterisation

Almost all of the OECD endpoints on physical-chemical testing have been completed for the principal OECD WPMN material, NM-400. Also the alternate materials, NM-401, NM-402, and NM-403 have been extensively characterised. The determination of the octanol water coefficient is not feasible for nanomaterials, as discussed at an OECD workshop in Mexico, March 2013, and was considered to be not relevant for insoluble and sparingly soluble nanomaterials. Analysis of intrinsic hydroxyl radical formation capacity, using the Benzoic acid probe for quantification, gave no detectable radical after 24 and 48-hour incubation.

The elemental analysis showed that the MWCNT NMs vary in purity, from 82 to 97 %wt carbon by TGA, and 90 to 93 %wt carbon by EDS. The MWCNT NMs were analysed using several techniques: EDS, ICP-MS, ICP-OES, TGA and DTA. In addition also XRD gave information about crystalline impurities. All the MWCNT NMs appear to contain some sodium (see Table 6) Thus, the elemental analyses performed were indicative, and the outcomes reflect also that the materials have an industrial origin, as within one NM not all vials contain the same impurities, and sub-samples of one vial may be of slightly different composition. More information regarding the nature of the impurities should be generated for the future.

Analysis of TEM micrographs showed that the general morphology of the nanomaterials may be grouped into two principally different types: highly bent MWCNT and straight-wall MWCNT. Within these groups, the general morphology of the MWCNTs was quite comparable.

Quantitative size analysis of the MWCNT based on TEM is also provided. NM-401 is classified as large-diameter MWCNT (ca. 70 to 80 nm average diameter), whereas NM-400, NM-402, and NM-403 are low-diameter MWCNT (ca. 10 to 17 nm average diameter). The number based thickness distribution is given in Figure 27. The large-diameter MWCNTs have a wide size distribution while the low-diameter MWCNT have a narrow size distribution (Figure 27). The large majority (87-90 %) of the large-diameter MWCNTs had a thickness of less than 100 nm. For the low diameter MWCNT all analysed tubes had a thickness of less than 100 nm. Due to the generally high degree of entanglement, it was only possible to complete manual analysis of the MWCNT dimensions.

The solubility of the MWCNT NMs in the BSA/water batch dispersion medium (i.e. the NANOGENOTOX dispersion protocol), Gambles solution and Caco2 medium was investigated; the solubility in pure water was not included. The MWCNT NMs dissolve partly

in all three media and are least soluble in the BSA/water solution applied in the NANOGENOTOX project.

O₂ reactivity tests showed some material and medium-dependent effects on dO₂, the difference between O₂ concentration in dosed and reference vials. NMs generally caused increased dO₂ values. Yet, NM-402 was the only material to notably increase dO₂ values in BSA-water.

The NMs dissolution and biodurability revealed material-dependent behaviour, partially linked to presence of associated impurity phases in MWCNT. The carbon materials in MWCNT are assumed to be highly durable in the selected incubation medium and test conditions. However, the associated metal impurities and catalysts have moderate to high levels of dissolution. When the most abundant elements included Al and/or Fe, the dissolved fractions were often in the range of 1-15 wt %, but some were notably higher. For NM-401 and NM-402 (relative high concentrations of Fe and Al + Fe, respectively), no dissolution was observed in BSA-water and Caco2 cell medium. For materials with Co, 13-16 wt % (NM-401) to 43-60 wt % (NM-403) was dissolved in all three media. The measured dissolved fraction sometimes exceeded 100%. This may be due to sensitivity of very low concentration levels, inhomogeneity and potentially incomplete extraction of the metals in the analysis of the powder materials.

Specific surface area measurements using BET show specific surface area values from 140.5 (NM-401) to 254 (NM-400) m²/g. The SAXS analysis gave some different results with a larger difference of specific surface area (from 30.5 (NM-401) to 189 (NM-400 and NM-403)

For dustiness the Vortex shaker (VS) methods was applied and are currently proposed as standardised test method for nanomaterials as the dustiness methods in EN15051 do not directly apply to nanomaterials. Both methods are based on agitation, and for both the determination of dustiness in respirable size-fractions were combined with number concentration and size-distribution analysis of the dust particles. For a few of the tests conducted with the VS method, electron microscopy (EM) observations were performed. Finally, particle-size distributions data were reported from measurements using Electrical Low-Pressure Impactor (ELPI™ Classic).

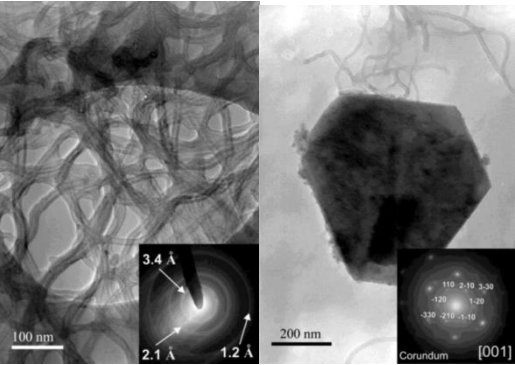
12.2. Summary of the characterisation of each MWCNT NM

Table 4 gives an overview of the physico-chemical characterisation performed, the methods used and the institutions involved in the testing. Table 30 to Table 33 summarise the results obtained in for the 4 different multi-walled carbon nanotubes.

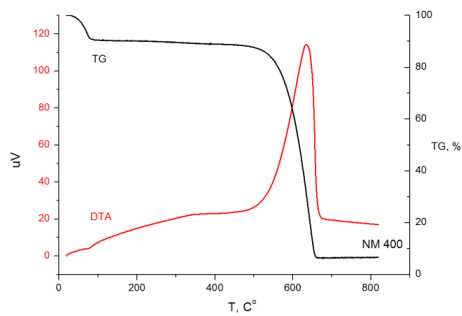
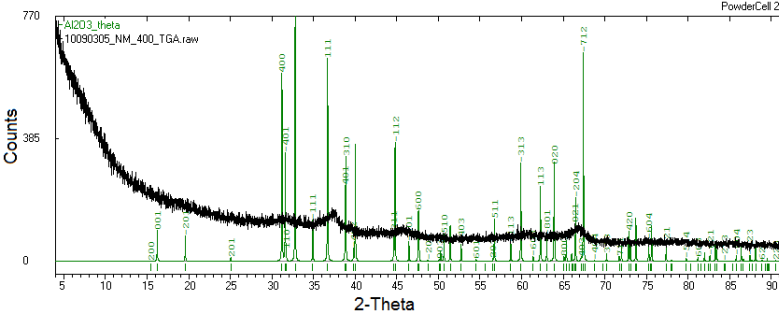
12.2.1. NM-400, summary of physico-chemical characterisation

Table 30. Overview of results from the physico-chemical characterisation of NM-400.

Method	Institution	Results for NM-400
Homogeneity		
Endpoint not investigated		
Agglomeration / aggregation		
Endpoint not relevant		
Water Solubility		
24-hour acellular <i>in vitro</i> incubation test	NRCWE	The 24-hour dissolution ratio of NM-400 was measured in three different media: 0.05% batch dispersion BSA in water, Gambles solution and Caco2 medium. In the dissolution experiments, the actual degradation of MWCNT cannot be assessed from pure elemental analyses. It is assumed that the tubular and graphite carbon material in the MWCNT NMs are non-degradable at the applied test conditions. However, the catalyst and impurity materials identified by elemental analysis and electron microscopy may behave differently. In this study, Al, Co, Fe and Ni were used as indicators for the catalyst dissolution. The measured concentrations of Al and Fe reach percent levels in NM-400 (1.0 wt % Al; 0.2 wt % Fe). The results from the analyses suggest slightly different behaviour of the catalyst materials in the three different incubation media. For very low concentration elements, higher percentages of dissolution were often found. Sometimes, the dissolved Ni fraction even exceeded 100 %. The fraction of dissolved Co was also relatively high in all test media (14 to 60 wt %). For these two elements, the observed high dissolved fractions may be due to MWCNT elemental concentrations being too low for quantification, material inhomogeneity, or too low yield in the elemental analyses on the powders.
Crystalline phase		
XRD	IMC-BAS	IMC-BAS investigated the possibility to detect catalyst, carbon allotropes and the MWCNT structure by XRD on powders from NM-400. The X-ray diffractograms show one significant broad reflection and some smaller ones. All peaks were ascribed to reflections from the carbon nanotubes. The carbon nanotube reflections were used to estimate the wall thickness based on the widths of the reflections. However, it should be strongly emphasized that there is no consensus on whether wall thickness can be properly calculated from powder X-ray diffraction data. Results from the XRD size calculations Standard: 2 nm Rietveld: 2.832 ± 0.641 nm Standard +Rietveld: 3.2 ± 0.6 nm
Raman	NRCWE	For MWCNT the intensity of the D-band increases as compared to the G-band with increasing number walls in the MWCNT. The results from the current analysis showed that NM-400 had a spectroscopic profile with a high G-band intensity and highest D-band.

Method	Institution	Results for NM-400
Dustiness		
Vortex Shaker Method	INRS	Respirable dustiness index (n=1) is inferior to 420 mg/kg (corresponding to the limit of detection in mass dustiness index)
Crystallite size		
Endpoint not relevant		
Representative TEM picture(s)		
TEM	CODA-CERVA, IMC-BAS	 <p>Corundum crystals (catalyst support material) were observed.</p>
Particle size distribution		
TEM	CODA-CERVA	Thickness 11 ± 3 nm Geodesic length 846 ± 446 nm
	IMC-BAS	Thickness 16.2 ± 3.5 nm
Specific Surface Area		
BET	IMC-BAS	254.00 (m ² /g)
SAXS	CEA	189.3 ± 8.1 (m ² /g)
Zeta Potential (surface charge)		
End-point not relevant for MWCNT		
Surface Chemistry		
End-point not relevant for MWCNT		
Photo-catalytic activity		
End-point not relevant for MWCNT		
Pour-density		
Weighing	INRS	0.08 g/cm ³
Porosity		
BET	IMC-BAS	Micropore volume (mL/g): 0.0
Octanol-water partition coefficient		
End-point not relevant		

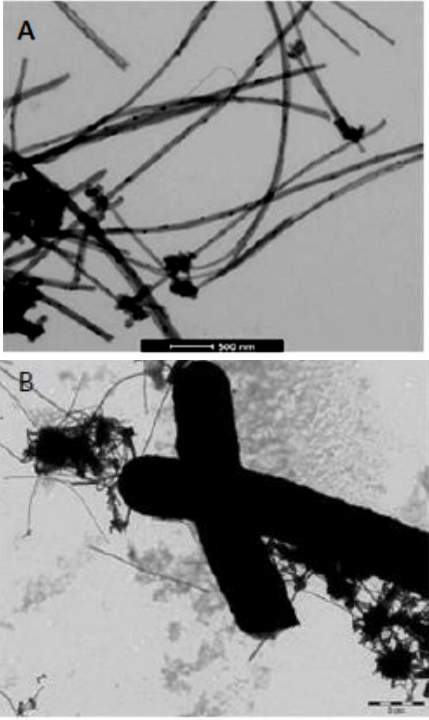
Method	Institution	Results for NM-400
Redox potential		
OxoDish fluorescence sensor plate for O ₂ detection	NRCWE	The evolution of O ₂ level during 24-hour incubation was measured in three different media. Different dO ₂ values were observed for all applied media. In BSA water dispersion NM-400 had minor to negligible effects on dO ₂ , and caused increased dO ₂ in Gambles solution and Caco2 medium. The maximum dO ₂ change is in the order of 40 μmol/ml. Considering the applied doses, this suggests that the particle reactivity easily can exceed 1 μmol O ₂ /mg.
Radical formation		
Endpoint not investigated		
Composition		
ICP-OES	CODA-CERVA	> 0.01 % : Al, Fe, Na, S 0.005 -0.01 % : Co 0.001-0.005 % : Ca, K After Calcination Al : 2540 ± 14 (mg/kg) Fe :387 ± 25 (mg/kg) Co : 161 ± 25 (mg/kg)
ICP-MS	LNE	Na 600 ppm, Cr 14 ppm, Mn 2 ppm, Fe 4300 ppm, Co 3700 ppm, Ni 17 ppm, Cu 1 ppm, As 5 ppm, Mo 1 ppm, Ag 0.3 ppm, Sn 0.5 ppm, Ba 0.3 ppm, Pb 1.5 ppm wt (%) of impurities 0.87
ICP-MS	Duke University	Na 1345 ± 151 ppm, Al 9951 ± 31 ppm, K 97 ± 3 ppm, Ca 3 ± 2 ppm, V 0 ppm, Cr 9 ± 1 ppm, Fe 1988 ± 26 ppm, Co 693 ± 26 ppm, Ni 4 ± 0 ppm, Cu 3 ± 0 ppm, Zn 2 ± 0 ppm, Ba 1 ± 0 ppm, Pb 1 ± 0 ppm wt (%) of impurities 1.41
EDS	IMC-BAS	C -89.81 (wt %), Al- 46100 ppm, Si- 400 ppm, Fe- 7600 ppm, Co 2500 ppm, Cu 2000 ppm, Zn 1900 ppm, O (wt%) calculated- 4.15
Presence of catalysts		
TGA	NRCWE	<div style="display: flex; justify-content: space-around;"> <div style="text-align: center;"> <p>TGA of NM400</p> </div> <div style="text-align: center;"> <p>1st derivative of TGA measurement on NM400</p> </div> </div> <p>NM-400 shows a strong, wide exothermic peak between 500 and 600 °C corresponding to the temperature range with high weight loss in TGA. The first derivative show more than one decomposition temperature for the two large samples, indicating more than one type of carbon material. The small sample appears to contain only one type of carbon nanotube. Comparing the data, a sample must contain at least 8 mg to be representative.</p>

Method	Institution	Results for NM-400
DTA	IMC-BAS	 <p>NM-400 shows a strong wide exothermic peak between 500 and 600 °C corresponding to the temperature range with high weight loss in TGA.</p>
XRD	IMC-BAS NRCWE	 <p>For NM-400, impurities were identified as $\gamma\text{Al}_2\text{O}_3$, or a closely related structure.</p>

12.2.2. NM-401, summary of physico-chemical characterisation

Table 31. Overview of results from the physico-chemical characterisation of NM-401.

Method	Institution	Results for NM-401
Homogeneity		
Endpoint not investigated		
Agglomeration / aggregation		
Endpoint not relevant		
Water Solubility		
24-hour acellular <i>in vitro</i> incubation test	NRCWE	The 24-hour dissolution ratio of NM-401 was measured in three different media: 0.05% BSA in water, Gambles solution and Caco2 medium. In the dissolution experiments with MWCNT, the actual degradation of MWCNT cannot be assessed from pure elemental analyses. It is assumed that the tubular and graphite carbon material in the MWCNT NMs are non-degradable at the applied test conditions. However, the catalyst and impurity materials identified by elemental analysis and electron microscopy may behave differently. In this study, Al, Co, Fe and Ni were used as indicators for the catalyst dissolution. The concentrations of the four selected elements may be too low in NM-401 (≤ 0.06 wt %) for reliable assessment even by ICP-OES. The results from the analyses suggest slightly different behaviour of the catalyst materials in the different incubation media. For NM-401, no dissolution was detected in BSA water and Caco2 cell medium. For very low concentration elements, higher percentages of dissolution were often found. For example, about half of the Ni was found to be dissolved in the test of NM-401. The observed high dissolved fractions may be due to MWCNT elemental concentrations too low for quantification, material inhomogeneity, or too low yield in the elemental analyses on the powders.
Crystalline phase		
XRD	IMC-BAS	IMC-BAS investigated the possibility to detect catalyst, carbon allotropes and the MWCNT structure by XRD on powders from NM-401. The X-ray diffractograms show one significant broad reflection and some smaller ones. All peaks were ascribed to reflections from the carbon nanotubes. Besides carbon nanotubes, graphite may be present in NM-401. The carbon nanotube reflections were used to estimate the wall thickness based on the widths of the reflections. However, it should be strongly emphasized that there is no consensus on whether wall thickness can be properly calculated from powder X-ray diffraction data. Results from the XRD size calculations <ul style="list-style-type: none"> • Standard: 9 nm (NM-401 + (graphite ?)) <ul style="list-style-type: none"> • Rietveld: 8.058 and 12.22 nm • Standard +Rietveld: 8.6 nm (for graphite 2H hkl 002 and 006)
Raman	NRCWE	For MWCNT the intensity of the D-band increases as compared to the G-band with increasing number walls in the MWCNT. NM-401 had a

Method	Institution	Results for NM-401
		spectroscopic profile with a high G-band intensity and low D-band which suggests a graphitic structure.
Dustiness		
Vortex Shaker Method	INRS	Respirable dustiness index (n=1) is inferior to 1700 (mg/kg)(correspond to the limit of detection in mass dustiness index)
Crystallite size		
End-point not relevant		
Representative TEM picture(s)		
TEM	CODA-CERVA, IMC-BAS	 <p>Inorganic catalyst particles are abundant in the sidewalls of NM-401 The second picture show some example of “megatubes” and dense aggregates and agglomerates</p>
Particle size distribution		
TEM	CODA-CERVA	Thickness 67 ± 24 nm Geodesic length 4048 ± 2371 nm
	IMC-BAS	Thickness 61.4 ± 24.4 nm
Specific Surface Area		
BET	IMC-BAS	140.46 (m ² /g)
SAXS	CEA	$> 30.5 \pm 1.5$ (m ² /g)
Zeta Potential (surface charge)		
End-point not relevant for MWCNT		
Surface Chemistry		
End-point not relevant for MWCNT		

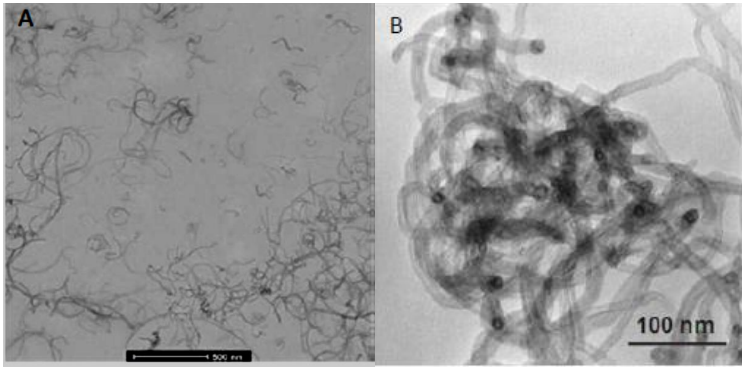
Method	Institution	Results for NM-401
Photo-catalytic activity		
End-point not relevant for MWCNT		
Pour-density		
Weighing	INRS	0.02 g/cm ³
Porosity		
BET	IMC-BAS	Micropore volume (mL/g): 0.0
Octanol-water partition coefficient,		
End-point not relevant		
Redox potential		
OxoDish fluorescent sensor plate for O ₂ detection	NRCWE	The evolution of O ₂ level during 24-hour incubation was measured in three different media. Different dO ₂ values were observed for all applied media. Limited reactivity was found in BSA water dispersions. The maximum dO ₂ change is in the order of 40 µmol/ml. Considering the applied doses, this suggests that the particle reactivity easily can exceed 1 µmol O ₂ /mg.
Radical formation		
Endpoint not investigated		
Composition		
ICP-OES	CODA-CERVA	> 0.01 % : S 0.005 -0.01 % :not detected 0.001-0.005 % : Ag
ICP-MS	Duke University	Na 581 ± 32 ppm, Mg 0 ± 32, Al 59 ± 4 ppm, K 57 ± 9 ppm, Ca 2 ± 1 ppm, V 1 ± 0 ppm, Cr 3 ± 1 ppm, Fe 379 ± 71 ppm, Ni 2 ± 0 ppm, Cu 3 ± 3 ppm, Zn 2 ± 1 ppm, Ba 1 ± 0 ppm, wt (%) of impurities 0.11
EDS	IMC-BAS	C-99.19 (wt %), Si- 500 ppm, , Cu 2300 ppm, Zn 2200 ppm, O (wt%) calculated - 0.6
Presence of catalysts		
TGA	NRCWE	<div style="display: flex; justify-content: space-around;"> <div style="text-align: center;"> <p>TGA of NM401</p> </div> <div style="text-align: center;"> <p>1st derivative of TGA measurement on NM401</p> </div> </div> <p>The curves for the decomposition of different NM-401 masses appear highly repeatable and the decomposition temperature is approximately the same for all runs. However, considering also the residual, there is a large amount of catalyst in the samples, based on which the material appears to be non-homogenous. It is estimated</p>

		that at least 4 mg is needed to get a representative sample
DTA	IMC-BAS	<p>A strong exothermic reaction peaking at ca. 750 °C corresponding well to the TGA is observed.</p>

12.2.3. NM-402, summary of physico-chemical characterisation

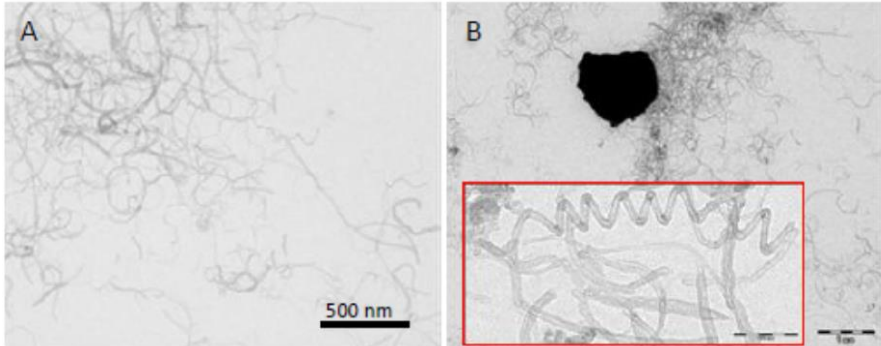
Table 32. Overview of results from the physico-chemical characterisation of NM-402.

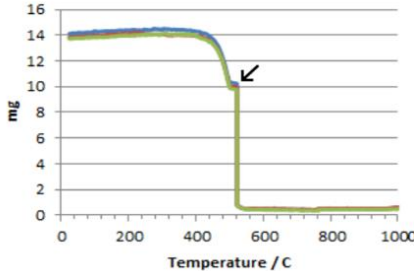
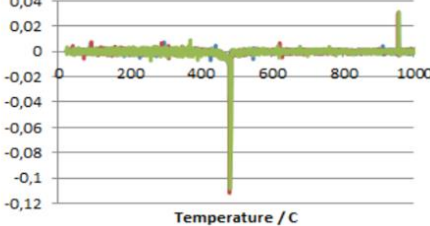
Method	Institution	Results for NM-402
Homogeneity		
Endpoint not investigated		
Agglomeration / aggregation		
Endpoint not relevant		
Water Solubility		
24-hour acellular <i>in vitro</i> incubation test	NRCWE	The 24-hour dissolution ratio of NM-402 was measured in three different media: 0.05% BSA in water, Gambles solution and Caco2 medium. In the dissolution experiments with MWCNT, the actual degradation of MWCNT cannot be assessed from pure elemental analyses. It is assumed that the tubular and graphite carbon material in the MWCNT NMs are non-degradable at the applied test conditions. However, the catalyst and impurity materials identified by elemental analysis and electron microscopy may behave differently. In this study, Al, Co, Fe and Ni were used as indicators for the catalyst dissolution. The measured concentrations of Al and Fe do reach percent levels in NM-402 (1.3 wt % Al; 1.6 wt % Fe) but no dissolution was observed in BSA water and Caco2 cell medium. Al (4.7 wt %) and Fe (1.6 wt %) was found to partially dissolve in Gambles solution.
Crystalline phase		
XRD	IMC-BAS	IMC-BAS investigated the possibility to detect catalyst, carbon allotropes and the MWCNT structure by XRD on powders from NM-402. The X-ray diffractograms show one significant broad reflection and some smaller ones. All peaks were ascribed to reflections from the carbon nanotubes. The carbon nanotubes reflections were used to estimate the wall thickness based on the widths of the reflections. However, it should be strongly emphasized that there is no consensus on whether wall thickness can be properly calculated from powder X-ray diffraction data. Results from the XRD size calculations Standard: 2 nm Rietveld: 2.939 ± 2.061 nm
Raman	NRCWE	For MWCNT the intensity of the D-band increases as compared to the G-band with increasing number walls in the MWCNT. The results from the current analysis showed that NM-402 had a spectroscopic profile with a high G-band intensity and highest D-band.
Dustiness		
Vortex Shaker Method	INRS	Respirable dustiness index (n=1) 4200 ± 0.0375 (mg/kg)
Crystallite size		
Endpoint not relevant		

Method	Institution	Results for NM-402
Representative TEM picture(s)		
TEM	CODA-CERVA, IMC-BAS	 <p>Inorganic catalyst particles appear to occur mainly at the tube ends in NM-402. The second picture shows showing the structure of dense “particle” areas, which consist of highly entangled MWCNT.</p>
Particle size distribution		
TEM	CODA-CERVA	Thickness 11 ± 3 nm Geodesic length 1372 ± 836 nm
	IMC-BAS	Thickness 14.3 ± 2.7 nm
Specific Surface Area		
BET	IMC-BAS	226.4 (m ² /g)
SAXS	CEA	130.3 ± 4.2 (m ² /g)
Zeta Potential (surface charge)		
End-point not relevant for MWCNT		
Surface Chemistry		
End-point not relevant for MWCNT		
Photo-catalytic activity		
End-point not relevant for MWCNT		
Pour-density		
Weighing	INRS	0.11 g/cm ³
Porosity		
BET	IMC-BAS	Micropore volume (mL/g): 0.0
Octanol-water partition coefficient		
End-point not relevant		
Redox potential		
OxoDish fluorescent sensor plate for O ₂ detection	NRCWE	The evolution of O ₂ level during 24-hour incubation was measured in three different media. Different dO ₂ values were observed for all applied media. NM-402 was able to induce significant increase in the oxygen level in BSA water dispersions. The maximum dO ₂ change is in the order of 40 μmol/ml L. Considering the applied doses, this suggests that the particle reactivity easily can exceed 1 μmol O ₂ /mg. NM-402 also caused increased dO ₂ in Gambles solution and Caco2 medium.
Radical formation		
Endpoint not investigated		

12.2.4. NM-403, summary of physico-chemical characterisation

Table 33. Overview of results from the physico-chemical characterisation of NM-403.

Method	Institution	Results for NM-403
Homogeneity		
Endpoint not investigated		
Agglomeration / aggregation		
Endpoint not relevant		
Water Solubility		
24-hour acellular <i>in vitro</i> incubation test	NRCWE	The 24-hour dissolution ratio of NM-403 was measured in three different media: 0.05% BSA in water, Gambles solution and Caco2 medium. In the dissolution experiments with MWCNT, the actual degradation of MWCNT cannot be assessed from pure elemental analyses. It is assumed that the tubular and graphite carbon material in the MWCNT NMs are non-degradable at the applied test conditions. However, the catalyst and impurity materials identified by elemental analysis and electron microscopy may behave differently. In this study, Al, Co, Fe and Ni were used as indicators for the catalyst dissolution. The measured concentrations of Al and Co do reach percent levels in NM-403 (1.0 wt % Al; 0.2 wt % Fe). The results from the analyses suggest slightly different behaviour of the catalyst materials in the three different incubation media. Al (BSA-water (ca. 3 wt %), Gambles solution (50 wt %), and Caco2 cell medium (ca. 3 wt %)) and Co (BSA-water (49 wt %), Gambles solution (60 wt %) and Caco2 cell medium (49 wt %))was found to partially dissolve in all three media: Co was found to partially dissolve in all three media.
Crystalline phase		
Endpoint not investigated		
Dustiness		
Vortex Shaker Method	INRS	Respirable dustiness index (n=1) 4900 ± 0.0439 (mg/kg)
Crystallite size		
Endpoint not relevant		
Representative TEM picture(s)		
TEM	CODA-CERVA, IMC-BAS	 <p>Micrometre unidentified impurity particles (Scale bar 1 µm) were observed. There were also some different morphologies particles such as bent and spiral shaped MWCNT.</p>

Method	Institution	Results for NM-403
Particle size distribution		
TEM	CODA-CERVA	Thickness 12 ± 7 nm Geodesic length 443 ± 222 nm
Specific Surface Area		
SAXS	CEA	189.0 ± 10.8 (m ² /g)
Zeta Potential (surface charge)		
End-point not relevant for MWCNT		
Surface Chemistry		
End-point not relevant for MWCNT		
Photo-catalytic activity		
End-point not relevant for MWCNT		
Pour-density		
Weighing	INRS	0.17 g/cm ³
Porosity		
Endpoint not investigated		
Octanol-water partition coefficient,		
End-point not relevant		
Redox potential		
Endpoint not investigated		
Radical formation		
Endpoint not investigated		
Composition		
ICP-OES	CODA-CERVA	> 0.01 % : Al, Co, Mg, Mn, Ca After Calcination Al : 431 ± 63 (mg/kg) Co : 40 ± 1 (mg/kg)
ICP-MS	Duke University	Na 893 ± 443 ppm, Mg 2231 ± 144 ppm, Al 2024 ± 168 ppm, K 88 ± 40 ppm, Ca 2 ± 1 ppm, V 0 ppm, Cr 3 ± 1 ppm, Mn 2706 ± 182 , Fe 7 ± 4 ppm, Co 2881 ± 190 ppm, Ni 58 ± 4 ppm, Cu 1 ± 0 ppm, Zn 5 ± 1 ppm, Ba 1 ± 1 ppm wt (%) of impurities 1.09
Presence of catalysts		
TGA	NRCWE	<div style="display: flex; justify-content: space-around;"> <div style="text-align: center;"> <p>TGA of NM403</p>  <p>The TGA plot shows weight (mg) on the y-axis (0 to 16) and Temperature (°C) on the x-axis (0 to 1000). The weight remains constant at approximately 14 mg until about 400°C, where it drops sharply to near 0 mg. An arrow points to the start of this weight loss.</p> </div> <div style="text-align: center;"> <p>1st derivative of TGA measurement on NM403</p>  <p>The 1st derivative plot shows the rate of weight change on the y-axis (-0.12 to 0.04) and Temperature (°C) on the x-axis (0 to 1000). A sharp negative peak is observed at approximately 400°C, corresponding to the weight loss event in the TGA plot.</p> </div> </div> <p>These analyses indicate that NM-403 is a very uniform material. The shape of the curves at approximately 400°C marked by an arrow shows a spontaneous combustion.</p>

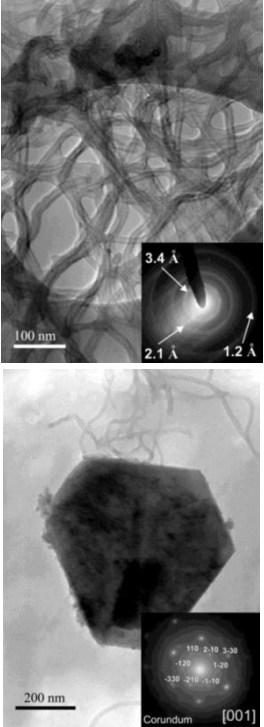
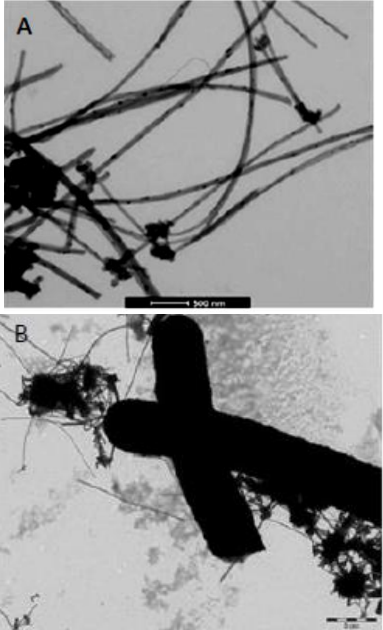
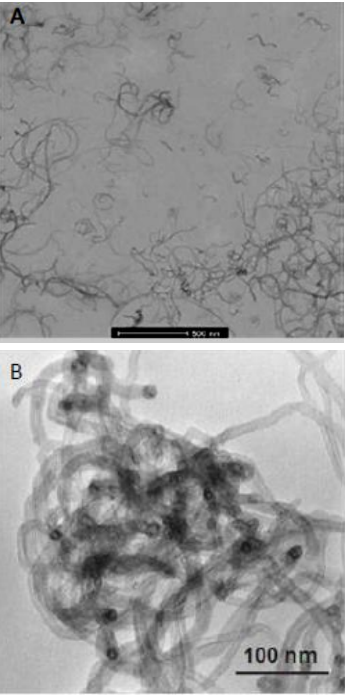
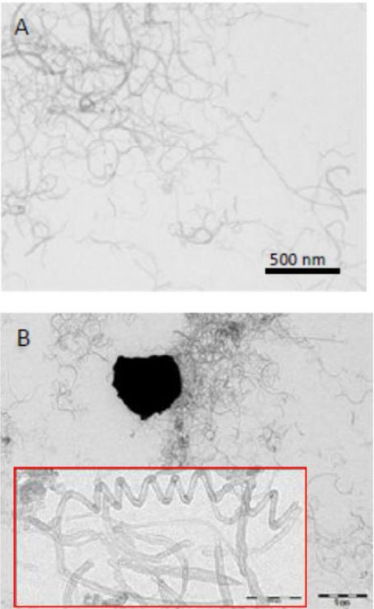
12.2.5. MWCNT NMs, overview of physico-chemical characterisation

Table 34 gives a comparative overview of the test results for the characterisation studies performed on the MWCNT NMs.

Table 34. Comparative overview of the outcome of the characterisation of NM-400, NM-401 , NM-402 and NM-403.

Physico-chemical Properties and Material Characterization (from OECD list) method	NM characterised			
	NM-400	NM-401	NM-402	NM-403
Homogeneity	Endpoint not investigated			
Agglomeration / aggregation	Endpoint not relevant			
<p>Water solubility SDR (24-hour acellular <i>in vitro</i> incubation test)</p> <p>The 24-hour dissolution ratio was measured in three different media: 0.05 % BSA in water, Gambles solution and Caco2 medium.</p>	<p>The 24-hour dissolution ratio of MWCNTs was measured in three different media: 0.05% batch dispersion BSA in water, Gambles solution and Caco2 medium. In the dissolution experiments, the actual degradation of MWCNT cannot be assessed from pure elemental analyses. It is assumed that the tubular and graphite carbon material in the MWCNT NMs are non-degradable at the applied test conditions. However, the catalyst and impurity materials identified by elemental analysis and electron microscopy may behave differently. In this study, Al, Co, Fe and Ni were used as indicators for the catalyst dissolution.</p>			
	<p>The measured concentrations of Al and Fe reach percent levels in NM-400 (1.0 wt % Al; 0.2 wt % Fe). The results from the analyses suggest slightly different behaviour of the catalyst materials in the three different incubation media. For very low concentration elements, higher percentages of dissolution were often found. Sometimes, the dissolved Ni fraction even exceeded 100 %. The fraction of dissolved Co was also relatively high in all test media (14 to 60 wt %). For these two elements, the observed high dissolved fractions may be due to MWCNT elemental concentrations being too low for quantification, material inhomogeneity, or too low yield in the elemental analyses on the powders.</p>	<p>The concentrations of the four selected elements may be too low in NM-401 (≤ 0.06 wt %) for reliable assessment even by ICP-OES. The results from the analyses suggest slightly different behaviour of the catalyst materials in the three different incubation media. For NM-401, no dissolution was detected in BSA water and Caco2 cell medium. For very low concentration elements, higher percentages of dissolution were often found. E.g., about half of the Ni was found to be dissolved. The observed high dissolved fractions may be due to MWCNT elemental concentrations too low for quantification, material inhomogeneity, or too low yield in the elemental analyses on the powders.</p>	<p>The measured concentrations of Al and Fe do reach percent levels in NM-402 (1.3 wt % Al; 1.6 wt % Fe) but no dissolution was observed in BSA water and Caco2 cell medium. Al (4.7 wt %) and Fe (1.6 wt %) was found to partially dissolve in Gambles solution.</p>	<p>The measured concentrations of Al and Co do reach percent levels in NM-403 (1.0 wt % Al; 0.2 wt % Fe). The results from the analyses suggest slightly different behaviour of the catalyst materials in the three different incubation media. Al (BSA-water (ca 3.wt %), Gambles solution (50 wt %), and Caco2 cell medium (ca. 3 wt %)) and Co (BSA-water (49 wt %), Gambles solution (60 wt %) and Caco2 cell medium (49 wt %)) was found to partially dissolve in all three media: Co was found to partially dissolve in all three media.</p>

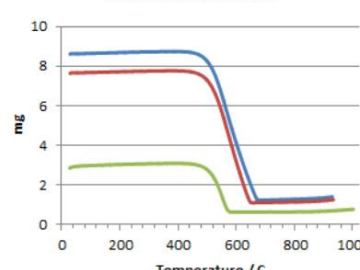
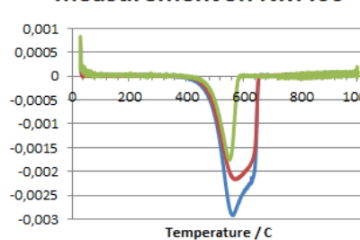
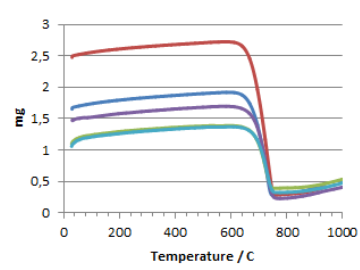
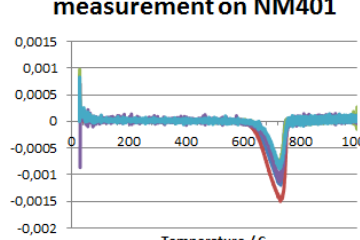
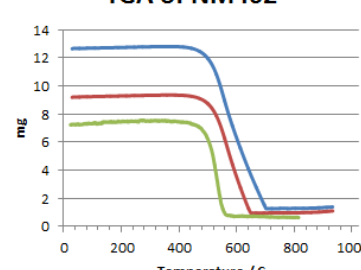
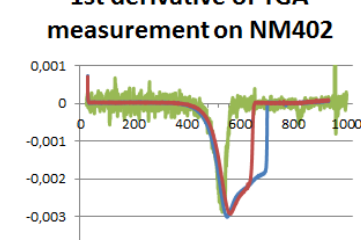
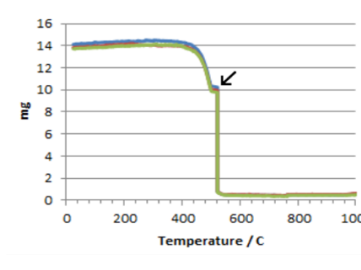
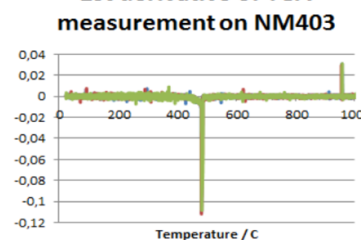
Crystalline phase XRD	<p>The possible detection of catalyst, carbon allotropes and the MWCNT structure by XRD on powders from NM-400 was investigated.</p> <p>The X-ray diffractograms show one significant broad reflection and some smaller ones. All peaks were ascribed to reflections from the MWCNT. The MWCNT reflections were used to estimate the wall thickness based on the widths of the reflections. However, it should be strongly emphasized that there is no consensus on whether wall thickness can be properly calculated from powder X-ray diffraction data.</p> <p>Results from the XRD size calculations Standard: 2 nm Rietveld: 2.832 ± 0.641 nm Standard + Rietveld: 3.2 ± 0.6 nm</p>	<p>The possible detection of catalyst, carbon allotropes and the MWCNT structure by XRD on powders from NM-401 was investigated.</p> <p>The X-ray diffractograms show one significant broad reflection and some smaller ones. All peaks were ascribed to reflections from the MWCNT. Besides MWCNT, graphite may be present in NM-401. The MWCNT reflections were used to estimate the wall thickness based on the widths of the reflections. However, it should be strongly emphasized that there is no consensus on whether wall thickness can be properly calculated from powder X-ray diffraction data.</p> <p>Results from the XRD size calculations</p> <ul style="list-style-type: none"> • Standard: 9 nm <p>(NM-401 + (graphite ?))</p> <ul style="list-style-type: none"> • Rietveld: 8.058 and 12.22 nm • Standard +Rietveld: 8.6 nm (for graphite 2H hkl 002 and 006) 	<p>The possible detection of catalyst, carbon allotropes and the MWCNT structure by XRD on powders from NM-402 was investigated.</p> <p>The X-ray diffractograms show one significant broad reflection and some smaller ones. All peaks were ascribed to reflections from the carbon nanotubes. The carbon nanotubes reflections were used to estimate the wall thickness based on the widths of the reflections. However, it should be strongly emphasized that there is no consensus on whether wall thickness can be properly calculated powder X-ray diffraction data.</p> <p>Results from the XRD size calculations Standard: 2 nm Rietveld: 2.939 ± 2.061 nm</p>	Endpoint not investigated
Raman	For MWCNT the intensity of the D-band increases as compared to the G-band with increasing number walls in the MWCNT.			Endpoint not investigated
Dustiness Vortex shaker method	Respirable dustiness index (n=1) is inferior to 420 mg/kg (corresponding to the limit of detection in mass dustiness index)	Respirable dustiness index (n=1) is inferior to 1700 mg/kg (corresponding to the limit of detection in mass dustiness index)	Respirable dustiness index (n=1) 4200 ± 0.0375 mg/kg	Respirable dustiness index (n=1) 4900 ± 0.0439 mg/kg
Crystallite size	Endpoint not relevant			

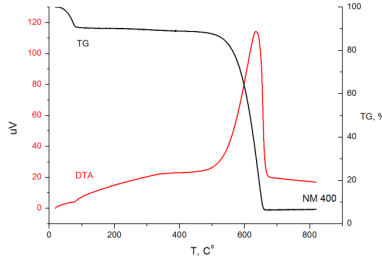
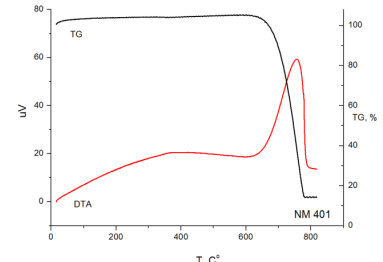
<p>Representative TEM picture(s) TEM</p>	 <p>Corundum crystals (catalyst support material) were observed.</p>	 <p>Inorganic catalyst particles are abundant in the sidewalls of NM-401. The second picture shows some examples of "megatubes" and dense aggregates and agglomerates.</p>	 <p>Inorganic catalyst particles appear to occur mainly at the tube ends in NM-402. The second picture shows the structure of dense "particle" areas, which consist of highly entangled MWCNT.</p>	 <p>Micrometre unidentified impurity particles (Scale bar 1 µm) were observed. There were also some different morphologies particles such as bent and spiral shaped MWCNT.</p>
<p>Particle size distribution TEM</p>	<p>Thickness 11 ± 3 nm Geodesic length 846 ± 446 nm</p>	<p>Thickness 67 ± 24 nm Geodesic length 4048 ± 2371 nm</p>	<p>Thickness 11 ± 3 nm Geodesic length 1372 ± 836 nm</p>	<p>Thickness 12 ± 7 nm Geodesic length 443 ± 222 nm</p>
<p>Specific surface area (SSA) BET</p>	<p>$254.00 \text{ m}^2/\text{g}$</p>	<p>$140.46 \text{ m}^2/\text{g}$</p>	<p>$226.4 \text{ m}^2/\text{g}$</p>	<p>-</p>
<p>SAXS</p>	<p>$189.3 \pm 8.1 \text{ m}^2/\text{g}$</p>	<p>$> 30.5 \pm 1.5 \text{ m}^2/\text{g}$</p>	<p>$130.3 \pm 4.2 \text{ m}^2/\text{g}$</p>	<p>$189.0 \pm 10.8 \text{ (m}^2/\text{g)}$</p>
<p>Zeta potential (surface charge)</p>	<p>End-point not relevant for MWCNT</p>			
<p>Surface chemistry</p>	<p>End-point not relevant for MWCNT</p>			

(where appropriate)				
Photo catalytic activity	End-point not relevant for MWCNT			
Redox potential	The evolution of O ₂ level during 24-hour incubation was measured in three different media: : 0.05% batch dispersion BSA in water, Gambles solution and Caco2 medium.			
	Different dO ₂ values were observed for all applied media. Limited reactivity was found in all BSA water dispersions. The maximum dO ₂ change is in the order of 40 µmol/ml. Considering the applied doses, this suggests that the particle reactivity easily can exceed 1 µmol O ₂ /mg.	Different dO ₂ values were observed for all applied media. Limited reactivity was found in all BSA water dispersions The maximum dO ₂ change is in the order of 40 µmol/ml. Considering the applied doses, this suggests that the particle reactivity easily can exceed 1 µmol O ₂ /mg.	Different dO ₂ values were observed for all applied media. NM-402 was able to induce significant increase in the oxygen level in BSA water dispersions. The maximum dO ₂ change is in the order of 40 µmol/ml L. Considering the applied doses, this suggests that the particle reactivity easily can exceed 1 µmol O ₂ /mg.	-
Radical formation	Endpoint not investigated			
Pour-density Weighing	0.08 g/cm ³	0.02 g/cm ³	0.11 g/cm ³	0.17 g/cm ³
Porosity BET	Micropore volume (mL/g): 0.0	Micropore volume (mL/g): 0.0	Micropore volume (mL/g): 0.0	
Octanol-water partition coefficient	End-point not relevant			
Other relevant information (where available)				
Elemental analysis/impurities Semi-quantitative ICP-OES	> 0.01 % : Al, Fe, Na, S 0.005 -0.01 % : Co 0.001-0.005 % : Ca, K After Calcination Al : 2540 ± 14 (mg/kg) Fe :387 ± 25 (mg/kg) Co : 161 ± 25 (mg/kg)	> 0.01 % : S 0.005 -0.01 % :not detected 0.001-0.005 % : Ag	> 0.01 % : Al, Fe, S After Calcination Al : 2025 ± 35 (mg/kg) Fe : 1255 ± 78 (mg/kg) Co : n.d.	> 0.01 % : Al, Co, Mg, Mn, Ca After Calcination Al : 431 ± 63 (mg/kg) Co : 40 ± 1 (mg/kg)
Elemental analysis/impurities Semi-quantitative EDS	C -89.81 (wt %), Al- 46100 ppm, Si- 400 ppm, Fe- 7600 ppm, Co 2500 ppm, Cu 2000 ppm, Zn 1900 ppm, O (wt%) calculated- 4.15	C-99.19 (wt %), Si- 500 ppm, , Cu 2300 ppm, Zn 2200 ppm, O (wt%) calculated - 0.6	C-92.97 (wt %), Al- 21100 ppm, Si- 500 ppm, Fe - 29800 ppm, Cu- 400 ppm, O (wt %) calculated- 1.93	
Elemental analysis/impurities ICP-MS	Na 600 ppm, Cr 14 ppm, Mn 2 ppm, Fe 4300 ppm, Co 3700 ppm, Ni 17 ppm, Cu 1 ppm, As 5 ppm, Mo 1		Cr 10 ppm, Mn 17 ppm, Fe 16000 ppm, Co 5 ppm, Ni 11 ppm, Cu 4 ppm, Zn 1 ppm, Mo 1 ppm, Ag 0.3 ppm, Sn 0.5 ppm, Ba 0.3 ppm, Pb 1.2 ppm, La	

Elemental analysis/impurities ICP-MS

Presence of catalysts

<p>ppm, Ag 0.3 ppm, Sn 0.5 ppm, Ba 0.3 ppm, Pb 1.5 ppm wt (%) of impurities 0.87</p>		<p>0.1 ppm, Ce 0.3 ppm wt (%) of impurities 1.6</p>	
<p>Na 1345 ± 151 ppm, Al 9951 ± 31 ppm, K 97 ± 3 ppm, Ca 3 ± 2 ppm, V 0 ppm, Cr 9 ± 1 ppm, Fe 1988 ± 26 ppm, Co 693 ± 26 ppm, Ni 4 ± 0 ppm, Cu 3 ± 0 ppm, Zn 2 ± 0 ppm, Ba 1 ± 0 ppm, Pb 1 ± 0 ppm wt (%) of impurities 1.41</p>	<p>Na 581 ± 32 ppm, Mg 0 ± 32, Al 59 ± 4 ppm, K 57 ± 9 ppm, Ca 2 ± 1 ppm, V 1 ± 0 ppm, Cr 3 ± 1 ppm, Fe 379 ± 71 ppm, Ni 2 ± 0 ppm, Cu 3 ± 3 ppm, Zn 2 ± 1 ppm, Ba 1 ± 0 ppm, wt (%) of impurities 0.11</p>	<p>Na 727 ± 120 ppm, Al 12955 ± 1530 ppm, K 85 ± 7 ppm, Ca 2 ± 1 ppm, V 1 ± 0 ppm, Cr 13 ± 1 ppm, Mn 9 ± 1 ppm, Fe 16321 ± 664 ppm, Co 2 ± 0 ppm, Ni 9 ± 1 ppm, Cu 4 ± 1 ppm, Zn 2 ± 0 ppm, Ba 1 ± 0 ppm, wt (%) of impurities 3.01</p>	<p>Na 893 ± 443 ppm, Mg 2231 ± 144 ppm, Al 2024 ± 168 ppm, K 88 ± 40 ppm, Ca 2 ± 1 ppm, V 0 ppm, Cr 3 ± 1 ppm, Mn 2706 ± 182, Fe 7 ± 4 ppm, Co 2881 ± 190 ppm, Ni 58 ± 4 ppm, Cu 1 ± 0 ppm, Zn 5 ± 1 ppm, Ba 1 ± 1 ppm wt (%) of impurities 1.09</p>
<p>TGA of NM400</p>  <p>1st derivative of TGA measurement on NM400</p>  <p>NM-400 shows a strong wide exothermic peak between 500 and 600 °C corresponding to the temperature range with high weight loss in TGA. The first derivative show more than one decomposition temperature for the two large samples, indicating more than one type of carbon material. The small sample appears to contain only one type</p>	<p>TGA of NM401</p>  <p>1st derivative of TGA measurement on NM401</p>  <p>The curves for the decomposition of different NM-401 masses appear highly repeatable and the decomposition temperature is approximately the same for all runs. However after considering the residual, there is a large amount of catalyst in NM-401. From the amount of</p>	<p>TGA of NM402</p>  <p>1st derivative of TGA measurement on NM402</p>  <p>The analyses of NM-402 indicate non-homogenous material. The three curves are all different (the green one has one decomposition temperature, the red one has two and the blue one has several peaks). From these data, more than 13 mg is necessary to get a</p>	<p>TGA of NM403</p>  <p>1st derivative of TGA measurement on NM403</p>  <p>Theses analyses indicate that NM-403 is a very uniform material. The shape of the curves at approximately 400°C marked by an arrow shows a spontaneous combustion.</p>

DTA	<p>of carbon nanotube. Comparing the data, a representative sample size is minimum 8 mg.</p>	<p>catalysts, the material appears to be non-homogenous and at least 4 mg is needed to obtain a representative sample.</p>	<p>representative sample.</p>	
	 <p>NM-400 shows a strong wide exothermic peak between 500 and 600 °C corresponding to the temperature range with high weight loss in TGA.</p>	 <p>A strong exothermic reaction peaking at ca. 750 °C corresponding well to the TGA is observed.</p>	-	-

13. References

- Baron P.A., Maynard A.D. and Foley M. (2002) Evaluation of Aerosol Release During the Handling of Unrefined Single Walled Carbon Nanotube Material. NIOSH DART-02-191
- Bau S., Witschger O., Gensdarmes F., Rastoix O. and Thomas D. (2010) A TEM-based method as an alternative to the BET method for measuring off-line the specific surface area of nanoaerosols. *Powder Technology*, 200(3), pp.190-201.
- Birkedal R., Shivachev, B., Dimova L., Petrov O., Nikolova, R., Mast, J., De Temmerman, P.-J., Waegeneers, N., Delfosse, L., Van Steen, F., Pizzolan, J.C. and De Temmerman, L., (2012) Deliverable 4.3: Crystallite size, mineralogical and chemical purity of NANOGENOTOX nanomaterials. Edited by Jensen K.A. and Thieret N., October 2012, pp. 71
- Brunauer S., Emmett P. H. & Teller E. (1938) Adsorption of gases in multimolecular layers. *J. Am. Chem. Soc.* 60, pp. 309
- Cedervall T., Lynch I., Lindman S., Berggård T., Thulin E., Nilsson H., Dawson K.A. and Linse S. (2007) Understanding the nanoparticle–protein corona using methods to quantify exchange rates and affinities of proteins for nanoparticles. *The National Academy of Sciences of the USA, PNAS*, 104 (7), pp. 2050
- Christensen V.R., Jensen S.L., Guldberg M. and Kamstrup O. (1995) Effects of chemical composition of man-made vitreous fibers on the rate of dissolution in vitro at different pHs. *Environmental Health Perspectives* 102 (5), pp.83
- Cho W.S., Duffin R., Howie S.E.M., Scotton C.J., Wallace W.A.H., MacNee W., Bradley M., Megson I.L. and Donaldson K. (2011) Progressive severe lung injury by zinc oxide nanoparticles; the role of Zn²⁺ dissolution inside lysosomes. *Particle and Fibre Toxicology*, 8 (27)
- De Temmerman, P.-J., van Van Doren E., Verleysen E., van Van der Stede Y., Francisco M.A.D. and Mast J. (2012) Quantitative characterization of agglomerates and aggregates of pyrogenic and precipitated amorphous silica nanomaterials by transmission electron microscopy. *Journal of Nanobiotechnology*, 10 (24)
- Dick C.A.J., Brown D.M., Donaldson K. and Stone V. (2003) The role of free radicals in the toxic and inflammatory effects of four different ultrafine particle types. *Inhalation toxicology* 15 (1), pp. 39
- EC (European Commission) (2011) Commission Recommendation of 18 October 2011 on the definition of nanomaterial (2011/696/EU). *OJ L 275*, 20.10.2011, pp. 38
- EFSA (2011) Guidance on the risk assessment of the application of nanoscience and nanotechnologies in the food and feed chain [<http://www.efsa.europa.eu/en/efsajournal/doc/2140.pdf>]
- Förster H. and Tiesler H. (1993) Contribution to comparability of in vitro and in vivo man-made mineral fibre (MMMMF) durability experiments. *Glastechnology Bereitung*, 66 (10), pp. 255
- Ge C., Lao F., Li W., Li Y., Chen C., Qiu Y., Mao X., Li B., Chai Z. and Zhao Y. (2008) Quantitative Analysis of Metal Impurities in Carbon Nanotubes: Efficacy of Different Pretreatment Protocols for ICPMS Spectroscopy. *Analytical Chemistry*, 80 (24), pp. 9426
- Isamu O, Hiromu S and Masashi G (2009) Dustiness testing of engineered nanomaterials. *J. Phys.: Conf. Series*, 012003
- ISO (2004) ISO 13322-1: Particle size analysis -Image analysis methods-. In: Part 1: Static image analysis methods.

- ISO (2008) ISO 9276-6: Part 6: Descriptive and quantitative representation of particle shape and morphology. In: Representation of results of particle size analysis. Geneva.
- Jensen K.A. et al. (2012). Presentation. "Nanomaterial dustiness. A comparison between three different methods" [http://www.nanosafe.org/home/liblocal/docs/Nanosafe2012/presentations%20orales/Session%205/O5c1%20Jensen%20et%20al_Dustiness%203%20Methods%20Comparison_NANOSAFE2012%20vs%20\[Mode%20de%20compatibilit%C3%A9\].pdf](http://www.nanosafe.org/home/liblocal/docs/Nanosafe2012/presentations%20orales/Session%205/O5c1%20Jensen%20et%20al_Dustiness%203%20Methods%20Comparison_NANOSAFE2012%20vs%20[Mode%20de%20compatibilit%C3%A9].pdf)
- Kim S.H., Mulholland G.W. and Zachariah M.R. (2009) Density measurement of size selected multiwalled carbon nanotubes by mobility-mass characterization. Carbon, 47, 1297-1302.
- Kumar M. and Ando Y. (2010) Chemical Vapor Deposition of Carbon Nanotubes: A review on Growth Mechanism and Mass production. Journal of Nanoscience and Nanotechnology, 10, 3739-3758
- Linsinger T., Roebben G., Gilliland D., Calzolari L., Rossi F., Gibson N. and Klein C. (2012) Requirements on measurements for the implementation of the European Commission definition of the term 'nanomaterial'. 52 pp. EUR 25404 EN
- Morris J., Willis J., Di Martinis D., Hansen B., Laursen H., Riego Sintes, J., Kearns P., Gonzalez, M. (2011) Science policy considerations for responsible nanotechnology decisions. Nature Nanotechnology, 6:73-77.
- Nordstöm, D.K. and Munoz, J.L. (1994) Geochemical Thermodynamics. Second edition. Blackwell Scientific Publications. 493 pp.
- OECD (2010). ENV/JM/MONO(2009)20-REV-ENG. Guidance Manual for Sponsors, OECD, Paris.
- OECD (2012). ENV/JM/MONO(2012)40. Guidance on sample preparation and dosimetry for the safety testing of manufactured nanomaterials, OECD, Paris.
- Olferta J.S., Symonds J.P.R. and Collings N. (2007) The effective density and fractal dimension of particles emitted from a light-duty diesel vehicle with a diesel oxidation catalyst. Journal of Aerosol Science, 38, pp. 69
- Osmond-McCloud, M.J., Poland C.A., Murphy F., Waddington L., Morris H., Hawkins S.C., Clark S., Aitken R., McCall M.J. and Donaldson K. (2011) Durability and inflammogenic impact of carbon nanotubes compared with asbestos fibres. Particles and Fibre Toxicology 8 (15)
- Roebben, G., Rasmussen, K., Kestens, V., Linsinger, T. P. J., Rauscher, H., Emons, H. and Stamm, H. (2013) Reference materials and representative test materials: the nanotechnology case. Journal of Nanoparticle Research, 15, pp. 1455
- SCENIHR (2009). Scientific Committee on Emerging and Newly Identified Health Risks (SCENIHR), Opinion on "Risk Assessment of Products of Nanotechnologies", Brussels.
- SCENIHR (2010) Scientific Basis for the Definition of the Term "Nanomaterial" [http://ec.europa.eu/health/scientific_committees/emerging/docs/scenih_r_o_030.pdf]
- Schneider T. and Jensen K.A. (2008) Combined single drop and rotating drum dustiness test of fine to nanosized powders using a small drum. Annals of Occupational Hygiene 52(1): pp. 23
- Schneider T. and Jensen K.A. (2009) Relevance of aerosol dynamics and dustiness for personal exposure to manufactured nanoparticles. Journal of Nanoparticle Research, 11, pp. 1637
- Sebastian K., Fellman J., Potter R., Bauer J., Searl A., de Meringo A., Maquin B., de Reydellet A., Jubb G., Moore M., Preininger R., Zoitos B., Boymel P., Steenberg T., Madsen A.L. and Guldborg M. (2002) EURIMA test guideline: In vitro acellular dissolution of man-made vitreous silicate fibres. Glass Science Technology 75(5), pp. 263

- Wiecinski, P.N., Metz K.M., Mangham, A.N., Jacobson, K.H., Hamers, R.J., and Pedersen, J.A (2009) Gastrointestinal biodurability of engineered nanoparticles: Development of an in vitro assay, *Nanotoxicology*, 3 (3), pp. 202-U66
- Witschger O., Brouwer D., Jensen K.A., Koponen I.K., Berges M., Jankowska E., Dahman D., Burdett G. and Bard D. (2011) DUSTINANO: A PEROSH initiative towards a harmonized approach for evaluating the dustiness of nanopowders. 5th International Symposium on Nanotechnology, Occupational and Environmental Health August 9 - August 12, 2011 — Boston, MA, USA, in abstract book, pp.178
- Xia T., Kovochich M., Brant J., Hotze M., Sempf J., Oberley T., Sioutas C., Yeh J.I., Wiesner M.R., and Nel, A.E. (2006) Comparison of the abilities of ambient and manufactured nanoparticles to induce cellular toxicity according to an oxidative stress paradigm, *Nano Letters*, 6 (8), pp. 1794
- Xinyuan L., Robert H.H. and Agnes K.B. (2010) Biodurability of single-walled carbon nanotubes depends on surface functionalization. *Carbon*, 48(7), pp.1961

A. Appendix. The Sensor Dish Reader System

The hydrochemical reactivity was assessed regarding acid-base reactivity and influence on the oxygen balance using a recently developed 24-well SDR (Sensor Dish Reader) system (PreSens Precision Sensing GmbH, Germany) intended for use for in vitro assays (Figure A1). Determination of the acid-base reactivity is particularly important in cell media, where a buffer usually is applied to ensure pH stability in the bioassay. However, if a NM is particularly reactive, this pH buffer may be insufficient at sufficiently high NM doses. The O₂ reactivity may be another important parameter and relates to hydrochemical reactions that consume or liberate oxygen. Deviations in the O₂-balance can be caused by different reactions including redox-reactions, protonation and deprotonation in the dispersion. These phenomena may be caused by catalytic reactions, but also dissolution, transformation of molecular speciation and precipitation in the medium under investigation.



Figure A1. Sensor Dish Reader, examples of sensor products and illustration of the SDR measurement principle. In this study we used the 24-well Oxy- and HydroDish for O₂ and pH monitoring. Source: PreSens Precision Sensing GmbH, Germany.

The pH variation was measured using the HydroDish® fluorescent sensor plate for pH detection with up to ± 0.05 pH resolution for pH 5 to 9. Measurement is not possible outside of this range.

The O₂ variation was measured using the OxoDish® fluorescent sensor plate for O₂ detection with ± 2 % air saturation resolution. The OxoDish® sensor can measure O₂ concentrations between 0 and 250% saturation, corresponding to 0 to 707.6 µmol/l.

In brief, the fluorescent sensor spots are placed at the bottom of each well in the dishes. For our study, we used 24 well plates. The sensor spot contains a luminescent dye. It is excited by the SensorDish® Reader using a laser diode, placed below the multidish, which is only active when analyses are done, and the sensor luminescence lifetime is detected through the transparent bottom. The luminescence lifetime of the dye varies with the oxygen partial pressure (OxoDish®) and the pH of the sample (HydroDish®), respectively. This signal is converted to oxygen and pH values by the instrument software. The sensor plates are pre-calibrated and the calibration data are uploaded and used for the specific plates used.

Experimental Procedure

Samples were prepared by prewetting the NMs with 0.5% v/v ethanol and dispersion in 0.05% w/v BSA water by probe-sonication following the generic NANOGENOTOX dispersion protocol. Chemically pre-analyzed and approved Nanopure filtered water was used for the batch dispersion to ensure minimum background contamination in the test.

The incubation media included 0.5% BSA-water, low-Ca Gambles solution and Caco2 medium. The BSA water was included in the study to assess the behaviour of the NMS in the batch dispersion medium, which is the first stage in all the biological tests in NANOGENOTOX. The reactivity was tested at doses 0.32, 0.16, 0.08 and 0 mg/ml and a total volume of 2 ml was entered into each well of the SDR plates. Figure A2 illustrates the general procedure.

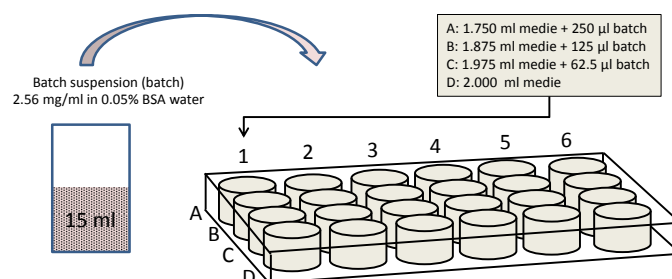


Figure A2. Principal sketch of the dosing into the SDR plates resulting in 2 ml test medium in each well. In this way six dose-response measurements can be made in one test round.

After 24-hours incubation, the maximum dose and control media from the pH and O₂ wells were retrieved by pipette, filtered through a 0.2 µm CAMECA syringe filter and centrifuged in Eppendorf tubes for 60 minutes at 20 000 x G RCF using a Ole Dich table top centrifuge. NM samples were placed in the outer ring and pure reference media in the inner ring. Then the upper 1.25 ml of each filtrate from the pH and O₂ wells were sampled, pooled (2.5 ml) in Eppendorf tubes and stabilized with 1 ml 2% HNO₃ water (sample diluted 5/7). The liquids

were then stored in darkness until sent for analyses. All vials were washed and rinsed in acid before use.

Data Treatment and Evaluation

The reactivity of each NM was evaluated qualitatively from the evolution of the pH and O₂ over time for each NM at the four dose levels, including the blank control. The SDR pH-values were plotted directly as function of time. The data were then evaluated visually comparing the SDR values of exposed wells with that of the un-exposed control media as well the readings from the initial medium readings in each of the wells to assess if there would be any systematic off-set in some of the sensors. This sensor-evaluation was always done using the blank control as the assumed correct internal reference value.

For the O₂ analyses, the difference between time-resolved readings from "exposure doses" and the medium control ($dO_2 = (O_{2,dose} - O_{2,medium\ control})$) were plotted as function of time.

For both pH and O₂, if the SDR readings from the dosed media showed no difference or followed the same trend as the reference media, the NM was assumed to have negligible pH reactivity or influence on the oxygen balance through redox reactivity or dissolution.

Nanomaterial dissolution and biodurability

The NM dissolution and biodurability was assessed from elemental analyses of the solute adjusted for background concentrations in the three test media. It was assumed that maximum dissolution would be observed at the 0.32 mg/ml dose and that equilibrium was reached in 24 hours. Consequently, if the elemental composition of the test materials is given, the results enable calculation of the solubility limit as well as the durability (the undissolved residual) of the specific NM in the batch dispersion, the lung lining fluid and the Caco2 medium. However, in this study, we have only semi-quantitative elemental composition data on the MWCNT.

Elemental analysis

The concentrations of dissolved Si elements in the media were analysed using Inductively Coupled Plasma-Optical Emission Spectroscopy. Ti, Al, Fe, Co, and Ni were determined by ICP Mass-spectrometry. Both element series were analysed as a commercial service by Eurofins, DK-6600 Vejen, Denmark. The elemental background concentrations in the three test media were determined on three doublet samples for each media. The elemental concentrations after dissolution were determined in two sub-samples for each NM.

B. Appendix. SOP for Small Angle X-ray Scattering.

This appendix describes the general procedure applied at CEA/LIONS (Laboratoire Interdisciplinaire sur l'Organisation Nanométrique et Supramoléculaire) to perform Small Angle X-ray Scattering measurements and the data treatment to extract physico-chemical properties of materials. This procedure was applied to characterize the SAS NMs as powders and in aqueous suspension.

General description

Small-Angle X-ray Scattering is a technique based on the interaction between X-rays and electrons to probe the structure of materials. The processed data is the number of X-rays scattered by a sample as a function of angular position of a detector, see Figure D1.

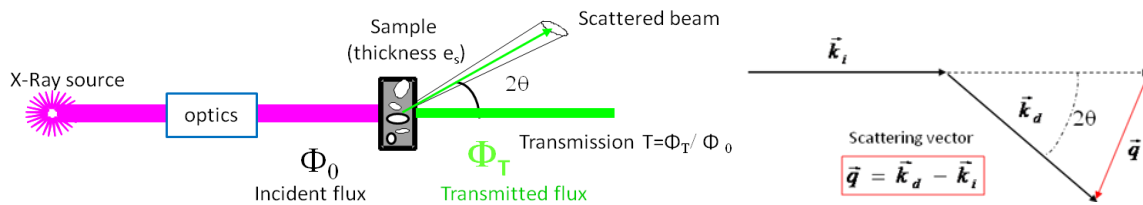


Figure D1. Schematic set up for SAXS and physical quantities

2D raw data images are converted into diffractograms displaying the **scattered intensity I** as a function of scattering vector q defined by:

$$q = \frac{4\pi \sin\theta}{\lambda}$$

λ : X-ray wavelength

The experimental scattering intensity is defined as the differential scattering cross-section per unit volume of sample and can be expressed as follows:

$$I(q) = \frac{1}{V} \frac{d\sigma}{d\Omega} = \frac{\eta_1 C_{ij}}{\eta_2 (\Phi_0 S T) dt \Delta\Omega e}$$

σ : scattering cross-section

V : volume of sample

C_{ij} : number of counts detected on a pixel ij during dt

η_1 : detector quantum efficiency when measuring the direct beam

η_2 : detector quantum efficiency for the count C_{ij}

(ϕ_0ST): flux (in detector unit counts/s) integrated over the whole beam transmitted by the sample

T: transmission of the sample

$\Delta\Omega$: solid angle covered by one pixel seen from the centre of the sample ($\Delta\Omega = p^2/D^2$ with p the pixel size and D the sample to detector distance)

The intensity is then expressed in **absolute scale** (in cm^{-1}) to be independent of the experimental set up parameters (X-ray wavelength, experimental background, time for acquisition, sample thickness, etc.).

General theorems of experimental physics have been developed to extract different properties of nanostructured material from the diffractograms, such as shape of nanoparticles, surface area, interactions occurring, etc. $I(q)$ curves can also be theoretically calculated from assumed nanostructures to fit the experimental curves.

In the simple case of binary samples, the scattering intensity is proportional to:

- the electronic contrast, more precisely the square of scattering length density difference between the two materials $(\Delta\rho)^2$,
- the concentration of the scattering object (in volume fraction), in case of suspensions for example.

Ultra Small Angle X-ray Scattering (USAXS) measurements give access to X-ray scattering data for a range of smaller q and then complement the SAXS diffractograms. It requires a specific and very precise set-up, different from the one used for SAXS.

Equipment

The experimental set up (X-ray source, optical elements, detectors, etc.) and the procedure for absolute scaling of data has been thoroughly described by Zemb (Zemb et al., 2003) and Né (Né et al., 2000).

Apparatus

The main set up components used for SAXS and USAXS experiments at CEA/LIONS are listed below:

- X-ray generator : Rigaku generator RUH3000 with copper rotating anode ($\lambda = 1.54 \text{ \AA}$), 3kW
- Homemade optic pathways and sample holders (with two channel-cut Ge (111) crystals in Bonse/Hart geometry for USAXS set up (Lambard et al., 1992)
- Flux measurement for SAXS set up : pico amperemeter Keithley 615
- Flux measurement for USAXS set up : DonPhysik ionization chamber

- Detector for SAXS set up : 2D image plate detector MAR300
- Detector for USAXS set up: 1D high count rate CyberStar X200 associated to a scintillator/ photomultiplier detector.

All experimental parameters are monitored by computer by a centralized control-command system based on TANGO, and interfaced by Python programming. 2D images are treated using the software *ImageJ* supplemented with some specific plugging developed at CEA/LIONS by Olivier Taché (Taché, 2006).

Calibration

A sample of 3 mm of Lupolen® (semi crystalline polymer) is used for the calibration of the intensity in absolute scale, the maximum intensity being adjusted to 6 cm⁻¹.

A sample of 1 mm of octadecanol is used for the calibration of the q range (calculation of sample-to-detector distance), the position of the first peak standing at 0.1525 Å⁻¹.

Calibrations in intensity and in q range are performed before each series of measurements.

Sample preparation

Almost any kind of material can be analysed by SAXS, whether as a powder, a colloidal suspension, a gel, or even self-supported hybrid materials, as long as the sample prepared meets some requirements of transmission and scattering properties.

Depending on the X-ray absorption coefficient of the material and its scattering properties, the sample thickness has to be adjusted to get a transmission as close as possible to the target transmission of 0.3 (optimal absorption/transmission ratio).

The sample thickness e is directly linked to the transmission T by the following equation:

$$e = -\frac{1}{\mu} \ln (T)$$

μ : X-ray absorption coefficient of the material,

T : transmission, $T = \text{transmitted flux} / \text{incident flux of the direct beam}$

If not self-supported (liquids, powders or gel), the material to be analysed is inserted in a cell, which can be made of glass (capillary), or X-ray transparent material such as Kapton® (polyimide). A measurement of the empty cell is performed and subtracted as a background for the sample measurement. See Figure D2 for examples of cells used at CEA/LIONS.

Powders

The absorption coefficient depends on the material and on the energy. For the Cu K-alpha emission (8 keV) used here, the coefficient, μ_{MWCNT} , for MWCNT is 6 cm^{-1} and the optimal sample thickness (equivalent thickness of dense material) to get a transmission of 0.3 is 2 mm.

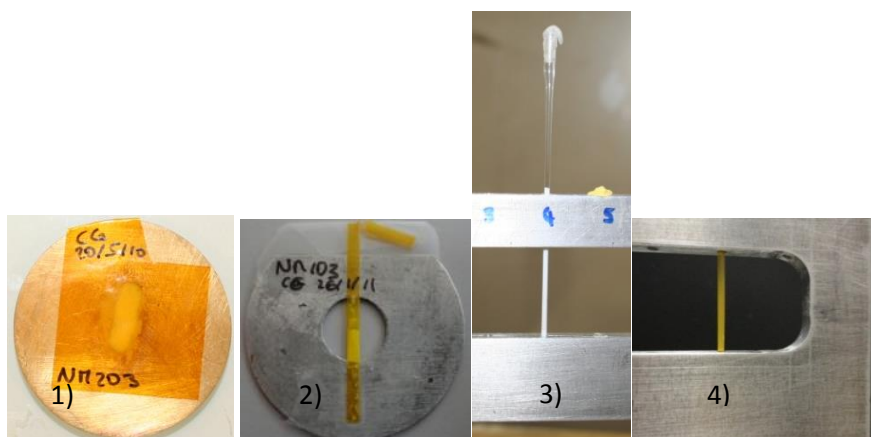


Figure D2. Examples of different type of cells used for SAXS measurements, 1) double sticky kapton® cell for powders, 2) 1.5 mm flattened polyimide capillary for powders, 3) 1.5 mm glass capillary for powder or liquid samples, 4) 1.5 mm polyimide capillary for powder or liquid samples.

SAXS measurements were performed by CEA using kapton capillaries of internal thickness 1.425 mm and run for 3600s.

Material	Cell	e_B (μm)	T_{exp}
NM-400	two sticky kapton films (5 mm cell)	745	0.64
NM-401	two sticky kapton films (15 mm cell)	1124	0.52
NM-402	two sticky kapton films (5 mm cell)	1190	0.5
NM-403	two sticky kapton films (5 mm cell)	1320	0.46

Aqueous suspensions

The usual thickness of aqueous samples for SAXS measurement is 1mm with an acquisition time of 1 hour. Dispersions for analysis are typically produced by sonication in a dispersion medium. The concentration required for analysis depends on the relative scattering length densities between particles and dispersion medium, and the density of materials. The sample must be stable within the time-frame of the measurement.

Measurements

In order to calculate the sample transmission, the flux of incident and transmitted beam are measured and averaged over 200 s before running the SAXS measurement. The time of acquisition necessary for SAXS experiment depends on the sample properties.

For aqueous suspensions prepared for NANOGENOTOX, SAXS measurements were performed in kapton capillaries of internal thickness 1.425 mm and run for 3600s, leading to transmissions of about 0.25. USAXS measurements were performed in 1 mm or 1.5 mm non-sticky double kapton cells, cell types are shown on Figure D2.

Data treatment

Raw data, translated into intensity as a function of the scattering vector q , are first normalized by parameters of the experiments such as acquisition time, sample thickness and calibration constants determined using reference samples, thus expressing data in absolute scale (cm^{-1}). Backgrounds are then subtracted. To get continuous diffractograms for the whole q range SAXS data obtained for short and long times are combined with USAXS data.

For powder samples, the Porod law is applied to extract specific surface areas of raw materials. Data from suspensions are fitted with a model describing fractal aggregates of primary particles. In this model, the whole q range is divided into sections reflecting different structural levels in the sample, and fitted by local Porod and Guinier scattering regimes. Intensity average parameters are then determined such as radius of gyration for the primaries and for the aggregates, and a fractal dimension for the aggregates. Invariants are calculated, which give a correlation between the sample concentration and the specific surface area obtained in suspension.

Raw data treatment

SAXS data

Radial averaging of 2D image (ImageJ)

2D images from the detector are converted into Intensity = $f(\text{scattering vector } q)$ graphs by the software ImageJ together with SAXS plugging. The process follows mainly these steps:

- Determination of the centre coordinates (direct beam position)
- Application of a mask to remove pixels corresponding to the beam stop and around the photodiode

- Radial averaging of the intensity, knowing pixel size, sample-detector distance and wavelength (example of parameters in Figure D3), conversion of pixel position into scattering vector q , and creation of a .rgr file containing $I(q)$ data.

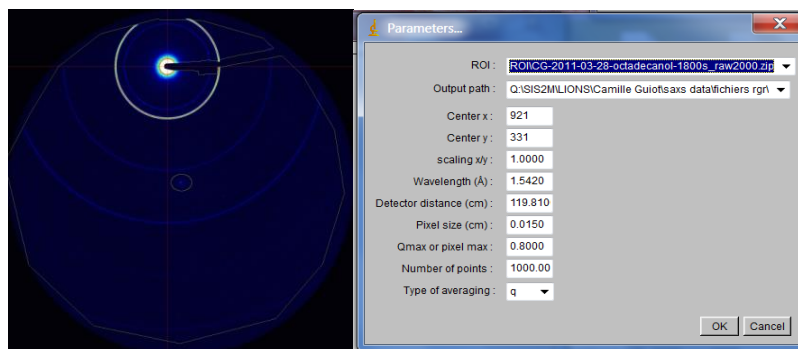


Figure D3. Example of raw 2D image (octadecanol) and parameters used for radial averaging with ImageJ

Absolute scaling of $I(q)$ (pySAXS)

In order to scale the data to the absolute scale in cm^{-1} , $I(q)$ data generated by *ImageJ* as .rgr files are treated by a homemade program called *pySAXS* and based on python programming.

The scaling involves a subtraction of the detector background and normalization by exposition time, sample transmission, sample thickness and K constant. The K constant is calibrated with Lupolen® sample and allows conversion of intensity in photons into absolute intensity in cm^{-1} . An example of parameters used for the scaling is shown on Figure D4.

The subtraction of the empty cell signal and normalization by the sample thickness can be done in a subsequent step.

USAXS data

Raw USAXS data are generated as intensity vs angle data in .txt files. Data treatment is achieved using *pySAXS* and involves the following steps:

- Subtraction of the “rocking curve” (signal with empty cell) normalized by the intensities at 0° (transmission).
- Desmearing, taking into account the effective size of the “punctual” detector (cf reference 0)
- Conversion of angle into q range
- Normalization by the sample thickness.



Figure D4. Example of SAXS scaling parameter file from PySAXS software

Data analysis

General theorems of X-ray scattering have been developed to analyse SAXS data. Here are presented some simple laws for **binary systems** (two phase samples) that may be of use in NANOGENOTOX framework.

Porod's Law

In the high q range, sample diffractograms display an intensity decreases in a q^{-4} trend, called the "Porod region". This region corresponds in the "real space" to the scale of the interfaces (for smooth interfaces).

Therefore, for a binary sample, the asymptotic limit of the so-called "Porod's plateau", when data are represented in Iq^4 , is related to the total quantity of interface Σ (in m^2/m^3) between the two phases, as follows:

$$\Sigma [m^{-1}] = \frac{\lim_{\text{plateau}} (I \cdot q^4)}{2\pi (\Delta\rho)^2}$$

where $\Delta\rho$ is the difference in scattering length density between the two phases. For a binary sample of **known thickness**, the volume fraction of a material φ_A , its specific surface area S_A/V_A (surface developed/ volume of A in the binary sample) and Σ are linked by the following relation:

$$\Sigma [m^{-1}] = \frac{S_A}{V_A} \varphi_A$$

For example, for a suspension of oxide in water, the determination of Porod plateau gives access to the concentration of the sample if the specific surface area of particles suspended is known (and vice versa).

Specific surface area determination from SAXS on powders

To treat raw SAXS data and get absolute intensities, the intensity by the thickness of the scattering material need to be normalised. However, for powder samples, the sample thickness is not well defined and cannot be precisely controlled as it depends on the powder compaction and the different scales of porosity, see Figure D5. To elude this problem, a model system is used, considering the effective thickness of material crossed by X-rays, called e_B , corresponding to an equivalent thickness if all the material would be arranged in a fully dense (no inner or outer porosity) and uniform layer.

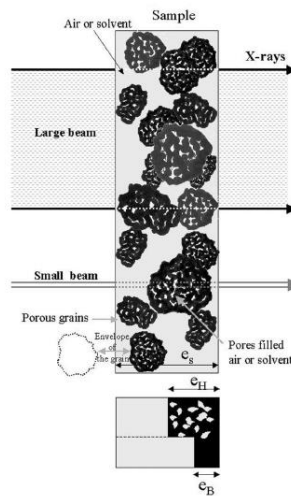


Figure D5. Schematic representation of a powder sample for SAXS measurement, and definitions of equivalent thick-nesses e_H and e_B .

The sample transmission is related to this equivalent thickness by the following equation:

$$e_B = -\frac{1}{\mu} \ln (T_{exp})$$

where μ is the material absorption coefficient for X-Ray ($\mu_{MWCNT} = 6 \text{ cm}^{-1}$) and T_{exp} is the **experimental transmission** (transmitted flux Φ_T / incident flux Φ_0), i.e. transmission of the sample with regard to the transmission of the empty cell (kapton® alone, empty capillary, etc.). The intensity scaled by this thickness e_B is called I_f . The Porod's law can then be applied for I_f to access the specific surface area of the powder.

Specific surface areas of powders are determined on the Porod plateau from the equation. The values in m^{-1} are then converted into m^2/g taking into account the material density ρ_m :

$$\sum \left[\frac{\text{m}^2}{\text{g}} \right] = \frac{\sum [\text{m}^{-1}]}{\rho_m \left[\frac{\text{g}}{\text{m}^3} \right]}$$

If no uncertainty is considered for the material density, the relative uncertainty of the specific surface area calculated is directly linked to the determination of the Porod plateau:

$$\frac{\Delta \Sigma[\frac{m^2}{g}]}{\Sigma[\frac{m^2}{g}]} = \frac{\Delta \Sigma[m^{-1}]}{\Sigma[m^{-1}]} = \frac{\Delta \lim(I)_1 q^4}{\lim(I)_1 q^4}$$

However, if we consider a quantifiable uncertainty on the material density, it is passed on to the calculated sample thickness e_B and the theoretical scattering length density of the material. Finally, the relative uncertainty on the specific surface area is increased by the uncertainty on the material density:

$$\frac{\Delta \Sigma[m^{-1}]}{\Sigma[m^{-1}]} = \frac{\Delta \lim(I)_1 q^4}{\lim(I)_1 q^4} + \frac{\Delta \rho_m}{\rho_m}$$

The uncertainty on the material density even contributes twice when the specific surface area is expressed in m^2/g :

$$\frac{\Delta \Sigma[\frac{m^2}{g}]}{\Sigma[\frac{m^2}{g}]} = \frac{\Delta \lim(I)_1 q^4}{\lim(I)_1 q^4} + 2 \frac{\Delta \rho_m}{\rho_m}$$

All specific surface area results, together with their uncertainty calculations are presented below. Errors on the Porod's plateaus have been determined manually for each diffractogram, and the uncertainty on the material density is considered to be about 5%.

Invariant theorem

When $I(q)$ can be extrapolated to zero values of q (no interaction at a large scale, i.e. a flat signal for low q) and at infinite q (usually with the Porod law), the following invariant theorem can be applied:

$$Q = \int_0^{\infty} I_{Abs} q^2 dq = 2\pi^2 \varphi (1 - \varphi) (\Delta\rho)^2$$

This implies that the invariant Q is a constant for a defined composition, which gives access to the volume fraction φ , or to the evolution of interactions for a fixed composition.

Guinier regime

For dilute samples of monodisperse objects (negligible position correlation between scattering objects, i.e. structure factor 1), the intensity in the low q region ($qR_G \ll 1$) can be approximated to:

$$I(q) \approx A \left(1 - \frac{(qR_G)^2}{3} + Bq^3 \right)$$

which gives access to the radius of gyration of the particles R_G with the slope of $\ln(I)=f(q^2)$.

Data fits

Assuming values of parameters such as volume fraction, size, shape and polydispersity of scattering objects for a model sample, it is possible to calculate theoretical curves of $I(q)$. Therefore, the adjustment of such parameters to fit experimental curves allows for the modelling of the sample properties.

Unified model of aggregates in suspension for SAXS data treatment

A unified fitting approach, developed by Beaucage et al. (Beaucage et al., 1996; Kammler et al., 2004; Kammler et al., 2005) was used to treat X-ray scattering data from SiO_2 suspensions composed of aggregates of primary particles. In this model, the whole q range is divided into sections reflecting different structural levels in the sample, and fitted by local Guinier, fractal and Porod scattering regimes, see Figure D6.

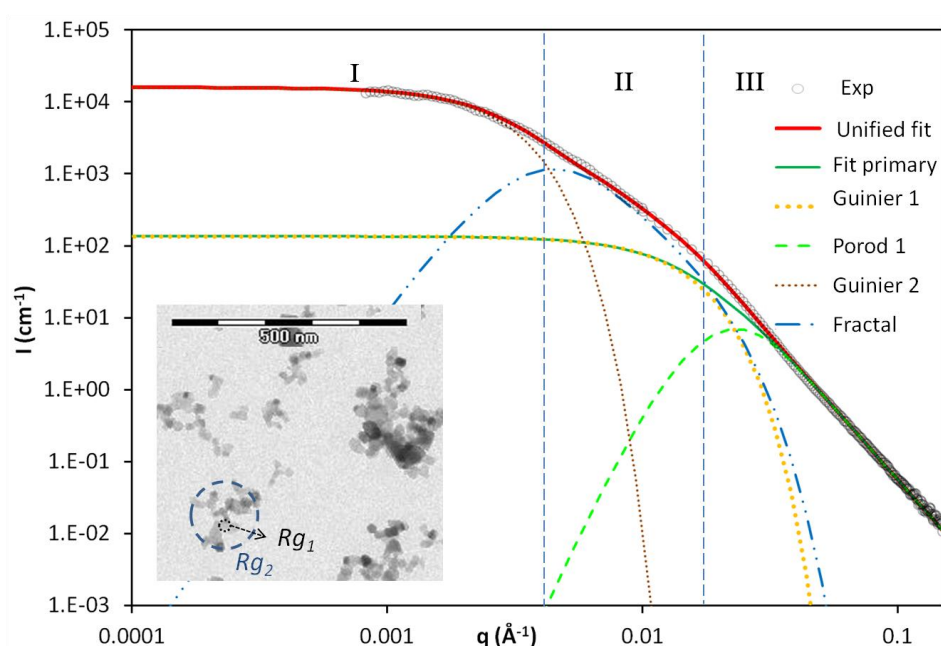


Figure D6. Example of SAXS diffractogram (NM-105, a TiO_2 , suspension sonicated at pH 2 as circles) illustrating the unified fit (solid red line) and its components prevailing in each q -domain (dashed-dotted lines). Insert of TEM micrograph (by CODA-CERVA) illustrating the gyration radius of primary particles (R_{g1}) and aggregates (R_{g2}) used in the model. Exp = experimental data.

The scattering vector q is homogeneous to the reverse of a length, so large q values actually corresponds to small observation scale in the direct space.

For a smooth surface of primary particles, **at large q** (the scale of interfaces) the intensity decays as a power-law of q^{-4} defining the Porod regime:

$$I_{\text{Porod } 1}(q) = B_1 q^{-4}$$

The coefficient B_1 is directly linked to the specific surface area of the primary particles:

$$B_1 = 2\pi N(\Delta\rho)^2 S$$

with N and S respectively the number density and the average surface area of primary particles and $\Delta\rho$ the difference of scattering length density between scattering object (MWCNT) and medium (water).

This Porod regime is preceded **at lower q** by a Guinier regime, signature of the size of primary particles, and is described by:

$$I_{\text{Guinier } 1}(q) = G_1 \exp\left(\frac{-q^2 Rg_1^2}{3}\right)$$

The sum of these two regimes (**Fit primary** in Figure D6) would describe scattering intensity resulting from individual uncorrelated primary particles, *i.e.* if they were perfectly dispersed and non-aggregated. It prevails in the large q range (domain III, Figure D6). The upturn of the intensity at small q is due to the association of primary particles into aggregates of finite size.

These aggregates also present a finite size and inner structure. Thus, a second Guinier regime is associated with the structural size of aggregates and prevails in the domain I defined in the Figure D6:

$$I_{\text{Guinier } 2}(q) = G_2 \exp\left(\frac{-q^2 Rg_2^2}{3}\right)$$

The coefficients G_1 and G_2 are defined by:

$$G_i = N_i (\Delta\rho)^2 V_i^2$$

where N_i and V_i are respectively the number density and volume of object i (primary particle or aggregate).

These two Guinier regimes give access to the radii of gyration of the primary particles, Rg_1 , and of the aggregates, Rg_2 .

The ratio of G_1 to B_1 is a measure of the anisotropy of the primary particles since

$$\frac{G_1}{B_1} \propto \frac{V^2}{2\pi S}$$

with V the volume of the particles and S their surface.

For intermediate q range between the scale of aggregates and the scale of primary particles (domain II in Figure D6), the intensity decays with a slope typical for the fractal regime of an aggregate and described by a power-law linked to the mass-fractal dimension D_f :

$$I_{\text{Fractal}}(q) = B_2 q^{-D_f}$$

The coefficient B_2 is linked to D_f , G_2 and Rg_2 by:

$$B_2 = \frac{G_2}{Rg_2^{D_f}} D_f \Gamma\left(\frac{D_f}{2}\right)$$

Γ is the gamma function.

The fractal dimension D_f is a measure of the degree of ramification and density of aggregates (value between 1 and 3), see Hyeon-Lee et al., 1998.

An average number of primary particles per aggregate can be derived from the Guinier coefficients:

$$N_{\text{part/agg}} = \frac{G_2}{G_1}$$

The global unified fit is obtained by addition of the different terms, see Bushell et al., 2002.

To fit the experimental diffractograms, the total model curve

$$I(q) = I_{\text{Porod 1}}(q) + I_{\text{Guinier 1}}(q) + I_{\text{Fractal}}(q) + I_{\text{Guinier 2}}(q)$$

is plotted and parameters (B_1 , G_1 , G_2 , D_f , Rg_1 and Rg_2) are adjusted manually so that the model fits the best the experimental data. Three parameters are there to describe the primary particles, and three are also necessary to describe the aggregates structures of primary particles. Also in TEM three independent parameters were required to describe the aggregates.

Some geometrical restrictions have to be respected ($D_f < 3$; volume of N primaries $<$ volume of aggregate, total surface area of primaries cannot be smaller than the corresponding surface area for ideal spheres).

All SAXS data are treated to be represented in the absolute scale (intensity in cm^{-1}). Therefore quantitative measurements are accessible and through the use of the invariant theorem and it is possible to calculate the exact concentration of samples, and then correlate the specific surface area developed in the suspension to the specific surface area of raw materials obtained from powder samples.

References

1. T. Zemb, O. Taché, F. Né, and O. Spalla; "A high-sensitivity pinhole camera for soft condensed matter"; J. Appl. Crystal., 36, 800-805, **2003**.
2. F. Né, I. Grillo, O. Taché, and T. Zemb.; "From raw image to absolute intensity: Calibration of a guinier-mering camera with linear collimation"; J. de Physique IV, 10(P10), 403-413, **2000**.
3. O. Spalla, S. Lyonnard, and F. Testard; "Analysis of the small-angle intensity scattered by a porous and granular medium"; J. Appl. Crystal., 36, 338-347, **2003**.
4. J. Lambard, P. Lessieur and Th. Zemb; "A triple axis double crystal multiple reflection camera for ultra small angle X-ray scattering"; J. de Physique I France, 2 , 1191-1213, **1992**. Lambard, J.; Lesieur, P.; Zemb, T., A triple axis double crystal multiple reflection camera for ultra small angle X-ray scattering. J. Phys. I France 1992, 2 (6), 1191-1213.
5. O. Taché; « Une architecture pour un système évolutif de contrôle commande d'expériences de physique », Engineer thesis, **2006**, available at <http://iramis.cea.fr/sis2m/lions/tango/tango-ds/memoire.pdf>
6. Beaucage, G., Small-Angle Scattering from Polymeric Mass Fractals of Arbitrary Mass-Fractal Dimension. J. Appl. Crystal. **1996**, 29 (2), 134-146.
7. Kammler, H. K.; Beaucage, G.; Mueller, R.; Pratsinis, S. E., Structure of Flame-Made Silica Nanoparticles by Ultra-Small-Angle X-ray Scattering. Langmuir **2004**, 20 (5), 1915-1921.
8. Kammler, H. K.; Beaucage, G.; Kohls, D. J.; Agashe, N.; Ilavsky, J., Monitoring simultaneously the growth of nanoparticles and aggregates by in situ ultra-small-angle x-ray scattering. J. Appl. Physics **2005**, 97 (5), 054309-11.
9. Hyeon-Lee, J.; Beaucage, G.; Pratsinis, S. E.; Vemury, S., Fractal Analysis of Flame-Synthesized Nanostructured Silica and Titania Powders Using Small-Angle X-ray Scattering. Langmuir **1998**, 14 (20), 5751-5756.
10. Bushell, G. C.; Yan, Y. D.; Woodfield, D.; Raper, J.; Amal, R., On techniques for the measurement of the mass fractal dimension of aggregates. Advances in Colloid and Interface Science **2002**, 95 (1), 1-50.
11. Porod, G.; Glatter, O.; Kratky, O., General theory: Small-angle X-ray scattering. Academic Press ed.; Academic Press: New York, **1982**.

Europe Direct is a service to help you find answers to your questions about the European Union
Freephone number (*): 00 800 6 7 8 9 10 11

(*) Certain mobile telephone operators do not allow access to 00 800 numbers or these calls may be billed.

A great deal of additional information on the European Union is available on the Internet.
It can be accessed through the Europa server <http://europa.eu>.

How to obtain EU publications

Our publications are available from EU Bookshop (<http://bookshop.europa.eu>),
where you can place an order with the sales agent of your choice.

The Publications Office has a worldwide network of sales agents.
You can obtain their contact details by sending a fax to (352) 29 29-42758.

European Commission

EUR 26796 EN – Joint Research Centre – Institute for Health and Consumer Protection

Title: Multi-walled Carbon Nanotubes, NM-400, NM-401, NM-402, NM-403: Characterisation and Physico-Chemical Properties

Authors: Kirsten Rasmussen, Jan Mast, Pieter-Jan De Temmerman, Eveline Verleysen, Nadia Waegeneers, Frederic Van Steen, Jean Christophe Pizzolon, Ludwig De Temmerman, Elke Van Doren, Keld Alstrup Jensen, Renie Birkedal, Per Axel Clausen, Yahia Kembouche, Nathalie Thieriet, Olivier Spalla, Camille Guiot, Davy Rousset, Olivier Witschger, Sébastien Bau, Bernard Bianchi, Boris Shivachev, Louiza Dimowa, Rositsa Nikolova, Diana Nihtianova, Mihail Tarassov, Ognyan Petrov, Snejana Bakardjieva, Charles Motzkus, Guillaume Labarraque, Caroline Oster, Giulio Cotogno and Claire Gailliard

Luxembourg: Publications Office of the European Union

2014 – 116 pp. – 21.0 x 29.7 cm

EUR – Scientific and Technical Research series –ISSN 1831-9424 (online), ISSN 1018-5593 (print)

ISBN 978-92-79-39648-9 (PDF)

ISBN 978-92-79-39649-6 (print)

doi:10.2788/10753

JRC Mission

As the Commission's in-house science service, the Joint Research Centre's mission is to provide EU policies with independent, evidence-based scientific and technical support throughout the whole policy cycle.

Working in close cooperation with policy Directorates-General, the JRC addresses key societal challenges while stimulating innovation through developing new methods, tools and standards, and sharing its know-how with the Member States, the scientific community and international partners.

Serving society
Stimulating innovation
Supporting legislation

doi:10.2788/10753

ISBN 978-92-79-39648-9

